AD-A236 696

2

DAMAGE MECHANICS OF COMPOSITE MATERIALS: CONSTITUTIVE MODELING AND COMPUTATIONAL ALGORITHMS

J.W. JU

Department of Civil Engineering & Operations Research
Princeton University
Princeton, N.J. 08544

21 April 1991

Final Technical Report

Prepared for

Air Force Office of Scientific Research

Building 410

Bolling AFB, D.C. 20332-6448

91 6 6 071

91-01453

REPORT DOCUMENTATION PAGE		Form Approved OMB No. 0704-0188

1a. REPORT SECURITY CLASSIFICATION Unclassified	1b. RESTRICTIVE MARKINGS

2a. SECURITY CLASSIFICATION AUTHORITY N/A	3. DISTRIBUTION/AVAILABILITY OF REPORT
2b. DECLASSIFICATION/DOWNGRADING SCHEDULE N/A	Approved for public release; distribution is unlimited.

4. PERFORMING ORGANIZATION REPORT NUMBER(S) PU/CEOR/SM-91-4	5. MONITORING ORGANIZATION REPORT NUMBER(S)

6a. NAME OF PERFORMING ORGANIZATION Princeton University	6b. OFFICE SYMBOL (If applicable)	7a. NAME OF MONITORING ORGANIZATION Air Force Office of Scientific Research

6c. ADDRESS (City, State, and ZIP Code) Dept. of Civil Engineering and Oper. Research Princeton University Princeton, NJ 08544	7b. ADDRESS (City, State, and ZIP Code) Building 410 Bolling AFB, D.C. 20332-6448

8a. NAME OF FUNDING/SPONSORING ORGANIZATION AFOSR	8b. OFFICE SYMBOL (If applicable) NA	9. PROCUREMENT INSTRUMENT IDENTIFICATION NUMBER AFOSR-89-0020

8c. ADDRESS (City, State, and ZIP Code) Bldg 410 Bolling AFB, DC 20332-6448	10. SOURCE OF FUNDING NUMBERS			
	PROGRAM ELEMENT NO. 61102F	PROJECT NO. 2302	TASK NO. B2	WORK UNIT ACCESSION NO.

11. TITLE (Include Security Classification) Damage Mechanics of Composite Materials: Constitutive Modeling and Computational Algorithms. (u)

12. PERSONAL AUTHOR(S) Ju, Jiann-Wen

13a. TYPE OF REPORT Final Technical	13b. TIME COVERED FROM 881001 TO 900930	14. DATE OF REPORT (Year, Month, Day) 91/4/21	15. PAGE COUNT 105

16. SUPPLEMENTARY NOTATION

17.	COSATI CODES		18. SUBJECT TERMS (Continue on reverse if necessary and identify by block number)
FIELD	GROUP	SUB-GROUP	Continuum Damage Mechanics. Micromechanical Damage Mechanics. Micromechanics of Composites.
09	02		
11	02		

19. ABSTRACT (Continue on reverse if necessary and identify by block number)

The present work is concerned with development of innovative damage mechanics models for constitutive modeling of modern composite materials. Special attention is focused on micro-mechanical damage theories to explain and model behavior of composites based on micromechanics and micro-geometry. In particular, basic studies are performed on the notion of isotropic and anisotropic damage variables in continuum damage mechanics. Futhermore, a micromechanical damage model is presented for uniaxially reinforced composites and is analytically derived based on micromechanical bi-material arc crack solutions. Finally, a novel three-dimensional statistical micromechanical theory is proposed to investigate the nonlinear behavior of microcrack-weakened brittle solids. The theory is fundamentally different from existing effective medium theories and deterministic microcrack interaction method.

20. DISTRIBUTION/AVAILABILITY OF ABSTRACT ☐ UNCLASSIFIED/UNLIMITED ☒ SAME AS RPT. ☐ DTIC USERS	21. ABSTRACT SECURITY CLASSIFICATION Unclassified
22a. NAME OF RESPONSIBLE INDIVIDUAL 1+ Col Steven C. Boyce	22b. TELEPHONE (Include Area Code) (202) 767-6963	22c. OFFICE SYMBOL AFOSR/NA

DD Form 1473, JUN 86   Previous editions are obsolete.   SECURITY CLASSIFICATION OF THIS PAGE

PREFACE

Accession For

NTIS GRA&I	☑
DTIC TAB	☐
Unannounced	☐
Justification	

By
Distribution/

Availability Codes

Dist	Avail and/or Special
A-1	

DTIC COPY INSPECTED 6

ABSTRACT

The present work is concerned with development of innovative damage mechanics models for constitutive modeling of modern composite materials. Special attention is focused on micromechanical damage theories to explain and model behavior of composites based on micromechanics, instead of using phenomenological models with arbitrary thermodynamic potential functions and arbitrary damage evolution equations. In particular, basic studies are performed on the notion of isotropic and anisotropic damage variables in continuum damage mechanics. It is demonstrated that "isotropic damage" does not necessarily imply "scalar damage" representation in general. Furthermore, a micromechanical damage model is presented for uniaxially reinforced composites with interfacial arc microcracks. All microcracks are assumed to occur in the fiber/matrix interfaces, and are modeled as *arc* microcracks. Microcrack-induced strains and overall compliances are analytically derived based on micromechanical bi-material arc crack solutions. Both "stationary" and "process" damage models are given. It is emphasized that the present work does not employ any arbitrary (fitted) "material constants". Finally, a novel three-dimensional statistical micromechanical theory is proposed to investigate the nonlinear behavior of microcrack-weakened brittle solids. The macroscopic stress-strain relations of elastic solids with interacting microcracks are micromechanically derived by taking the *ensemble average* (over all possible realizations) and *volume average*. The proposed statistical micromechanical theory accounts for random microcrack location, distribution, and interaction without using Monte Carlo simulations. The theory is fundamentally different from existing effective medium theories and deterministic microcrack interaction method.

RESEARCH OBJECTIVES

The proposed research work is concerned with development of innovative damage mechanics theories and constitutive modeling of modern composite materials. Micromechanically based damage theories and models will be actively pursued. Particular attention will be focused on the construction of physical underlying damage mechanisms based on microstructural considerations. The general goal is to physically understand and mathematically model the fundamental damage mechanisms at the local level so that we can simulate randomly oriented distributed microcracks and perform failure analysis of composite solids and structures. The specific objectives of the proposed research are the following:

1. Develop proper micromechanically based "damage mode tensors" for different modes of failure mechanisms.

2. Develop a set of physical damage loading/unloading fracture criteria for microcracks initiation, growth, coalescence and arrest.

3. Derive micromechanically-based evolution equations for microcrack growth.

4. Derive progressively damaged material properties (complainces) and obtain damaged anisotropic multi-phase stress-strain constitutive laws based on micromechanics solutions.

5. Develop efficient and accurate computational constitutive algorithms for the micromechanically-based damage models proposed, and perform experimental verification of the models obtained.

LIST OF PAPERS FOR PUBLICATION IN JOURNALS

[1] J.W. Ju, "Isotropic and Anisotropic Damage Variables in Continuum Damage Mechanics," *Journal of Engineering Mechanics*, ASCE, Vol. 116, No. 12, Dec. 1990, pp. 2764--2770.

[2] J.W. Ju, "A Micromechanical Damage Model for Uniaxially Reinforced Composites with Interfacial Arc Microcracks," *Journal of Applied Mechanics*, accepted for publication, in press.

[3] J.W. Ju and K.W. Tseng, "A Three-Dimensional Statistical Micromechanical Theory for Brittle Solids with Interacting Microcracks," to be submitted to *Mechanics of Materials* shortly.

[4] J.W. Ju, "A Complete Second Order 3-D Statistical Micromechanical Theory for Brittle Solids with Interacting Microcracks," in preparation.

LIST OF NAMES OF PARTICIPATING PROFESSIONALS

[1] Dr. X. Lee, Post-Doctoral Research Associate.

[2] Mr. K.W. Tseng, Graduate Research Assistant.

Table of Contents

PART I:

On the Notion of Isotropic and Anisotropic Damage Variables in Continuum Damage Mechanics

I.0. Abstract

The present work analyzes the implication and limitation of some "scalar damage" models. In particular, thermodynamic potential and "effective stress concept" are re-examined. It is demonstrated that "isotropic damage" does not necessarily imply "scalar damage" representation in general. The notion of isotropic and anisotropic damage variables in continuum damage mechanics is then discussed. In addition, some results from micromechanical analyses are applied to show the direct relationship between the fourth-order damage tensor and the damage-induced compliance tensor characteristic of microcrack-weakened brittle matrix composite materials. It is shown that even for isotropic damage one should employ an isotropic fourth-order damage tensor (not a scalar damage variable) to characterize the state of damage in materials, in accordance with the *effective stress* concept. In general, however, a damage tensor is anisotropic and should be derived from micromechanical damage analysis when possible.

I.1. Introduction

Since the first introduction of the *scalar damage concept* by Kachanov (1958) and Rabotnov (1963) for creep of metals, continuum damage mechanics has become an emerging field of active research. Extensive phenomenological damage models were proposed in the literature to describe and predict macroscopic constitutive behavior of ductile and brittle materials containing distributed microdefects such as microvoids and microcracks. We refer to Lemaitre (1984), Krajcinovic (1984,1986,1989), Kachanov (1986), and Ju (1989a) for a literature review. In addition, *micromechanical* "non-process" (stationary) and "process" (propagating) damage models for brittle solids with many microcracks were proposed by, e.g., Budiansky and O'Connel (1976), Horii and Nemat-Nasser (1983,1985), Kachanov (1987), Krajcinovic and Fanella (1986), Sumarac and Krajcinovic (1987,1989), Fanella and Krajcinovic (1988), Krajcinovic and Sumarac (1989), and Ju (1989b).

The predictive utility of a damage model depends heavily on its particular choice of a "*damage variable*" which serves as a macroscopic approximation in describing the underlying micromechanical processes of microdefects. In the current literature, there are many ways to phenomenologically *define* or micromechanically *derive* damage variables; see, Krajcinovic (1989) for a state-of-the-art review. In particular, scalar damage variables were widely used for *isotropic* or *one-dimensional* phenomenological damage models; see, e.g., Lemaitre and Chaboche (1978,1985) for excellent work. In addition, vectorial, second-order and fourth-order tensorial damage variables were often used for *anisotropic* phenomenological damage models; see, e.g, Krajcinovic and Fonseka (1981), Vakulenko and Kachanov (1971), Kachanov (1980), Murakami and Ohno (1981), Chaboche (1979), Cordebois and Sidoroff (1979,1982), and Ju (1989a) for interesting examples. The simplicity of a scalar damage representation is indeed very attractive. However, a scalar damage model is somewhat of limited use in practice. A vectorial damage representation is appealing because microcrack areas and orientations are captured and a vectorial representation is a direct extension of the original Kachanov's model. Nevertheless, a vector damage model to some extent suffers microcrack shape-indifference and tensor operation problems related to general stress transformation. A second-order damage tensor representation is also attractive since microcrack areas and orientations are captured, too. It is, however, incapable of describing general anisotropy. Therefore, as noted by several researchers, an appropriate description of anisotropic damage generally involves a *fourth-order* or even an eighth-order damage tensor representation. In practice,

an eighth-order damage representation is perhaps too complicated. A fourth-order damage representation, on the other hand, can be handled reasonably well and and has nice correspondence with the fourth-order overall stiffness tensor.

In spite of the direct intuition that "isotropic damage" necessarily warrants a *scalar* damage representation (see, e.g., Lemaitre and Chaboche (1978), Lemaitre (1984), Mazars (1984), Kachanov (1986)), this is, surprisingly, not always true from the viewpoint of the *effective stress concept* and *thermodynamic potential*. The present work shows that isotropic damage actually only implies that the (fourth-order) damage tensor is *isotropic*, not necessarily reducing to a scalar. On the other hand, anisotropic damage implies that damage tensor is anisotropic. Further, the implication of scalar damage representation upon overall elastic-damage moduli is discussed within the framework of the effective stress concept. Some results from micromechanical analyses are also applied to demonstrate the physical meaning of the fourth-order damage tensor in the case of microcrack-weakened brittle solids.

I.2.   Implication of scalar damage variable

In the case of spatially perfectly randomly distributed microcracks or microvoids in all directions, isotropic damage model is certainly an appropriate choice. In particular, in a *scalar* damage model, the virgin (undamaged) material is often assumed to be linearly elastic and isotropic in the absence of plastic flow. In the literature, some researchers consider the following rational elastic-damage potential energy based on the physically appealing *effective stress concept* (Lemaitre and Chaboche (1978), Lemaitre (1984), Mazars (1984), etc.):

$$\psi^e = \tfrac{1}{2}\,(1 - d)\,\epsilon^e : \mathbf{C}^o : \epsilon^e \tag{1}$$

where d is a scalar damage variable (ranging from 0 to 1), ϵ^e is the elastic strain tensor, $\mathbf{C}^o$ is the virgin linear elasticity tensor, and " : " signifies tensor contraction. From the Clausius-Duhem inequality for isothermal processes, one obtains the homogenized stress σ:

$$\sigma = (1 - d)\,\mathbf{C}^o : \epsilon^e \tag{2}$$

Hence, it is clear that the overall elastic-damage stiffness tensor C takes the form:

$$\mathbf{C} = (1 - d)\,\mathbf{C}^o \tag{3}$$

such that $\sigma = \mathbf{C} : \epsilon^e$. As a consequence, a component of the overall elastic-damage stiffness tensor can be obtained by scaling down the corresponding component of the virgin elastic stiffness tensor by a *common* factor $(1 - d)$. Moreover, the effective stress $\bar{\sigma}$ is often defined as (within the framework of isotropic damage):

$$\bar{\sigma} = \frac{\sigma}{1 - d} \tag{4}$$

Thus, we have $\bar{\sigma} = \mathbf{C}^o : \epsilon^e$. The above formulation is indeed excellent for one-dimensional problems and is entirely consistent with Kachanov's (1958) original concept of damage measure.

In a *three-dimensional* setting, nevertheless, Eqs. (1)-(4) are less attractive. This can be proved by simply noting from Eq. (3) that *damaged* bulk and shear moduli become $K = (1 - d)K_o$ and $G = (1 - d)G_o$, respectively, with K_o and G_o denoting the *virgin* bulk and shear moduli. It follows that $G/K = G_o/K_o$. Therefore, the above scalar damage formulation inherently implies that Poisson's ratio always remains *constant*, i.e., $\nu \equiv \nu_o$. This is somewhat too restrictive and not universal even among isotropic damage processes. This anomaly is due to the *one-dimensional* nature of Eq. (4).

I.3.   Notion of isotropic and anisotropic damage variables

As discussed in the previous section, "scalar damage" is only a special case of "isotropic damage". "Isotropic damage" only states that the fourth-order damage tensor $\mathbf{D}$ is *isotropic*. In addition, isotropic damage does *not* require the virgin elasticity tensor $\mathbf{C}^o$ to be isotropic. It is emphasized that isotropic damage will *preserve* the directional characteristics of the virgin elasticity tensor $\mathbf{C}^o$. That is, if $\mathbf{C}^o$ is isotropic, then the elastic-damage stiffness $\mathbf{C}$ is also isotropic. On the other hand, if $\mathbf{C}^o$ is orthotropic (or anisotropic), then $\mathbf{C}$ is also orthotropic (or anisotropic). By contrast, general anisotropic damage will *change* the directional properties of $\mathbf{C}^o$.

The anomaly in the aforementioned scalar damage formulation can be easily resolved by re-examining the effective stress concept and the elastic-damage energy potential. In particular, the following formulation is free of the previous anomaly in three-dimension:

$$\psi^e = \tfrac{1}{2} \, \epsilon^e : [\mathbf{M}(\mathbf{D}) \cdot \mathbf{C}^o] : \epsilon^e \tag{5}$$

where $\mathbf{M}(\mathbf{D})$ is a fourth-order tensorial function of the fourth-order damage tensor $\mathbf{D}$. The Clausius-Duhem inequality then renders

$$\sigma = [\mathbf{M}(\mathbf{D}) \cdot \mathbf{C}^o] : \epsilon^e \tag{6}$$

According to the *effective stress* concept, the effective stress can be expressed as $\bar{\sigma} = \mathbf{C}^o : \epsilon^e$. Consequently, Eq. (6) can be rephrased as

$$\sigma = \mathbf{M}(\mathbf{D}) : \bar{\sigma} \tag{7}$$

Clearly, $\mathbf{M}(\mathbf{D})$ is the transformation tensor relating the homogenized and effective stresses. Moreover, from Eq. (6), we obtain the elastic-damage stiffness tensor $\mathbf{C}$:

$$\mathbf{C} = \mathbf{M}(\mathbf{D}) \cdot \mathbf{C}^o \tag{8}$$

A rational choice of $\mathbf{M}(\mathbf{D})$ may be $\mathbf{M}(\mathbf{D}) \equiv \mathbf{I} - \mathbf{D}$, with $\mathbf{I}$ denoting the rank-four unit tensor. If this choice is made, then Eq. (7) and (8) can be recast as (see also Krajcinovic (1989))

$$\bar{\sigma} = [\mathbf{I} - \mathbf{D}]^{-1} : \sigma \tag{9}$$

$$\mathbf{C} = [\mathbf{I} - \mathbf{D}] \cdot \mathbf{C}^o \quad or \quad \mathbf{D} = \mathbf{I} - \mathbf{C} \cdot \mathbf{C}^{o-1} \tag{10}$$

It is worth noting that Eq. (10) shows the direct relationship between the damage tensor $\mathbf{D}$ and the elastic-damage stiffness tensor $\mathbf{C}$. Therefore, damage tensor $\mathbf{D}$ must be *isotropic* (not necessarily reducing to a scalar representation) for an isotropic damage state. Moreover, the appropriate expression for the effective stress concept is Eq. (7) or (9), not Eq. (4) even in the case of isotropic damage. On the other hand, $\mathbf{D}$ and hence $\mathbf{C}$ become anisotropic in the case of an anisotropic damage state.

I.4. Application of micromechanical analyses for isotropic damage

In this section, we apply some results from micromechanical analyses for two-dimensional microcrack-weakened brittle solids under tension (Horii and Nemat-Nasser (1983), Sumarac and Krajcinovic (1987)). Applications can be made to brittle matrix fiber or particle composites as well as ceramics, etc. It is assumed that the virgin material is isotropic and linearly elastic, and that line microcracks are *always* open and perfectly randomly distributed in all directions with uniform size $2a$. The microcrack size $2a$, however, may grow *uniformly* during the loading history. Therefore, the overall material response remains isotropic. Furthermore, the overall elastic-damage compliance tensor S takes the form:

$$S = S^o + S^*$$ (11)

where S^o is the virgin elastic compliance (i.e., inverse of C^o) and S^* denotes the damage-induced additional inelastic compliance.

For two-dimensional problems, it is more convenient to use the Voigt's notation and express the compliance tensor as a three by three matrix. Based on microcrack opening displacement formulas, S^* can be micromechanically computed by (assuming plane stress condition):

$$S^* = \frac{2\,N\,a^2}{E\,A} \int_0^\pi \hat{g}(\theta)\,d\theta$$ (12)

where N = the number of microcracks per unit cell surface, A = the surface area of representative unit cell, Γ = the damaged overall "Young's modulus", and $\hat{g}(\theta)$ is a tensorial function of the orientation angle θ ; see Sumarac and Krajcinovic (1989, Eq. (17)). Notice that S^* is indeed an isotropic tensor.

In the case of the *Taylor's model*, microcrack interaction is completely ignored. By actually evaluating the integral in Eq. (12), we obtain the overall elastic-damage moduli for plane stress as follows (see Sumarac and Krajcinovic (1989, Eq. (22)))

$$\frac{E}{E_o} = \frac{\nu}{\nu_o} = \frac{1}{1+\omega}$$ (13)

where $\omega \equiv N\pi a^2/A$ is the non-dimensional microcrack density parameter, and E_o and ν_o are the virgin elastic moduli. Clearly, $\nu < \nu_o$ and therefore the scalar damage representation discussed in Sec. 2 is inadequate. It is also noteworthy from Eq. (12) that S^* is factually a function of the microcrack density parameter ω . Nevertheless, one should not confuse the scalar microcrack density parameter ω with the isotropic damage tensor D .

Similarly, in the case of the *self-consistent model*, S* can be micromechanically derived and the plane stress elastic-damage moduli are (Horii and Nemat-Nasser (1983)):

$$\frac{E}{E_o} = \frac{\nu}{\nu_o} = 1 - \omega \tag{14}$$

One observes that $\nu < \nu_o$, and hence the previous scalar damage formulation is again improper.

Moreover, one may define an alternative damage tensor $\hat{D}$ through

$$I + \hat{D} \equiv [I - D]^{-1} \tag{15}$$

so that one may write

$$S = S^o \cdot [I + \hat{D}] \tag{16}$$

From Eq. (11) and (16), we make the following identification:

$$S^* = S^o \cdot \hat{D} \quad or \quad \hat{D} = C^o \cdot S^* \tag{17}$$

Thus, it is actually possible *derive* the fourth-order damage tensor $\hat{D}$ (or D) from micromechanics (i.e., the microcrack-induced inelastic compliance S*). Obviously, if microcracks are spatially randomly distributed in a representative volume element, then S* and hence $\hat{D}$ (or D) are isotropic (given linearly elastic and isotropic C°). If there are preferred orientations in microcrack distribution, then S* will be anisotropic and therefore damage tensor $\hat{D}$ (or D) becomes anisotropic. Finally, one notes that if S* = d S° then D = d I , and hence the scalar damage model discussed in Sec. 2 is recovered.

I.5. Conclusion

The present work analyzes the implication and limitation of some scalar damage models. It is demonstrated that isotropic damage does not necessarily imply scalar damage representation in general. The notion of isotropic and anisotropic damage variables in continuum damage mechanics is discussed. In addition, some results from micromechanical analyses are applied to show the direct relationship between the fourth-order damage tensor $\mathbf{D}$ (or $\hat{\mathbf{D}}$) and the damage-induced compliance tensor $\mathbf{S}^*$. It is concluded that, even for isotropic damage, one should employ an isotropic fourth-order damage tensor (not a scalar damage variable) to characterize the state of damage in materials. In general, however, a damage tensor is anisotropic. Finally, it is preferable to *derive* general anisotropic damage tensors from micromechanical formulations, instead of postulating them arbitrarily.

I.6. References

1. BUDIANSKY, B. AND R. J. O'CONELL, (1976), "Elastic Moduli of a Cracked Solid", *Int. J. Solids & Struct.*, Vol. 12, pp. 81–97.

2. CHABOCHE, J. L., (1979), "Le Concept de Contrainte Effective Applique a L'elasticite et a la Viscoplasticite en Presence d'un Endommagement Anisotrope", *Mechanical Behavior of Anisotropic Solids*, Proc. Euromech Colloque 115, June 1979, Edited by J. P. Boehler, pp. 737–760, Martinus Nijhoff.

3. CORDEBOIS, J. P. AND F. SIDOROFF, (1979), "Damage Induced Elastic Anisotropy", *Mechanical Behavior of Anisotropic Solids*, Proc. Euromech Colloque 115, June 1979, Edited by J. P. Boehler, pp. 761–774, Martinus Nijhoff.

4. CORDEBOIS, J. P. AND F. SIDOROFF, (1982), "Endommagement Anisotrope en Elasticite et Plasticite", *J. Mech. Theor. Appl.*, No. special, pp. 45–59.

5. FANELLA, D. AND D. KRAJCINOVIC, (1988), "A Micromechanical Model for Concrete in Compression", *Eng. Fract. Mech.*, Vol. 29, No. 1, pp. 49–66.

6. HORII, H. AND S. NEMAT-NASSER, (1983), "Overall Moduli of Solids with Microcracks: Load Induced Anisotropy", *J. Mech. Phys. Solids*, Vol. 31, No. 2, pp. 155–171.

7. HORII, H. AND S. NEMAT-NASSER, (1985), "Elastic Fields of Interacting Inhomogeneities", *Int. J. Solids & Struct.*, Vol. 21, No. 7, pp. 731–745.

8. JU, J. W., (1989a), "On Energy-Based Coupled Elastoplastic Damage Theories: Constitutive Modeling and Computational Aspects", *Int. J. Solids & Struct.*, Vol. 25, No. 7, pp. 803–833.

9. JU, J. W., (1989b), "On Two-Dimensional Self-Consistent Micromechanical Damage Models for Brittle Solids", *Int. J. Solids & Struct.*, accepted for publication, in press.

10. KACHANOV, L. M., (1958), "Time of the Rupture Process under Creep Conditions", *Izvestia Akademii Nauk*, USSR, Nauk 8, pp. 26–31.

11. KACHANOV, L. M., (1986), "Introduction to Continuum Damage Mechanics", Martinus Nijhoff Publishers, Dordrecht, Netherlands.

12. KACHANOV, M., (1980), "A Continuum Model of Medium with Cracks", *J. Eng. Mech. Div.*, ASCE, Vol. 106, pp. 1039–1051.

13. KACHANOV, M., (1987), "Elastic Solids with Many Cracks: A Simple Method of Analysis", *Int. J. Solids & Struct.*, Vol. 23, No. 1, pp. 23–43.

14. KRAJCINOVIC, D., (1984), "Continuum Damage Mechanics", *Appl. Mech. Rev.*, Vol. 37, Jan., pp. 1–6.

15. KRAJCINOVIC, D., (1985), "Constitutive Theories for Solids with Defective Microstructure", in *Damage Mechanics and Continuum Modeling*, ed. N. Stubbs and D. Krajcinivic, ASCE, pp. 39–56.

16. KRAJCINOVIC, D., (1986), "Update to Continuum Damage Mechanics", *Appl. Mech. Update*, pp. 403–406.

17. KRAJCINOVIC, D., (1989), "Damage Mechanics", *Mech. of Materials*, to appear.

18. KRAJCINOVIC, D. AND D. FANELLA, (1986), "A Micromechanical Damage Model for Concrete", *Eng. Fract. Mech.*, Vol. 25, No. 5/6, pp. 585–596.

19. KRAJCINOVIC, D. AND G. U. FONSEKA, (1981), "The Continuous Damage Theory of Brittle Materials", *J. Appl. Mech.*, Vol. 48, pp. 809–824.

20. KRAJCINOVIC, D. AND D. SUMARAC, (1989), "A Mesomechanical Model for Brittle Deformation Processes: Part I", *J. Appl. Mech.*, Vol. 56, No. 3, pp. 51–56.

21. LEMAITRE, J., (1984), "How to Use Damage Mechanics", *Nuclear Eng. and Design*, Vol. 80, pp. 233–245.

22. LEMAITRE, J. AND J. L. CHABOCHE, (1978), "Aspect Phenomenologique de la Rupture par Endommagement", *J. de Mech. Applique*, Vol. 2, pp. 317–365.

23. LEMAITRE, J. AND J. L. CHABOCHE, (1985), *Mechanique des Materiaux Solids*, Dunod, Paris.

24. MAZARS, J., (1984), "Application de la Mechanique de l'Endommagement au Comportement non Lineaire et a la Rupture du Beton de Structure", These de Doctorate d'Etat, L.M.T., Universite Paris, France.

25. MURAKAMI, S. AND N. OHNO, (1981), "A Continuum Theory of Creep and Creep Damage", in *Creep of Structures*, IUTAM Symp., Ed. A.R.S. Ponter, Springer-Verlag, Berlin, pp. 422–444.

26. RABOTNOV, I. N., (1963), "On the Equations of State for Creep", in *Progress in Applied Mechanics–The Prager Anniversary Volume*, MacMillan, New York, pp. 307–315.

27. SUMARAC, D. AND D. KRAJCINOVIC, (1987), "A Self-Consistent Model for Microcrack-Weakened Solids", *Mech. Mater.*, Vol. 6, pp. 39–52.

28. SUMARAC, D. AND. KRAJCINOVIC, (1989), "A Mesomechanical Model for Brittle Deformation Processes: Part II", *J. Appl. Mech.*, Vol. 56, No. 3, pp. 57–62.

29. VAKULENKO, A. A. AND M. KACHANOV, (1971), "Continuum Theory of Cracked Media", *Izv. AN SSSR, Mekh. Tverdogo Tela*, Vol. 4, pp. 159–166.

PART II:

A Micromechanical Damage Model for Uniaxially Reinforced Composites with Interfacial Arc Microcracks

II.0. Abstract

A micromechanical damage model is presented in this work for fiber/matrix interfacial micro-crack-weakened uniaxially reinforced brittle matrix composites. It is assumed that the undamaged fibers and matrix materials are linearly elastic and isotropic. All microcracks are assumed to occur in the fiber/matrix interfaces, and are modeled as *arc* microcracks under "cleavage 1" deformation processes. Microcrack-induced inelastic strains and overall elastic-damage compliances are analytically derived based on micromechanical bi-material (interfacial) arc-microcrack opening displacements and probabilistic distributions of arc microcracks. In addition, thermodynamic basis is rendered. The present work is entirely different from existing phenomenological continuum damage models for composite materials since it is based on micromechanical derivations. Both "*stationary*" and "*process*" damage models are given in the present work. In particular, microcrack kinetic equations are constructed based on micromechanical fracture criterion and microstructural geometry in a representative volume element. Simple and efficient computational algorithms as well as some numerical uniaxial tension tests are also presented to illustrate the proposed micromechanical damage model for composites. It is emphasized that the present work does not employ any arbitrary (fitted) "material constants".

II.1. Introduction

Initiated by Kachanov (1958) and Rabotnov (1963) for one-dimensional creep damage of metals, continuum damage mechanics has been extensively explored and applied by many outstanding applied mechanics researchers. Basically, there are two types of continuum damage formulations – *phenomenological* and *micromechanical* damage models. Most existing work are classified as phenomenological damage models; see, e.g., Krajcinovic (1984,1986,1989) and Bazant (1986) for a comprehensive literature review. There are, however, some micromechanical "stationary" or "process" damage models proposed in the literature; see, e.g., Budiansky and O'Connel (1976), Horii and Nemat-Nasser (1983, 1985), Kachanov (1987), Krajcinovic and Fanella (1986), Fanella and Krajcinovic (1988), Sumarac and Krajcinovic (1987), and Ju (1989b).

In particular, excellent studies on damage mechanics in modern composite materials were presented by Weitsman (1987a,1987b,1988), Talreja (1985a,1985b,1985c,1986,1987), Allen et al. (1987a,1987b,1987c), and Harris et al. (1987) for distributed matrix cracks and delamination within the framework of *phenomenological* damage models. On the other hand, some noteworthy micromechanical (primarily "stationary") damage models for composites were proposed by, e.g., Wang et al. (1984), Laws et al. (1983) and Hashin (1985) for transverse (parallel) matrix crack systems. It is noted that existing phenomenological continuum damage models of Weitsman, Talreja and Allen et al. employed either vector-valued or second-rank (symmetric or non-symmetric) "damage tensors" (treated as internal state variables) to characterize the state of damage in composite materials. However, a vector or a second-rank damage tensor is inherently incapable of describing general anisotropy in composites. An appropriate description of anisotropic damage generally involves a *fourth-rank* (or even eighth-rank) damage tensor representation; see, Chaboche (1979), Cordebois and Sidoroff (1979,1982), Ju (1989a), and Krajcinovic (1989) for further remarks. In addition, in spite of the solid and attractive thermodynamic basis, the specific functional forms of *the Helmholtz or Gibbs free energy potentials* in phenomenological damage models are to some extent *arbitrary* (heuristic). Therefore, the resulting overall stiffness-damage relationships and stress-strain laws are also somewhat arbitrary. Moreover, in order to have constitutive *predictive* capability, phenomenological damage models must arbitrarily or empirically postulate functional forms for damage "evolution (growth) equations". In the thermodynamic free energy potentials and damage evolution equations, nevertheless, existing phenomenological damage models typically rely on the use of many (perhaps up to 100 or even 200) *fitted* "material constants". As a

consequence, it becomes very difficult to identify these fitted constants from actual experimental data of composites.

Hence, as pointed out by Krajcinovic and Fanella (1986) and Weitsman (1988), micromechanical damage theories for composites are warranted to incorporate microstructural geometry, micromechanical deformations and microcrack growth into the damage mechanics framework. Most currently available micromechanical damage models for composites focused on the effects of transverse *stationary* matrix cracks on overall (damaged) compliance tensors. The present paper, on the other hand, considers the damage effects on uniaxially reinforced composites due to the *existence* and *growth* of an ensemble of randomly oriented microcracks at the fiber/matrix *interfaces* within the context of micromechanical damage mechanics. This circumstance corresponds to an ensemble of randomly distributed *arc microcracks* at the interfaces between cyclindrical inclusions and extended exterior regions under *plane strain*. In the case of a single arc crack at the fiber/matrix interface subjected to remote tension field (plane strain), solutions are available in England (1966), Perlman and Sih (1967), Toya (1974), and Piva (1982). In particular, Toya's solution is the most suitable for our damage mechanics formulation because it provides analytical (micromechanical) expressions for microcrack opening displacements and arc microcrack fracture energy criteria; see also remarks made in Weitsman (1988).

In the present work, it is assumed that the undamaged fibers and matrix materials have different properties but are both linearly elastic and isotropic. All arc microcracks are assumed to occur in the fiber/matrix interfaces under "cleavage 1" deformation processes (i.e., due to pre-existing arc microcracks). New microcrack nucleations ("cleavage 2" processes) are not considered in this work. Moreover, at this stage of the development, arc-microcrack interactions are assumed to be negligible (Taylor's model); i.e., dilute microcrack concentrations are considered. In the absence of a micromechanical solution for partially closed or entirely closed arc microcrack (namely, a "mixed crack-and-contact problem"), we assume that all arc microcracks are entirely *open* under a remote tension field.

An outline of this paper is as follows. The representation of the fourth-rank damage and thermodynamic basis for microcrack-weakened brittle composites are presented in Sec. II.2 within the context of homogenization for multiphase inhomogeneous materials. It is assumed that distributed arc microcrack concentration justifies the use of effective continuum medium theory. Based on Toya's (1974) micromechanical solution of bi-material (interface) arc-crack opening displacements, damage-induced inelastic strains and inelastic compliances are systematically derived in

Sec. II.3 for an ensemble of randomly oriented open arc microcracks. This corresponds to a *stationary* (non-process) micromechanical damage model. In Sec. II.4, microcrack growth (evolution) is considered based on Toya's (1974) micromechanical fracture criterion for a single arc microcrack under uniaxial tension. The extension to account for biaxial tension loadings can be readily made. "Stable" and "unstable" domains are identified for stationary and propagating arc microcracks, respectively. As a consequence, a "process model" is rendered. It is emphasized that the present work does not employ any arbitrary (fitted) "material constants". Simple and efficient computational algorithms are given in Sec. II.5. In addition, some numerical uniaxial tension tests are presented in Sec. II.5 to illustrate the potential capability of the proposed micromechanical damage model for composites.

II.2. Thermodynamic basis

In the case of general anisotropy, a scalar, a vectorial, or a second-rank tensorial representation of damage variable is not adequate; see Krajcinovic (1989) for more details. In this work, we employ a fourth-rank anisotropic damage tensor to represent the state of damage in anisotropic composite materials. It is worth mentioning that the fourth-rank damage tensor employed has an appealing correspondence with the fourth-rank overall stiffness (or compliance) tensor.

Within the framework of homogenization concept for inhomogeneous effective continuum medium, one may define the homogenized Gibbs free energy as

$$\chi \equiv \tfrac{1}{2}\,\sigma : [S^{\circ} \cdot (I + D)] : \sigma \tag{1}$$

where σ is the *volume-average* stress tensor (Hill (1965)), S° is the undamaged linear elastic compliance (obtained by the rule of mixture) of a composite material, I is the fourth-rank unit tensor, D denotes the fourth-rank damage tensor, and " : " denotes the tensor contraction operation. By the Clausius-Duhem inequality for isothermal process, we have (with ϵ denoting the volume-average strain)

$$\dot{\chi} - \dot{\sigma} : \epsilon \geq 0 \tag{2}$$

The standard Coleman's method then leads to the following macroscopic stress-strain law and overall elastic-damage compliance tensor S :

$$\epsilon = [S^{\circ} \cdot (I + D)] : \sigma \tag{3}$$

$$S \equiv S^{\circ} \cdot (I + D) \tag{4}$$

together with the damage dissipative inequality:

$$\tfrac{1}{2}\,\sigma : \dot{S} : \sigma \geq 0 \tag{5}$$

From Eq. (5), it is observed that the evolution $\dot{S}$ plays an essential role in microcrack energy dissipation and growth. Further, Eq. (3) is entirely consistent with the "effective stress" concept in continuum damage mechanics (Kachanov (1958), Rabotnov (1963), Lemaitre and Chaboche (1978)). During a damage *loading* process, the total strain tensor ϵ is amenable to an additive decomposition:

$$\epsilon = \epsilon^{e} + \epsilon^{*} \tag{6}$$

where ϵ^e and ϵ^* denote the elastic and inelastic (damage-induced) strains, respectively. In addition, it is assumed that $\epsilon^* \approx 0$ upon complete unloading; namely, the residual strain at zero stress is negligible for brittle composite materials. The elastic-damage compliance tensor is also suitable for an additive decomposition:

$$S = S^o + S^* \qquad (7)$$

where S^* signifies the damage-induced inelastic compliance (Mura (1982), Horii and Nemat-Nasser (1983)). In fact, from Eqs. (4) and (7), the relationship between S^* and D can be formally expressed as

$$S^* = S^o \cdot D \qquad (8)$$

Therefore, if one can micromechanically *derive* the damage-induced inelastic compliance S^*, then one can explicitly express the fourth-rank damage tensor D by means of micromechanics in stead of postulating D and $\dot{D}$ heuristically. This is precisely the motivation of the following development.

II.3. Microcrack-induced inelastic strains and overall compliances

In this section, damage-induced inelastic strains and inelastic compliances are derived for an ensemble of randomly distributed fiber/matrix interfacial arc microcracks. Microcrack interactions are neglected at this stage of our development, and shall be subject of future study. According, only "Taylor's model" (not self-consistent model) is constructed. The microcrack opening displacement formulas for a single interfacial arc microcrack are based on Toya's (1974) solution. All interfacial microcracks are assumed to be entirely open. If micromechanical solutions for partially closed or entirely closed interfacial arc microcrack become available in the future, however, the present framework can be readily modified to accommodate those circumstances. The development in this section can be classified as "stationary" (or "non-process") model according to the terminology of Krajcinovic and Fanella (1986).

II.3.1. Microcrack-induced inelastic strains

In Toya's (1974) solution, the fiber (inclusion) and the matrix materials are assumed to have different linear elastic properties. Nevertheless, both fiber and matrix constituents are assumed to be homogeneous and isotropic. Toya (1974) actually provides solutions for stresses, displacements, and debonding criteria for an *open* arc crack at the bi-material interface under remote uniaxial and biaxial tension loadings. In what follows, for simplicity, we only consider the case of uniaxial tension loadings.

As remarked by Toya (1974), both stresses and displacements *oscillate* violently at the immediate regions near the crack tips. This is quite typical for the mixed boundary-value problem for interfacial cracks at bi-material boundaries. However, the extent of the oscillating regions is very small. Consequently, Toya (1974) concludes that his solutions provide a good approximation to the physical state of the body at the bi-material interface *except* in the immediate vicinity of the crack tips. Although some recent results of oscillation-free bi-material stress and displacement analyses were reported in several technical symposiums and journals (see, e.g., Qu and Bassani (1989a, 1989b), Bassani and Qu (1989)), they were derived for line (straight) microcracks at the interface of two dissimilar semi-infinite materials, not valid in our arc crack problem. Therefore, Toya's solution is adopted in the present work.

The global (unprimed) and local (primed) Cartesian coordinate systems as well as the local polar coordinate system (at a typical arc point) are shown in Figure 1. In particular, α denotes the

half-angle expanded by an arc microcrack, a denotes the radius of the fiber (inclusion), ϕ denotes the angle between the x'-axis and y-axis, and ψ ($= \pi/2 - \phi$) signifies the angle between the y-axis and y'-axis. The uniaxial tension p is applied in the y-axis direction. Counterclockwise direction is taken as positive, and θ is measured from the x'-axis. In addition, $\mathbf{n}'$ and (u'_r, u'_θ) represent the outward unit normal vector and the polar coordinates at a typical point along the arc, respectively. The expressions for u'_r and u'_θ under remote uniaxial tension are given by Eq. (3.57) in Toya (1974) by means of a complex variable form. Note that the real part is u'_r and the imaginary part is u'_θ. Let us first transform the local polar coordinates at a typical arc point to the local Cartesian coordinate defined at the *mid-point* of the arc:

$$u'_x = u'_r \cos\theta - u'_\theta \sin\theta \tag{9a}$$

$$u'_y = u'_r \sin\theta + u'_\theta \cos\theta \tag{9b}$$

Furthermore, the Cartesian components of the unit outward normal vector at a typical arc point are:

$$n'_x = \cos\theta \quad ; \quad n'_x = \cos\theta \tag{10}$$

Since the present work is concerned with the mechanical behavior of interfacial microcrack-weakened uniaxially reinforced brittle composites, it is appropriate to focus on the case of *plane strain* (orthogonal to the fiber direction). The virgin brittle composite material under consideration is actually transversely isotropic. Thus, in a plane strain framework, the virgin composite material is isotropic. However, if the composite contains an ensemble of microcracks, it may become anisotropic, depending on the microcrack sizes and orientations. By the standard definition of Cartesian strain tensor, the inelastic plane strain components (in Voigt's notation) due to a *single* (k-th) arc microcrack take the form:

$$\epsilon_1^{*(k)'} \equiv \epsilon_{xx}^{*(k)'} = \frac{a}{A} \int_{-\alpha}^{\alpha} u'_x \cos\theta \, d\theta = \frac{a}{A} \int_{-\alpha}^{\alpha} (u'_r \cos^2\theta - u'_\theta \sin\theta \cos\theta) \, d\theta \tag{11}$$

$$\epsilon_2^{*(k)'} \equiv \epsilon_{yy}^{*(k)'} = \frac{a}{A} \int_{-\alpha}^{\alpha} u'_y \sin\theta \, d\theta = \frac{a}{A} \int_{-\alpha}^{\alpha} (u'_r \sin^2\theta + u'_\theta \sin\theta \cos\theta) \, d\theta \tag{12}$$

$$\epsilon_6^{*(k)'} \equiv 2\epsilon_{xy}^{*(k)'} = \frac{a}{A} \int_{-\alpha}^{\alpha} (u'_x \sin\theta + u'_y \cos\theta) \, d\theta = \frac{a}{A} \int_{-\alpha}^{\alpha} (u'_r \sin 2\theta - u'_\theta \cos 2\theta) \, d\theta \tag{13}$$

where A is the surface area of a representative volume element in two-dimension.

In the above equations, it is implicitly assumed that the k-th arc microcrack is entirely *open*. That is, the radial crack opening displacement u'_r is always positive. Therefore, there exist some

restrictions on the arc microcrack size 2α and the orientation ϕ; see Toya (1974) for further remarks. For example, in the case of the epoxy matrix (shear modulus $\mu_1 = 346$ KSI or 2.39 GN/m^2, Poisson's ratio $\eta_1 = 0.35$) and glass fiber (shear modulus $\mu_2 = 6410$ KSI or 44.2 GN/m^2, Poisson's ratio $\eta_1 = 0.22$) composite material, the range of "entirely open" arc microcracks is approximately defined by:

$$|\phi| + \alpha \leq 65° \tag{14}$$

See Fig. 2 in Toya (1974) for more information regarding allowable (ϕ, α) region.

The inelastic strains due to an ensemble of non-interacting arc microcracks can be evaluated by performing the following integration:

$$\epsilon_i^* = N \int_\Omega g_{ji}^{(k)} \epsilon_j^{*(k)'} \, P(\phi, \alpha) \, d\Omega \tag{15}$$

where N is the number of open (active) arc microcracks; $i, j = 1, 2, 6$; $P(\phi, \alpha)$ is a joint probability density function of arc microcrack orientations and sizes; Ω is the domain of all open (active) microcracks, and $g_{ji}^{(k)}$ is the component of the following local-global transformation matrix (Horii and Nemat-Nasser (1983))

$$[\mathbf{g}^{(k)}] = \begin{bmatrix} \cos^2 \psi & \sin^2 \psi & \sin 2\psi \\ \sin^2 \psi & \cos^2 \psi & -\sin 2\psi \\ -\frac{1}{2}\sin 2\psi & \frac{1}{2}\sin 2\psi & \cos 2\psi \end{bmatrix} \tag{16}$$

Eq. (15) can be numerically computed by double Gauss quadrature, as will be discussed in Sec. II.5.

The total strain components can be obtained by adding ϵ_i^* to the elastic contributions ϵ_i^e, with ϵ_i^e expressed as

$$\epsilon_i^e = S_{ij}^o \, \sigma_j \tag{17}$$

Remark 3.1. In the case of *biaxial* tension loadings, ϵ^* can be obtained by the same procedure as above. The only modification required is to use Eq. (3.43) (not Eq. (3.57)) in Toya (1974) when integrating arc crack opening displacements. ∎

II.3.2. Overall elastic-damage compliances

To derive the damage-induced inelastic compliance matrix $\mathbf{S}^*$, Eqs. (11)–(13) must be modified. The key step is to construct the inelastic strain-stress relationship ($\epsilon^{*(k)'}$ vs. σ') in *local*

Cartesian coordinates. However, this local relationship is not readily available from (3.57) in Toya (1974) since crack opening displacements are related to *global* tension stress p instead of *local* stress field in Toya's work. The local stresses can be easily obtained as follows

$$\sigma_1' \equiv \sigma_{xx}' = p \, \cos^2 \phi \tag{18}$$

$$\sigma_2' \equiv \sigma_{yy}' = p \, \sin^2 \phi \tag{19}$$

$$\sigma_6' \equiv \sigma_{xy}' = \frac{p}{2} \, \sin 2\phi \tag{20}$$

After a lengthy but straightforward derivation, Eqs. (11)–(13) (due to a single arc microcrack only) can be recast as

$$\epsilon_1^{*(k)'} = \frac{a}{A} \left\{ \sum_i \left[\int_{-\alpha}^{\alpha} (u'_{ri} \cos^2 \theta - u'_{\theta i} \sin \theta \cos \theta) \, d\theta \right] \sigma_i' \right\} \tag{21}$$

$$\epsilon_2^{*(k)'} = \frac{a}{A} \left\{ \sum_i \left[\int_{-\alpha}^{\alpha} (u'_{ri} \sin^2 \theta + u'_{\theta i} \sin \theta \cos \theta) \, d\theta \right] \sigma_i' \right\} \tag{22}$$

$$\epsilon_6^{*(k)'} = \frac{a}{A} \left\{ \sum_i \left[\int_{-\alpha}^{\alpha} (u'_{ri} \sin 2\theta - u'_{\theta i} \cos 2\theta) \, d\theta \right] \sigma_i' \right\} \tag{23}$$

where the summation is for $i = 1, 2, 6$, and the expressions for u'_{ri} and $u'_{\theta i}$ are

$$
\begin{aligned}
u'_{r1} = &-A_1 a \left[\sin \tfrac{1}{2}(\alpha - \theta) \sin \tfrac{1}{2}(\alpha + \theta) \right]^{\frac{1}{2}} e^{\lambda(\pi - \alpha)} \times \\
&\times \left\{ \left[\frac{1 - (\cos \alpha + 2\lambda \sin \alpha)e^{2\lambda(\pi - \alpha)} + (1 - k)(1 + 4\lambda^2) \sin^2 \alpha}{2 - k - k(\cos \alpha + 2\lambda \sin \alpha)e^{2\lambda(\pi - \alpha)}} - \frac{1}{k} - \right. \right. \\
&\left. - \frac{2(1 - k)}{k} e^{2\lambda(\alpha - \pi)} \cos \theta \right] \cos \left(\tfrac{1}{2}\theta - \lambda \ln \left[\frac{\sin \tfrac{1}{2}(\alpha - \theta)}{\sin \tfrac{1}{2}(\alpha + \theta)} \right] \right) + \\
&\left. + \left[\frac{2(1 - k)}{k} e^{2\lambda(\alpha - \pi)} \sin \theta \sin \left(\tfrac{1}{2}\theta - \lambda \ln \left[\frac{\sin \tfrac{1}{2}(\alpha - \theta)}{\sin \tfrac{1}{2}(\alpha + \theta)} \right] \right) \right] \right\}
\end{aligned} \tag{24}
$$

$$
\begin{aligned}
u'_{\theta 1} = &-A_1 a \left[\sin \tfrac{1}{2}(\alpha - \theta) \sin \tfrac{1}{2}(\alpha + \theta) \right]^{\frac{1}{2}} e^{\lambda(\pi - \alpha)} \times \\
&\times \left\{ - \left[\frac{1 - (\cos \alpha + 2\lambda \sin \alpha)e^{2\lambda(\pi - \alpha)} + (1 - k)(1 + 4\lambda^2) \sin^2 \alpha}{2 - k - k(\cos \alpha + 2\lambda \sin \alpha)e^{2\lambda(\pi - \alpha)}} - \frac{1}{k} - \right. \right. \\
&\left. - \frac{2(1 - k)}{k} e^{2\lambda(\alpha - \pi)} \cos \theta \right] \sin \left(\tfrac{1}{2}\theta - \lambda \ln \left[\frac{\sin \tfrac{1}{2}(\alpha - \theta)}{\sin \tfrac{1}{2}(\alpha + \theta)} \right] \right) + \\
&\left. + \left[\frac{2(1 - k)}{k} e^{2\lambda(\alpha - \pi)} \sin \theta \cos \left(\tfrac{1}{2}\theta - \lambda \ln \left[\frac{\sin \tfrac{1}{2}(\alpha - \theta)}{\sin \tfrac{1}{2}(\alpha + \theta)} \right] \right) \right] \right\}
\end{aligned} \tag{25}
$$

$$u'_{r2} = -A_1 a \left[\sin \tfrac{1}{2}(\alpha - \theta) \sin \tfrac{1}{2}(\alpha + \theta) \right]^{\frac{1}{2}} e^{\lambda(\pi - \alpha)} \times$$

$$\times \left\{ \left[\frac{1 - (\cos \alpha + 2\lambda \sin \alpha) e^{2\lambda(\pi - \alpha)} - (1 - k)(1 + 4\lambda^2) \sin^2 \alpha}{2 - k - k(\cos \alpha + 2\lambda \sin \alpha) e^{2\lambda(\pi - \alpha)}} - \frac{1}{k} + \right. \right.$$

$$\left. + \frac{2(1 - k)}{k} e^{2\lambda(\alpha - \pi)} \cos \theta \right] \cos \left(\tfrac{1}{2}\theta - \lambda \ln \left[\frac{\sin \tfrac{1}{2}(\alpha - \theta)}{\sin \tfrac{1}{2}(\alpha + \theta)} \right] \right) -$$

$$\left. - \left[\frac{2(1 - k)}{k} e^{2\lambda(\alpha - \pi)} \sin \theta \sin \left(\tfrac{1}{2}\theta - \lambda \ln \left[\frac{\sin \tfrac{1}{2}(\alpha - \theta)}{\sin \tfrac{1}{2}(\alpha + \theta)} \right] \right) \right] \right\} \tag{26}$$

$$u'_{\theta 2} = -A_1 a \left[\sin \tfrac{1}{2}(\alpha - \theta) \sin \tfrac{1}{2}(\alpha + \theta) \right]^{\frac{1}{2}} e^{\lambda(\pi - \alpha)} \times$$

$$\times \left\{ - \left[\frac{1 - (\cos \alpha + 2\lambda \sin \alpha) e^{2\lambda(\pi - \alpha)} - (1 - k)(1 + 4\lambda^2) \sin^2 \alpha}{2 - k - k(\cos \alpha + 2\lambda \sin \alpha) e^{2\lambda(\pi - \alpha)}} - \frac{1}{k} + \right. \right.$$

$$\left. + \frac{2(1 - k)}{k} e^{2\lambda(\alpha - \pi)} \cos \theta \right] \sin \left(\tfrac{1}{2}\theta - \lambda \ln \left[\frac{\sin \tfrac{1}{2}(\alpha - \theta)}{\sin \tfrac{1}{2}(\alpha + \theta)} \right] \right) -$$

$$\left. - \left[\frac{2(1 - k)}{k} e^{2\lambda(\alpha - \pi)} \sin \theta \cos \left(\tfrac{1}{2}\theta - \lambda \ln \left[\frac{\sin \tfrac{1}{2}(\alpha - \theta)}{\sin \tfrac{1}{2}(\alpha + \theta)} \right] \right) \right] \right\} \tag{27}$$

$$u'_{r6} = -2A_1 a \left[\sin \tfrac{1}{2}(\alpha - \theta) \sin \tfrac{1}{2}(\alpha + \theta) \right]^{\frac{1}{2}} e^{\lambda(\pi - \alpha)} \times$$

$$\times \left\{ - \frac{2(1 - k)}{k} e^{2\lambda(\alpha - \pi)} \sin \theta \cos \left(\tfrac{1}{2}\theta - \lambda \ln \left[\frac{\sin \tfrac{1}{2}(\alpha - \theta)}{\sin \tfrac{1}{2}(\alpha + \theta)} \right] \right) - \right.$$

$$- \left[\frac{(1 - k)(1 + 4\lambda^2) \sin^2 \alpha}{k[1 + (\cos \alpha + 2\lambda \sin \alpha) e^{2\lambda(\pi - \alpha)}]} - \frac{2(1 - k)}{k} e^{2\lambda(\alpha - \pi)} \cos \theta \right] \times \tag{28}$$

$$\left. \times \sin \left(\tfrac{1}{2}\theta - \lambda \ln \left[\frac{\sin \tfrac{1}{2}(\alpha - \theta)}{\sin \tfrac{1}{2}(\alpha + \theta)} \right] \right) \right\}$$

$$u'_{\theta 6} = -2A_1 a \left[\sin \tfrac{1}{2}(\alpha - \theta) \sin \tfrac{1}{2}(\alpha + \theta) \right]^{\frac{1}{2}} e^{\lambda(\pi - \alpha)} \times$$

$$\times \left\{ \frac{2(1 - k)}{k} e^{2\lambda(\alpha - \pi)} \sin \theta \sin \left(\tfrac{1}{2}\theta - \lambda \ln \left[\frac{\sin \tfrac{1}{2}(\alpha - \theta)}{\sin \tfrac{1}{2}(\alpha + \theta)} \right] \right) - \right.$$

$$- \left[\frac{(1 - k)(1 + 4\lambda^2) \sin^2 \alpha}{k[1 + (\cos \alpha + 2\lambda \sin \alpha) e^{2\lambda(\pi - \alpha)}]} - \frac{2(1 - k)}{k} e^{2\lambda(\alpha - \pi)} \cos \theta \right] \times \tag{29}$$

$$\left. \times \cos \left(\tfrac{1}{2}\theta - \lambda \ln \left[\frac{\sin \tfrac{1}{2}(\alpha - \theta)}{\sin \tfrac{1}{2}(\alpha + \theta)} \right] \right) \right\}$$

In the above equations, k, λ, and A_1 are given material properties (related to elastic shear moduli and Poisson's ratios of fiber and matrix), and are defined in (3.9), (3.3), (3.39) in Toya (1974). For convenience, they are given in what follows:

$$k \equiv \frac{\beta}{1 + \nu} \quad ; \quad \beta \equiv \frac{\mu_1(1 + \kappa_2)}{(\mu_1 + \kappa_1 \mu_2)} \quad ; \quad \nu \equiv \frac{(\mu_2 + \kappa_2 \mu_1)}{(\mu_1 + \kappa_1 \mu_2)} \tag{30}$$

$$\kappa_1 \equiv 3 - 4\eta_1 \quad ; \quad \kappa_2 \equiv 3 - 4\eta_2 \tag{31}$$

$$\lambda \equiv -\frac{\ln \nu}{2\pi} \qquad (32)$$

$$A_1 \equiv \frac{k}{4} \left[\frac{1+\kappa_1}{\mu_1} + \frac{1+\kappa_2}{\mu_2} \right] \qquad (33)$$

Therefore, Eqs. (21)–(23) can be rewritten as $(i, j = 1, 2, 6)$

$$\epsilon_i^{*(k)'} = S_{ij}^{*(k)'} \sigma_j' \qquad (34)$$

where $S_{ij}^{*(k)'}$ is the local two-dimensional microcrack-induced inelastic compliance component. In particular, the inelastic compliance matrix components take the form:

$$S_{1i}^{*(k)'} = \frac{a}{A} \int_{-\alpha}^{\alpha} (u'_{ri} \cos^2 \theta - u'_{\theta i} \sin \theta \cos \theta) \, d\theta \qquad (35)$$

$$S_{2i}^{*(k)'} = \frac{a}{A} \int_{-\alpha}^{o} (u'_{ri} \sin^2 \theta + u'_{\theta i} \sin \theta \cos \theta) \, d\theta \qquad (36)$$

$$S_{6i}^{*(k)'} = \frac{a}{A} \int_{-\alpha}^{\alpha} (u'_{ri} \sin 2\theta - u'_{\theta i} \cos 2\theta) \, d\theta \qquad (37)$$

It is noticed that the inelastic compliance matrix $\mathbf{S}^{*(k)'}$ due to a single arc microcrack is in fact *non-symmetric*; i.e., $S_{ij}^{*(k)'} \neq S_{ji}^{*(k)'}$ for $i \neq j$. The integrals in Eqs. (35)-(37) can be effectively evaluated by means of numerical integration procedures; see Sec. II.5 for details. In addition, in terms of global Cartesian coordinates, $S_{ij}^{*(k)'}$ can be rephrased as

$$S_{ij}^{*(k)} = g_{mi}^{(k)} g_{nj}^{(k)} S_{mn}^{*(k)'} \qquad (38)$$

Consequently, the total inelastic compliance $\mathbf{S}^*$ due to an ensemble of randomly oriented interfacial arc microcracks can be expressed as

$$S_{ij}^* = N \int_{\Omega} S_{ij}^{*(k)} P(\phi, \alpha) \, d\Omega \qquad (39)$$

From Eqs. (35)–(37), it is observed that $\mathbf{S}^*$ is actually a tensorial function of the *mean* "arc microcrack density parameter" $< \omega >$, with $\omega \equiv N(a\alpha)^2/A$. Finally, the overall elastic-damage compliance $\mathbf{S}$ is obtained simply by writing

$$\mathbf{S} = \mathbf{S}^o + \mathbf{S}^* \qquad (40)$$

Therefore, the inelastic compliances and fourth-rank damage tensors of interfacial microcrack-weakened brittle composites can actually be derived from micromechanics, instead of postulating them arbitrarily or heuristically.

II.4. Microcrack kinetic equations

It is characteristic that brittle composite solids have some pre-existing arc microcracks along the fiber/matrix interfaces even before specimens are first loaded. Some of these initial microcracks may grow (propagate) later upon application of adequate loads. In this section, we transform the stationary ("non-process") damage model presented in Sec. II.3 into a "process" damage model so that the model possesses a constitutive *predictive* capability. That is, "cleavage 1" (pre-existing) microcrack *growth* and the *evolution* of S (or S*) are considered based on micromechanical considerations. The importance of micromechanically-based microcrack growth relations were also recognized by Weitsman (1988). It is recalled that although some existing phenomenological damage models are in principle capable of providing damage evolution equations for composites, they may require some 100 (or even more) fitted "material constants" in the microcrack evolution laws.

The present work is *not* restricted to monotonically increasing loads. In fact, loading/unloading sequences can be easily accommodated by computing and checking whether there is *undergoing* microcrack growth (excluding those previously propagating and currently arrested microcracks). If there is no (ϕ, α) region in which *additional* microcrack growth is now taking place, then the current incremental load step is in an *unloading* state. Therefore, "active microcrack growth" is the valid current loading condition, regardless of prior existence of certain (ϕ, α) regions where microcracks previously experienced growth. Moreover, the damage-induced inelastic compliance S* takes the form:

$$S^* = S^*_u + S^*_i + S^*_f \qquad (41)$$

where S^*_u = the compliance contribution from undergoing microcrack growth, S^*_i = the contribution from stationary microcracks having *initial* sizes, and S^*_f = the contribution from arrested microcrack growth due to *previous* microcrack growth. In particular, if $S^*_u = 0$, then the current load level p is not high enough to cause further damage, and therefore all existing microcracks are arrested. Finally, S* is added to S° to obtain the overall compliance S.

II.4.1. Interfacial microcrack fracture criterion

The mixed mode bi-material fracture criterion was provided in Eq. (4.8) in Toya (1974) for a non-interacting, entirely open arc microcrack along the fiber/matrix interface under uniaxial tension. It is implicitly assumed that the bonding strength between the fiber and matrix is sufficiently

small compared with the fracture toughness of the matrix, so that an initial (existing) arc micro-crack will always grow along the bi-material interface. Thus, microcrack kinking into the matrix is not considered here. Toya's bi-material, local stress fracture criterion for a *tip* of an arc microcrack under uniaxial tension reads:

$$\frac{1}{16}p^2 ka A_1 (1 + 4\lambda^2)\pi N_0 \bar{N}_0 \sin \alpha \; e^{2\lambda(\pi - \alpha)} = 2\gamma^{if} \tag{42}$$

where γ^{if} is the specific surface tension energy of the interface (i.e., critical energy release rate), and N_0 together with its complex conjugate $\bar{N}_0$ are functions of ϕ, α, and elastic material properties (see Eq. (4.9) in Toya (1974)). Eq. (42) is only valid for an open microcrack; i.e., $u'_r \geq 0$ is required for any θ value along an arc microcrack. In addition, one tip of a microcrack may reach the fracture criterion (4.2) before the other tip does. Hence, one tip may be propagating while the other tip is arrested.

When the energy release rate reaches its critical value (or when tension reaches a critical value p_{cr}), an arc microcrack may grow in a stable or unstable fashion, according to Fig. 3 in Toya (1974). Within a limited range of the (ϕ, α) region, Eq. (42) may have two solutions for α and ϕ. Thus, one tip or both tips may actually grow in a *stable* manner. This implies that the *final* microcrack size α_f and orientation ϕ_f can be analytically obtained. However, for other ranges of the (ϕ, α) region, there is only one solution for Eq. (42). Therefore, an arc microcrack may grow in an *unstable* manner outside the limited range of the two-solution (ϕ, α) domain. Moreover, with further increase of the tensile stress p ($> p_{cr}$), even an originally stable arc microcrack will grow continuously in an unstable manner.

In the case of many randomly distributed open arc microcracks, Eq. (42) is systematically checked for every permissible microcrack orientation ϕ and size α to numerically determine the domains of "growth zone" and "stationary zone" for a given tensile stress p and known elastic material properties. Because of the preferred microcrack growth orientations, the overall material compliances become even more anisotropic. These issues will be further addressed in Sec. II.5.

It is worth noting that the interfacial fracture criterion for a tip of an arc microcrack under *biaxial* tension field is also available from Eq. (4.7) in Toya (1974). Therefore, the regions of microcrack "growth zone" can be numerically identified, too.

II.4.2. Microcrack growth – a process model

As previously mentioned, it is presumed that all arc microcracks are entirely open and no microcrack kinking (into matrix) is considered. These assumptions are made because solutions for mixed boundary-value problems are not yet available for partially closed, entirely closed (mode II frictional sliding), or kinked arc microcracks. When these solutions do become available, the proposed process model must be properly modified.

In addition, it is recalled that the region of "stable microcrack growth" (from an initial microcrack orientation and size (ϕ_i, α_i) to a final stable configuration (ϕ_f, α_f) is quite limited and is only applicable at certain critical stress level, according to Fig. 3 in Toya (1974). Therefore, it appears rational and practical to simplify the distributed microcrack growth kinetics as follows. If *one* tip of an arc microcrack reaches or exceeds the critical surface energy required to initiate microcrack growth, then *both* tips of the arc microcrack may grow continuously (generally in a *non-symmetric* fashion) until the half-angle size reaches an α_f and the central crack "orientation" $\phi_f \approx 0^\circ$ (i.e., approximately aligned with the applied tensile loading direction). In the case of the aforementioned epoxy-glass composites, $\alpha_f = 65^\circ$ is a reasonable choice since it is the maximum allowable half-angle size for an arc microcrack to remain *open*. It is noted that the arc-microcrack central orientation indeed will change due to crack growth; see Toya (1974) for more discussions. Therefore, according to the proposed simplified treatment, an arc microcrack may either be stable (no growth, with original geometry) or unstable (with $\alpha_f = 65^\circ$ and $\phi_f = 0^\circ$). Clearly, damage-induced anisotropy is bound to be a natural consequence.

In the case of randomly distributed arc microcracks, Eq. (4.2) should be used to numerically (iteratively) define the *bounds* of (ϕ, α) regions undergoing microcrack growth under a *particular* tensile stress p, a given interface toughness γ^{if} and a given initial microcrack geometry. For simplicity, in what follows, we assume that all arc microcracks are of *equal* initial size α_i and are such oriented that $|\phi| + \alpha_i \leq 65^\circ$ (opening) always holds. Thus, for a specified interface toughness γ^{if}, one can perform numerical iteration to obtain the minimum tension stress p_{cr} required to cause the first arc microcracks to propagate. The corresponding initial central microcrack orientations are denoted by $\pm\phi_{cr}$. When p is greater than p_{cr}, the unstable microcrack domains will increase accordingly.

The proposed microcrack growth kinetic sequence proceeds as follows.

(1) As $p < p_{cr}$, all arc microcracks are stable and of initial size α_i. Due to preferred initial microcrack orientations to ensure opening, the overall stress-strain response is anisotropic even if virgin composites are isotropic (in plane strain). Although the overall response is linear and reversible under the present stress level p, the material state is really *elastic-damage* (inelastic). In fact, the current elastic-damage compliance S is greater than the virgin undamaged elastic compliance S^o.

(2) As $p = p_{cr}$, those microcracks with central orientations ϕ_{cr} become unstable, and increase their lengths to $\alpha_f = 65°$ as well as change their orientations to $\phi_f = 0$. The contributions from partially closed and entirely closed portions are neglected here.

(3) As $p \equiv p_1 > p_{cr}$, the unstable microcrack growth regions Ω_{act} increase. Therefore, some microcracks in specific orientation domains $(-\phi_l, -\phi_h)$ and (ϕ_h, ϕ_l) become activated and increase in size to $\alpha_f = 65°$ as well as change their orientations to $\phi_f = 0$. The material behaves anisotropically and the elastic-damage compliance increases. It is noted that ϕ_l and ϕ_h values depend on p_1, p_{cr}, α_i and γ^{ij}, and can be obtained by numerical iteration. The compliance contributions S_u^* and S_i^* in Eq. (41) can be computed (integrated) through Eq. (35) and (39):

$$S_u^* = N \int_{\Omega_{act}} \mathbf{g}^{(k)T} \mathbf{S}^{*(k)'}(\phi, \alpha_f) \mathbf{g}^{(k)} P(\phi) d\phi \tag{43}$$

$$S_i^* = N \int_{\Omega_{in}} \mathbf{g}^{(k)T} \mathbf{S}^{*(k)'}(\phi, \alpha_i) \mathbf{g}^{(k)} P(\phi) d\phi \tag{44}$$

where $P(\phi)$ is the assumed probability density function of microcrack orientation and Ω_{in} is the stable (no growth) domain.

(4) As $p_{cr} < p < p_1$, the *unloading* case is taking place. There is no further microcrack growth because the apparent "active orientation fans" shrink. Therefore, $S_u^* = 0$. It is emphasized that the *actual* "orientation fans" (featuring α_f size) does *not* reduce owing to the *irreversible* nature of damage. Hence, the elastic-damage compliance remains its previous value.

(5) As $p > p_1$, more microcracks are activated. The "unstable growth" domains can be computed similar to step (3). However, S_u^* in step (3) should be replace by the sum of S_u^* and S_j^* in this step.

(6) At some higher stress level $p = p_c$, the energy release rate reaches the critical value of the matrix energy barrier. Therefore, microcracks having size α_f will resume to propagate (kink) into the matrix, and eventually lead to final failure.

As was commented by Sumarac and Krajcinovic (1987), the above scheme implicitly assumes that ultimate failure prefers "runaway cracks" in comparison with "localization modes". Some numerical simulations will be given in Sec. II.5.

II.5. Computational algorithms and numerical simulations

In this section, computational integration algorithms are given for the proposed micromechanical damage model. Furthermore, a number of uniaxial tension numerical simulations are presented. In the absence of suitable *plane strain* experimental data at this stage, however, actual experimental validation is not included here. Experimental verification of the proposed models should be performed in the future once they become available. Nonetheless, the presented numerical simulations demonstrate the potential capability of the proposed damage model, **without** resorting to any fitted "material parameters" commonly utilized in phenomenological continuum damage models.

II.5.1. Computational integration algorithms

The proposed micromechanical damage model does not include microcrack interaction effects, and therefore falls into the category of "Taylor's model". That is, one employs the undamaged elastic material properties (not overall elastic-damage moduli) to compute microcrack opening displacements. Thus, the proposed process model does not require the use of an iterative scheme when computing the single microcrack-induced inelastic compliance $S^{*(k)}$ (see Eqs. (35)–(38)). In order to determine the *bounds* of unstable crack growth regions under a particular applied tension stress, nevertheless, one needs to perform numerical iterations, as commented in Sec. II.4.2. The computational schemes involved in solving the proposed stress-controlled micromechanical damage models proceed as follows. It is assumed that all initial arc microcracks are of equal size α_i and open.

(1) For a given load level p, compute "unstable orientation bounds" $(-\phi_l , -\phi_h)$ and (ϕ_h , ϕ_l) according to the fracture criterion Eq. (42). For example, one may use the bi-section method to locate the very *first* unstable microcrack orientations $\pm\phi_{cr}$, and later the *bounds* defining the crack growth domains. These "unstable orientation bounds" should be stored as *history variables* since they are irreversible.

(2) Obtain the individual and total damage-induced inelastic compliance $S^{*(k)}$ and S^* by actually evaluating the double integral involved in Eq. (39) (in conjunction with Eqs. (35)–(38)). Note that stable microcracks have the size α_i while unstable microcracks reach the size α_f (= 65° in our case). Numerical integration of Eq. (39) can be efficiently performed by two separate "Gauss quadratures" – one for stable and the other for unstable regions. In particular, one needs

to integrate the compliance contributions from *every* θ angle-coordinate along an arc, and from *every* open arc microcrack. at different orientations. Here, we use Gauss quadrature rule with 60 integration points for each stable or unstable region.

(3) Obtain new overall elastic-damage compliance S by adding S^* to S^o.

(4) Apply the next load p and go to step (1).

II.5.2. Some uniaxial tension tests

A number of mixed-mode plane strain uniaxial tension tests are considered in this section for various different fiber sizes a, microcrack concentrations ω ($\equiv N(a\alpha)^2/A$), and initial microcrack half-angle sizes α. Both stationary and process (kinetic) damage models are employed to predict the continuous changes in overall elastic-damage compliances and stress-strain responses based on micromechanics. The composite material considered here is epoxy for matrix and glass for fiber. Both epoxy and fibers are isotropic and linear elastic. The shear modulus and Poisson's ratio of the epoxy matrix are μ_1 = 346 KSI (2.39 GN/m^2) and η_1 = 0.35, respectively. In addition, the shear modulus and Poisson's ratio of the glass fibers are μ_2 = 6410 KSI (44.2 GN/m^2) and η_2 = 0.22, respectively. The composite volume ratio of the matrix and fiber constituents are 0.8 and 0.2, respectively. The (plane strain) overall composite Young's modulus and Poisson's ratio is found to be E = 1151 KSI (7.93 GN/m^2) and η = 0.3481, respectively, by means of the elementary rule of mixture (see, e.g., Jones (1975)). Therefore, the plane strain elastic compliance matrix takes the form: (unit = KSI^{-1})

$$[S^o] = \begin{bmatrix} 0.00076383 & -0.00040784 & 0 \\ -0.00040784 & 0.00076383 & 0 \\ 0 & 0 & 0.0023433 \end{bmatrix} \tag{45}$$

Moreover, the interfacial specific surface tension energy (fracture toughness) $2\gamma^{if}$ is taken as 0.001 Kips/in. (0.175 KN/m).

First, we examine the effects of different initial microcrack concentrations ω_i on stress-strain responses and compliances of the uniaxially reinforced epoxy-glass composite. The initial microcrack concentration parameter ω_i is increased gradually (with 256 increments) from 0 to 0.64. All microcracks are assumed to be stationary (no growth), open, and of the half-angle size α_i = 10°. In view of Fig. 2 in Toya (1974), $|\phi| + \alpha \leq 65^\circ$ is required for crack opening. Therefore, arc microcracks are assumed to be perfectly (uniformly) randomly oriented between ϕ = -55° and ϕ

$= 55°$; i.e., the probability density of orientation is $P(\phi) = 0.521$. The uniaxial tension stress is applied in the 2-direction, and the lateral direction is denoted as the 1-direction. The axial-stress (KSI) versus the axial- and lateral-strain (curves corresponding to monotonically increasing values of ω_i are displayed in Fig. 2. The elastic stress-strain response is also shown in Fig. 2 for comparison purpose. The elastic-damage compliance components S_{22} and S_{12} vs. ω_i parameter are shown in Fig. 3 and Fig. 4, respectively. It is clear that as microcrack concentration increases, the compliance components S_{22} and S_{12} increase monotonically.

Next, we perform "process model" uniaxial tension tests. Let the fiber radius be $a = 0.1$ in. and microcrack number density be $N/A = 100$. Two initial half-angle sizes of arc microcracks are considered: $\alpha_i = 10°$ and $\alpha_i = 20°$, respectively. The axial-stress vs. the axial- and lateral-strain responses are recorded in Fig. 5. It is noted that before the load p reaches a certain critical value p_{cr}, the stress-strain response is linear (stationary damage model) for either $\alpha_i = 10°$ or $\alpha_i = 20°$. After the critical values p_{cr} are reached, the overall responses then become nonlinear. Double Gauss quadrature is employed to integrate inelastic compliances and strains contributions from various microcrack orientations and sizes. For example, in the case of $\alpha_i = 10°$, it is found (by numerical iteration) that the first microcracks to become unstable (propagating) are oriented in the direction $\phi_{cr} = 5.01°$. Later, as p increases, more "orientation fans" are enclosed within the ϕ-angle bounds (obtained by numerical iteration) of microcrack growth. Therefore, more and more microcracks experience growth and finally have $\phi_f = 0°$ and $\alpha_f = 65°$. In the case of $\alpha_i = 20°$, on the other hand, it is found that $\phi_{cr} = 10.59°$. It is also observed from Fig. 5 that larger initial microcrack size $\alpha_i = 20°$ results in lower critical load level p_{cr} for microcrack growth.

Let us now fix the initial microcrack size $\alpha_i = 10°$ and vary the fiber sizes and microcrack number densities: (i) $a = 0.05$ in. and $N/A = 40$, and (ii) $a = 0.1$ in. and $N/A = 100$, respectively. The axial-stress vs. the axial- and lateral-strain responses are shown in Fig. 6. The changes in overall elastic-damage compliances S_{22}, S_{11} and S_{12} versus axial stresses are plotted in Fig. 7, 8 and 9. It is observed that S_{22} and S_{11} increase as tensile stress level p increases. However, S_{12} is negative and decreases as the stress increases; i.e., $|S_{12}|$ increases monotonically.

The above uniaxial tension tests are repeated for fixed initial microcrack size $\alpha_i = 20°$. Again, two sets of fiber sizes and microcrack number densities are considered: (i) $a = 0.05$ in. and $N/A = 40$, and (ii) $a = 0.1$ in. and $N/A = 100$. The axial-stress vs. the axial- and lateral-strain responses are shown in Fig. 10. The changes in overall elastic-damage compliances S_{22}, S_{11} and S_{12} versus

axial stresses are plotted in Fig. 11, 12 and 13. Similarly, S_{22} and S_{11} increase as tensile stress level p increases. In addition, S_{12} decreases as the stress increases.

The above numerical simulations illustrate the potential capability of the proposed micromechanical damage models to qualitatively explain and quantitatively predict the overall stress-strain behavior and compliance evolutions. Not a single fitted "material parameter" is employed in the proposed model. It is also emphasized that the numerical tests presented in this section is for "cleavage 1" damage processes. Thus, nucleation of new arc microcracks is not included. Further, partially or entirely closed arc microcracks, or microcrack kinking (into the matrix) are not incorporated into the present model. These issues will be topics of future research.

II.6. Conclusion

A micromechanical damage model is presented in this work, based on Toya's (1974) micromechanics solutions and general damage mechanics framework, for uniaxially reinforced brittle matrix fibrous composites. All microcracks are assumed to exist along the fiber/matrix interfaces, and are modeled as *arc* microcracks under "cleavage 1" plane strain deformation processes. Thermodynamic basis is rendered based on a fourth-rank damage tensor. Microcrack-induced inelastic strains and elastic-damage compliances are analytically derived based on micromechanical bi-material arc-microcrack opening displacements and probabilistic distributions of arc microcracks. It is noted that the (plane strain) overall elastic-damage compliance matrix is *non-symmetric*. Both "*stationary*" and "*process*" damage models are given in the present work. In particular, microcrack kinetic equations are given based on micromechanical fracture criterion and microstructural geometry in a representative volume (area) element. Moreover, simple computational algorithms and a number of uniaxial tension tests are presented to illustrate the potential capability of the proposed micromechanical damage model for fibrous composites. It is emphasized that the present work does not employ any arbitrary (fitted) "material constants". The proposed framework can be readily extended to account for biaxial tension loadings, as addressed in **Remark 3.1**. Issues related to microcrack interaction, closed microcracks, microcrack kinking, and microcrack nucleation mechanisms warrant further studies in the future to extend the proposed method.

II.7. References

1. ALLEN, D. H., C. E. HARRIS, AND S. E. GROVES, (1987a), "Thermomechanical Constitutive Theory for Elastic Composites with Distributed Damage. Part I: Theoretical Development", *Int. J. Solids & Struct*, Vol. 23, No. 9, pp. 1301–1318.

2. ALLEN, D. H., C. E. HARRIS, AND S. E. GROVES, (1987b), "Thermomechanical Constitutive Theory for Elastic Composites with Distributed Damage. Part II: Application to Matrix Cracking in Laminated Composites", *Int. J. Solids & Struct*, Vol. 23, No. 9, pp. 1319–1338.

3. ALLEN, D. H., C. E. HARRIS, S. E. GROVES, AND R. G. NORVELL, (1987c), "Characterization of Stiffness Loss in Crossply Laminates with Curved Matrix Cracks", *Composites '86: Recent Advances in Japan and the United States*, K. Kawata, S. Umekawa & A. Kobayashi, eds., Proc. Japan-U.S. CCM-III, Tokyo, 1986, pp. 223–229.

4. BASSANI, J. L. AND J. QU, (1989), "Finite Crack on Bimaterial and Bicrystal Interfaces", *J. Mech. Phys. Solids*, Vol. 37, No. 4, pp. 435–453.

5. BAZANT, Z., (1986), "Mechanics of Distributed Cracking", *Appl. Mech. Rev.*, Vol. 39, No. 5 pp. 675–705.

6. BUDIANSKY, B. AND R. J. O'CONELL, (1976), "Elastic Moduli of a Cracked Solid", *Int. J. Solids & Struct.*, Vol. 12, pp. 81–97.

7. CHABOCHE, J. L., (1979), "Le Concept de Contrainte Effective Applique a L'elasticite et a la Viscoplasticite en Presence d'un Endommagement Anisotrope", *Mechanical Behavior of Anisotropic Solids*, Proc. Euromech Colloque 115, June 1979, Edited by J. P. Boehler, pp. 737–760, Martinus Nijhoff.

8. CORDEBOIS, J. P. AND F. SIDOROFF, (1979), "Damage Induced Elastic Anisotropy", *Mechanical Behavior of Anisotropic Solids*, Proc. Euromech Colloque 115, June 1979, Edited by J. P. Boehler, pp. 761–774, Martinus Nijhoff.

9. CORDEBOIS, J. P. AND F. SIDOROFF, (1982), "Endommagement Anisotrope en Elasticite et Plasticite", *J. Mech. Theor. Appl.*, No. special, pp. 45–59.

10. ENGLAND, A. H., (1966), "An Arc Crack Around a Circular Elastic Inclusion", *J. Appl. Mech.*, Vol. 33, pp. 637–640.

11. FANELLA, D. AND D. KRAJCINOVIC, (1988), "A Micromechanical Model for Concrete in Compression", *Eng. Fract. Mech.*, Vol. 29, No. 1, pp. 49–66.

12. HARRIS, C. E., D. H. ALLEN, AND E. W. NOTTORF, (1987), "Damage-Induced Changes in the Poisson's Ratio of Cross-Ply Laminates: An Application of a Continuum Damage Mechanics Model for Laminated Composites", Proc. ASME Winter Annual Meeting, Dec. 13–18, Boston, pp. 17–23.

13. HASHIN, Z., (1985), "Analysis of Cracked Laminates: A Variational Approach", *Mech. of Mater.*, Vol. 4, pp. 121–136.

14. HILL, R., (1965), "A Self-Consistent Mechanics of Composite Materials", *J. Mech. Phy. Solids*, Vol. 13, pp. 213–222.

15. HORII, H. AND S. NEMAT-NASSER, (1983), "Overall Moduli of Solids with Microcracks: Load Induced Anisotropy", *J. Mech. Phys. Solids*, Vol. 31, No. 2, pp. 155–171.

16. HORII, H. AND S. NEMAT-NASSER, (1985), "Elastic Fields of Interacting Inhomogeneities", *Int. J. Solids & Struct.*, Vol. 21, No. 7, pp. 731–745.

17. JONES, R. M., (1975), *Mechanics of Composite Materials*, McGraw-Hill Book Company.

18. JU, J. W., (1989a), "On Energy-Based Coupled Elastoplastic Damage Theories: Constitutive Modeling and Computational Aspects", *Int. J. Solids & Struct.*, Vol. 25, No. 7, pp. 803–833.

19. JU, J. W., (1989b), "On Two-Dimensional Self-Consistent Micromechanical Damage Models for Brittle Solids", *Int. J. Solids & Struct.*, in press.

20. KACHANOV, L. M., (1958), "Time of the Rupture Process under Creep Conditions", *Izvestia Akademii Nauk*, USSR, Nauk 8, pp. 26–31.

21. KACHANOV, M., (1987), "Elastic Solids with Many Cracks: A Simple Method of Analysis", *Int. J. Solids & Struct.*, Vol. 23, No. 1, pp. 23–43.

22. KRAJCINOVIC, D., (1984), "Continuum Damage Mechanics", *Appl. Mech. Rev.*, Vol. 37, Jan., pp. 1–6.

23. KRAJCINOVIC, D., (1986), "Update to Continuum Damage Mechanics", *Appl. Mech. Update*, pp. 403–406.

24. KRAJCINOVIC, D., (1989), "Damage Mechanics", *Mech. of Materials*, to appear.

25. KRAJCINOVIC, D. AND D. FANELLA, (1986), "A Micromechanical Damage Model for Concrete", *Eng. Fract. Mech.*, Vol. 25, No. 5/6, pp. 585–596.

26. LAWS, N., G. J. DVORAK, AND M. HEJAZI, (1983), "Stiffness Changes in Unidirectional Composites Caused by Crack Systems", *Mech. of Mater.*, Vol. 2, pp. 123–137.

27. LEMAITRE, J. AND J. L. CHABOCHE, (1978), "Aspect Phenomenologique de la Rupture par Endommagement", *J. de Mech. Applique*, Vol. 2, pp. 317–365.

28. MURA, T., (1982), *Micromechanics of Defects in Solids*, Nijhoff Publishers, The Hague.

29. PERLMAN, A. B. AND G. C. SIH, (1967), "Elastostatic Problems of Curvilinear Cracks in Bonded Dissimilar Materials", *Int. J. Eng. Sci.*, Vol. 5, pp. 845–867.

30. PIVA, A., (1982), "Crack Along a Circular Interface Between Dissimilar Media", *Meccanica*, Vol. 17, pp. 85–90.

31. QU, J. AND J. L. BASSANI, (1989a), "Interface Cracks Between Anisotropic Elastic Solids", in Proc. *Bonding, Structure and Mechanical Properties of Metal/Ceramic Interfaces*, University of California, Santa Barbara, Jan. 1989.

32. QU, J. AND J. L. BASSANI, (1989b), "Cracks on Bimaterial and Bicrystal Interfaces", *J. Mech. Phys. Solids*, Vol. 37, No. 4, pp. 417–433.

33. RABOTNOV, I. N., (1963), "On the Equations of State for Creep", in *Progress in Applied Mechanics–The Prager Anniversary Volume*, MacMillan, New York, pp. 307–315.

34. SUMARAC, D. AND D. KRAJCINOVIC, (1987), "A Self-Consistent Model for Microcrack-Weakened Solids", *Mech. Mater.*, Vol. 6, pp. 39–52.

35. TALREJA, R., (1985a), "A Continuum Mechanics Characterization of Damage in Composite Materials", *Proc. R. Soc. London*, Vol. 399A, pp. 195–216.

36. TALREJA, R., (1985b), "Residual Stiffness Properties of Cracked Composite Laminates", *Advances in Fracture Research*, Proc. Sixth Int. Conf. Fracture, New Delhi, India, Vol. 4, pp. 3013–3019.

37. TALREJA, R., (1985c), "Transverse Cracking and Stiffness Reduction in Composite Laminates", *Composite Mater.*, Vol. 21, pp. 355–375.

38. TALREJA, R., (1986), "Stiffness Properties of Composite Laminates with Matrix cracking and Interior Delamination", *Eng. Fract. Mech.*, Vols. 5–6, pp..751–762.

39. TALREJA, R., (1987), "Modeling of Damage Development in Composites Using Internal State Variables Concepts", Proc. ASME Winter Annual Meeting, Dec. 13–18, Boston, pp. 11–16.

40. TOYA, M., (1974), "A Crack Along the Interface of a Circular Inclusion Embedded in an Infinite Solid", *J. Mech. Phys. Solids*, Vols. 22, pp.325–348.

41. WANG, A. S. D., P. C. CHOU, AND S. C. LEI, (1984), "A Stochastic Model for the Growth of Matrix Cracks in Composite Laminates", *J. Composite Mater.*, Vol. 18, May, pp. 239–254.

42. WEITSMAN, Y., (1987a), "Environmentally Induced Damage in Composites", Proc. Fifth Int. Symp. Continuum Models of Discrete Systems, A.J.M. Spencer, ed., pp. 187–192, Nottingham, U.K.

43. WEITSMAN, Y., (1987b), "Coupled Damage and Moisture-Transport in Fiber-Reinforced, Polymeric Composites", *Int. J. Solids & Struct.*, Vol. 23, No. 7, pp. 1003–1025.

44. WEITSMAN, Y., (1988), "Damage Coupled with Heat Conduction in Uniaxially Reinforced Composites", *J. Appl. Mech.*, Vol. 55, pp. 641–647.

II.8.   Figure captions

Figure 1. The local (primed) and global Cartesian coordinates, as well as the polar coordinates at a typical arc point.

Figure 2. The axial-stress vs. the axial- and lateral-strain under different microcrack concentrations ω (varying from 0 to 0.64). Note that $\omega \equiv N(a\alpha)^2/A$. The dotted lines are the undamaged elastic stress-strain responses.

Figure 3. The overall compliance S_{22} vs. microcrack concentration ω for various stationary damage model simulations. The dotted line is the elastic response.

Figure 4. The overall compliance S_{12} vs. ω for various stationary damage model simulations.

Figure 5. The axial-stress vs. the axial- and lateral-strain for two different initial microcrack sizes: $\alpha_i = 10°$ and $\alpha_i = 20°$. Note that $a = 0.1$ in. and $N/A = 100$. These are "process model" simulations.

Figure 6. The axial-stress vs. the axial- and lateral-strain for two different fiber sizes and microcrack number densities. Note that $\alpha_i = 10°$.

Figure 7. The overall compliance S_{22} vs. the axial stress p for two different sets of a and N/A values. Note that $\alpha_i = 10°$.

Figure 8. The overall compliance S_{11} vs. the axial stress p for two different sets of a and N/A values. Note that $\alpha_i = 10°$.

Figure 9. The overall compliance S_{12} vs. the axial stress p for two different sets of a and N/A values. Note that $\alpha_i = 10°$.

Figure 10. The axial-stress vs. the axial- and lateral-strain for two different fiber sizes and microcrack number densities. Note that $\alpha_i = 20°$.

Figure 11. The overall compliance S_{22} vs. the axial stress p for two different sets of a and N/A values. Note that $\alpha_i = 20°$.

Figure 12. The overall compliance S_{11} vs. the axial stress p for two different sets of a and N/A values. Note that $\alpha_i = 20°$.

Figure 13. The overall compliance S_{12} vs. the axial stress p for two different sets of a and N/A values. Note that $\alpha_i = 20°$.
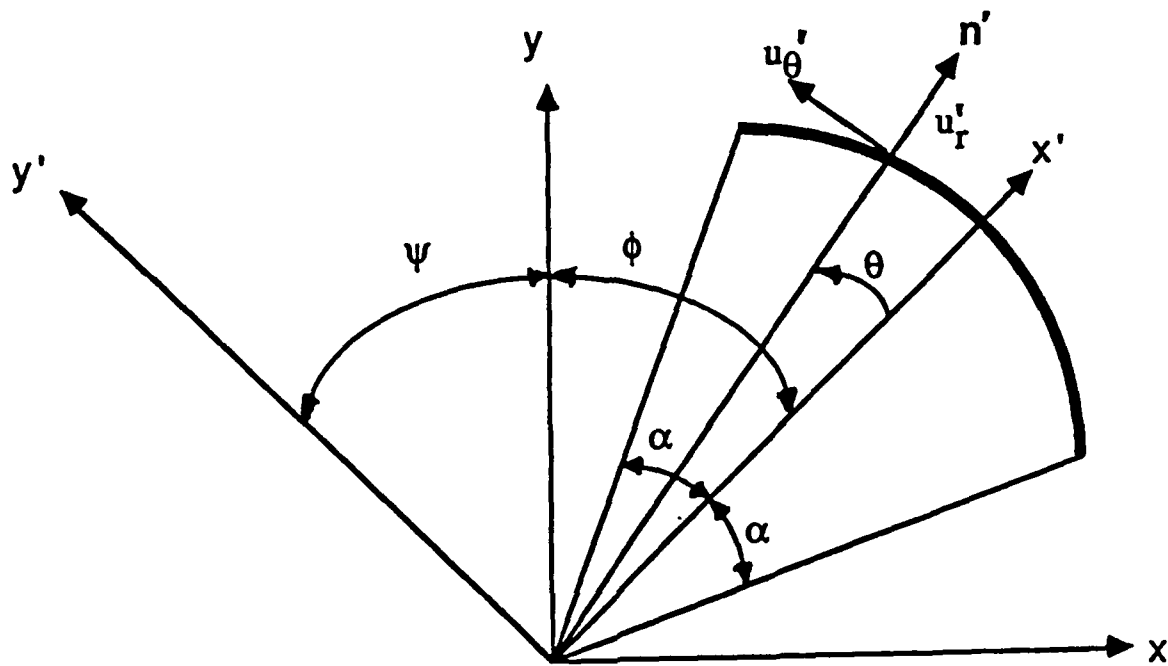
Figure 1. The local (primed) and global Cartesian coordinates, as well as the polar coordinates at a typical arc point.

Figure 2. The axial-stress vs. the axial- and lateral-strain under different microcrack concentrations ω (varying from 0 to 0.64). Note that $\omega \equiv N(a\alpha)^2/A$. The dotted lines are the undamaged elastic stress-strain responses.

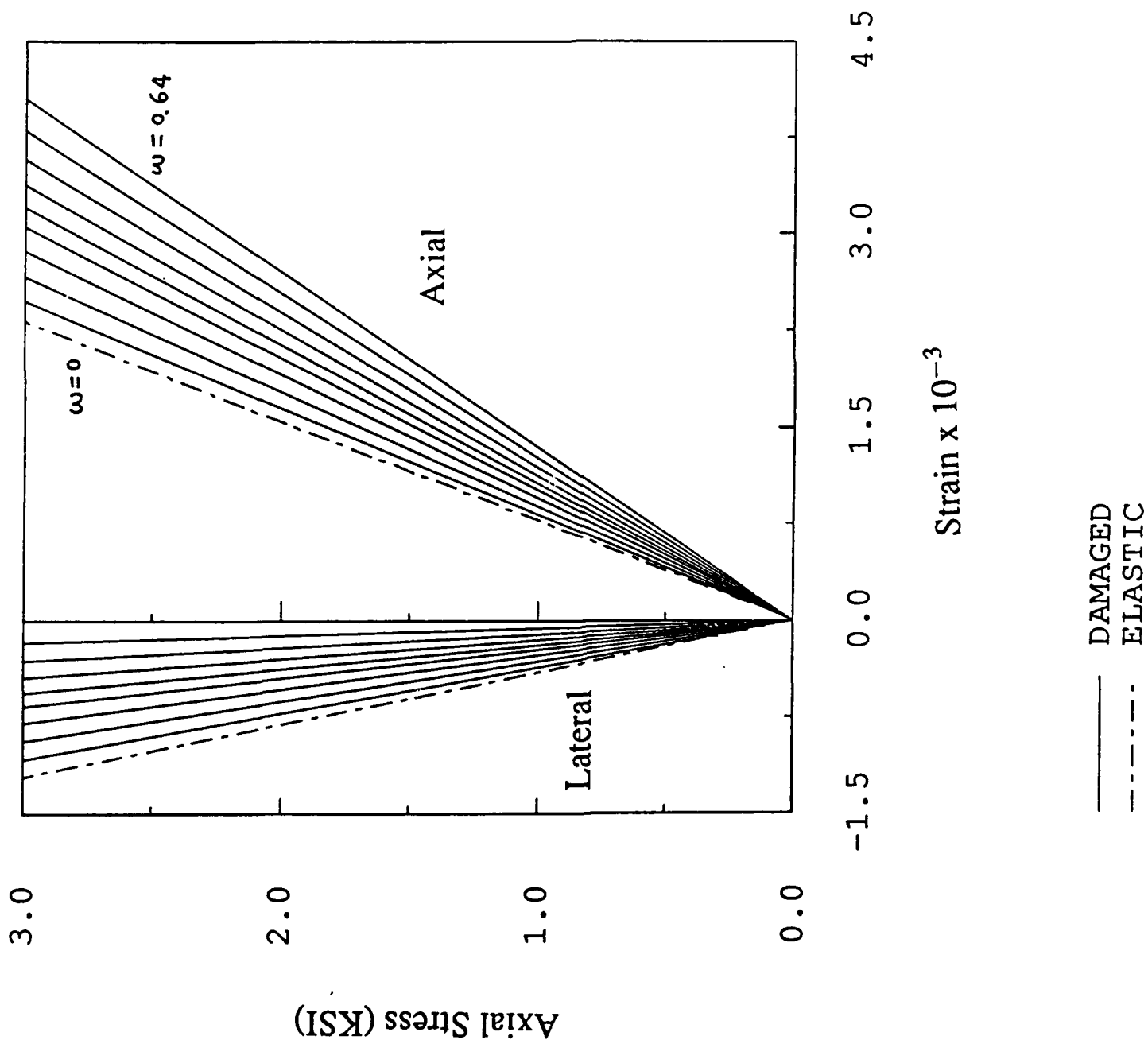**Figure 3.** The overall compliance S_{22} vs. microcrack concentration ω for various stationary damage model simulations. The dotted line is the elastic response.
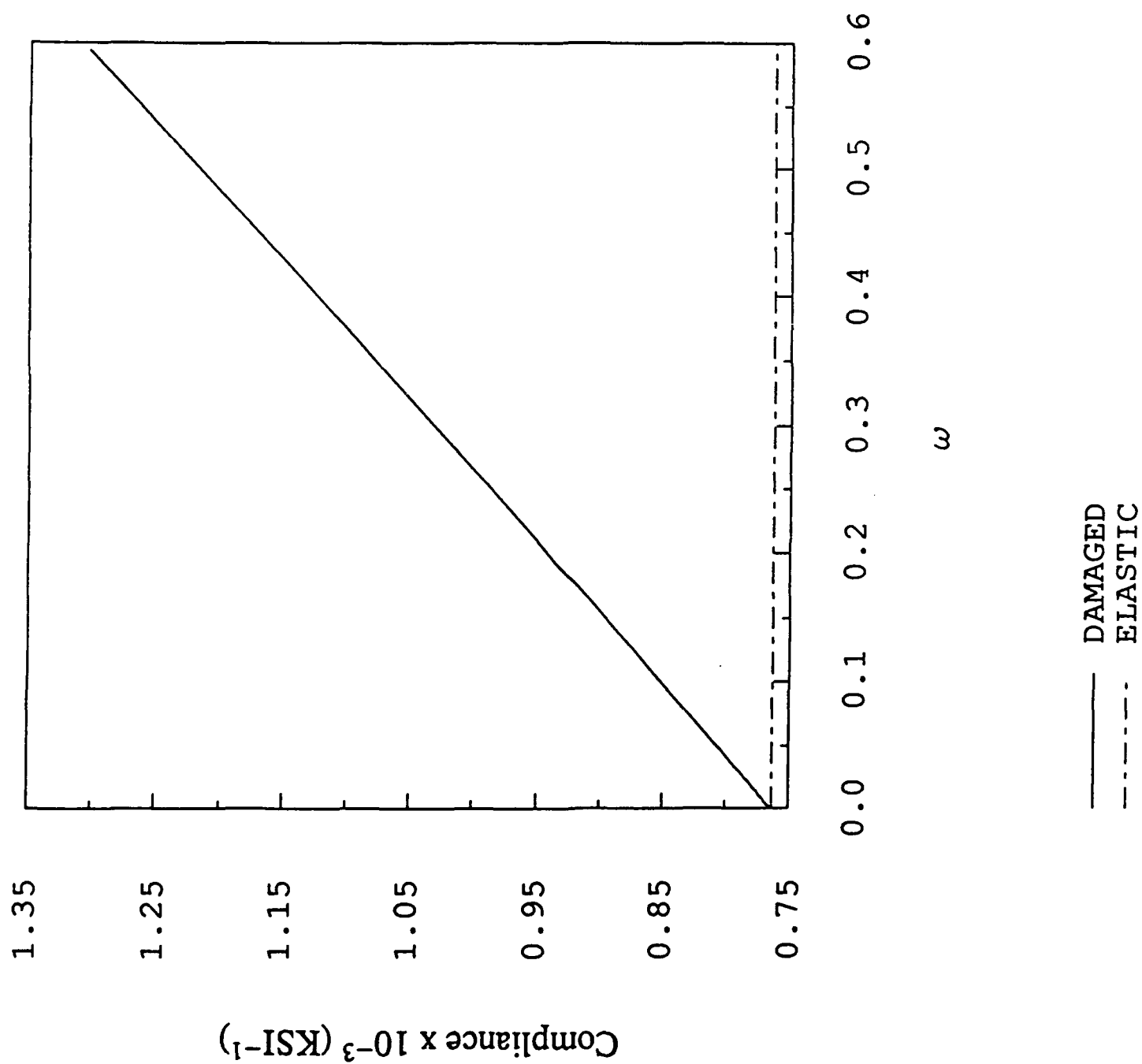
Figure 4. The overall compliance S_{12} vs. ω for various stationary damage model simulations.
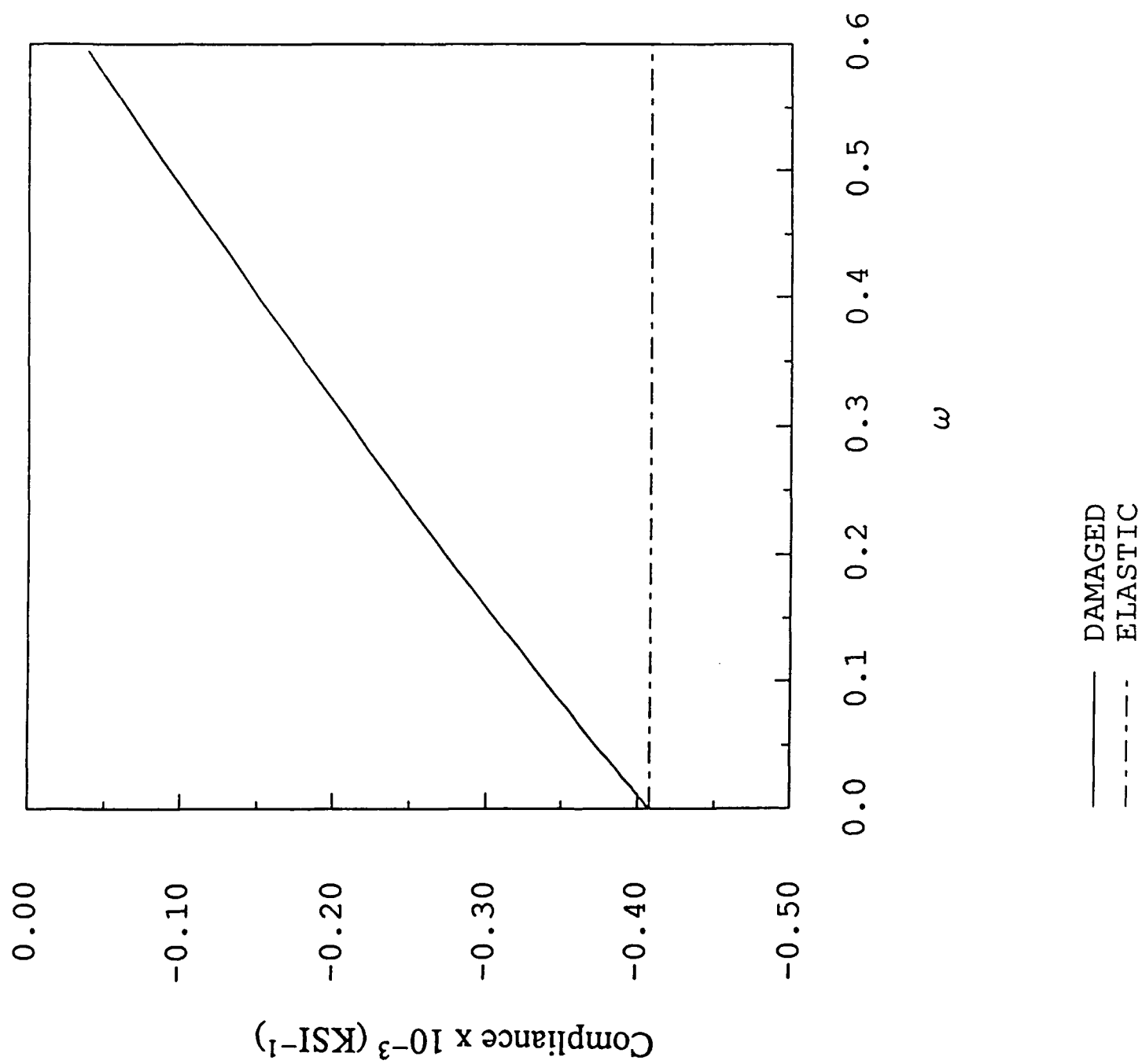
Figure 5. The axial-stress vs. the axial- and lateral-strain for two different initial microcrack sizes: $\alpha_i = 10°$ and $\alpha_i = 20°$. Note that $a = 0.1$ in. and $N/A = 100$. These are "process model" simulations.
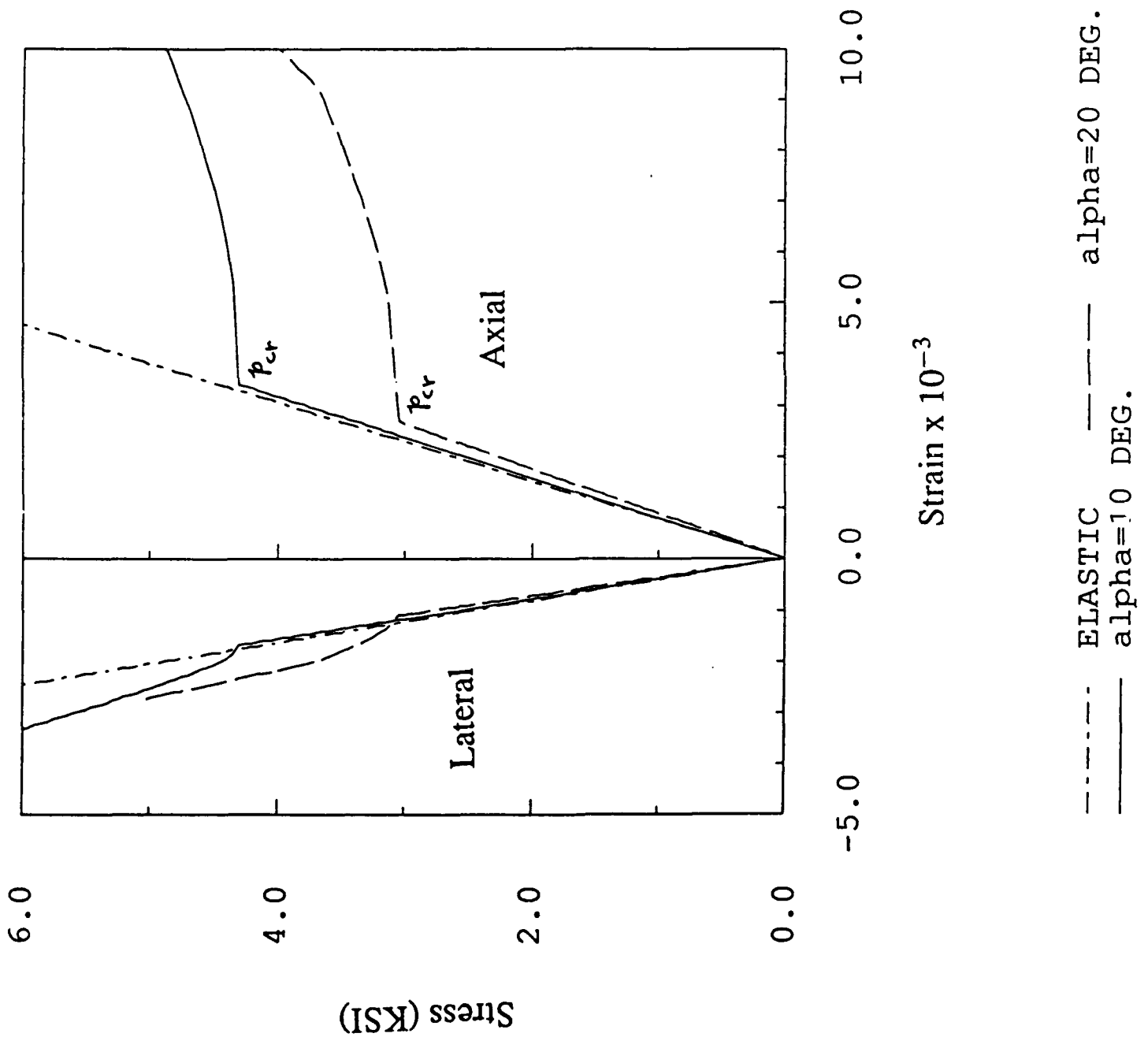
Figure 6. The axial-stress vs. the axial- and lateral-strain for two different fiber sizes and microcrack number densities. Note that $\alpha_i = 10°$.

Figure 7. The overall compliance S_{22} vs. the axial stress p for two different sets of a and N/A values. Note that $\alpha_i = 10°$.

Figure 8. The overall compliance S_{11} vs. the axial stress p for two different sets of a and N/A values. Note that $\alpha_i = 10°$.

Figure 9. The overall compliance S_{12} vs. the axial stress p for two different sets of a and N/A values. Note that $\alpha_i = 10°$.

Figure 10. The axial-stress vs. the axial- and lateral-strain for two different fiber sizes and microcrack number densities. Note that $\alpha_i = 20°$.
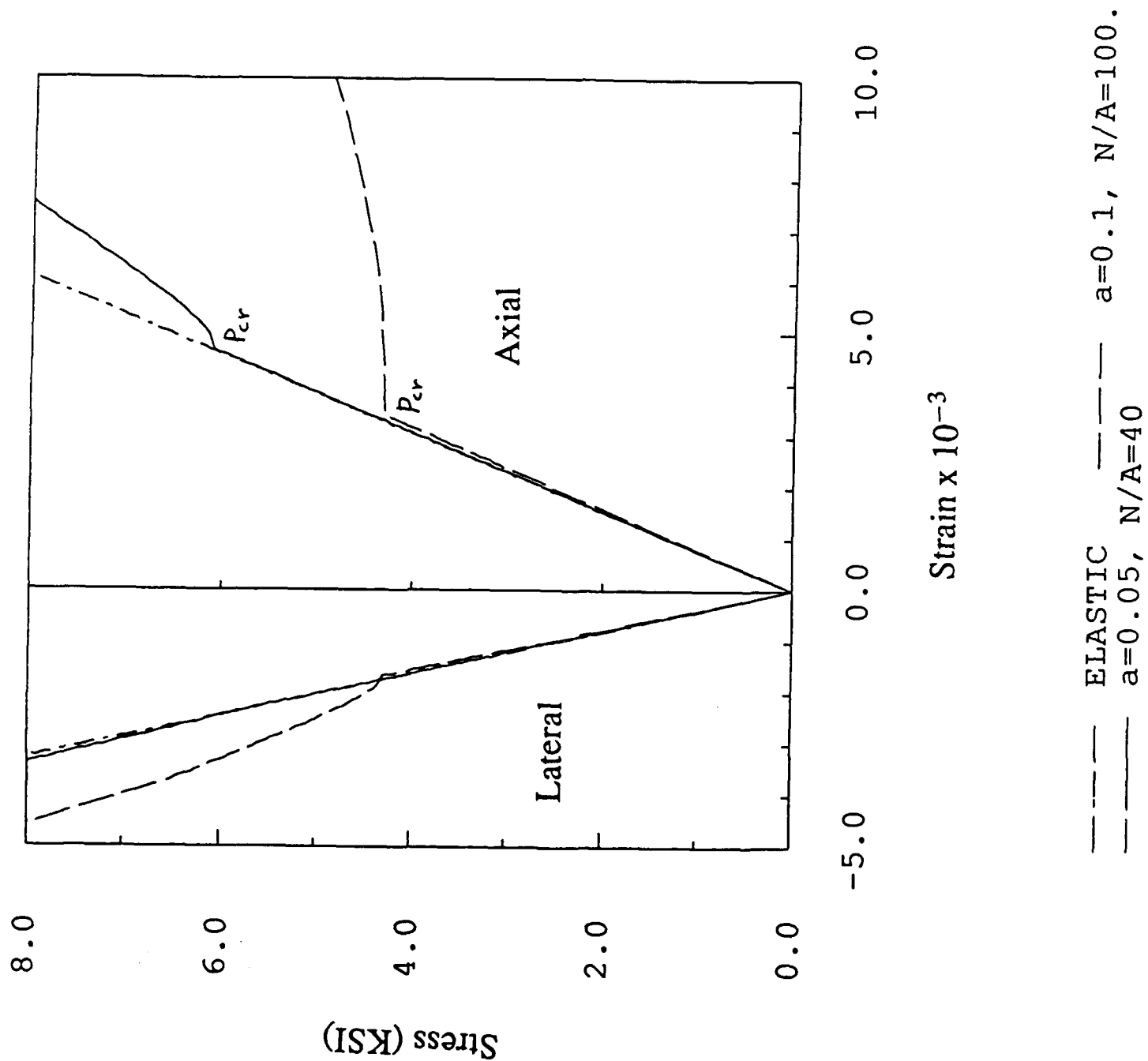
Figure 11. The overall compliance S_{22} vs. the axial stress p for two different sets of a and N/A values. Note that $\alpha_i = 20°$.
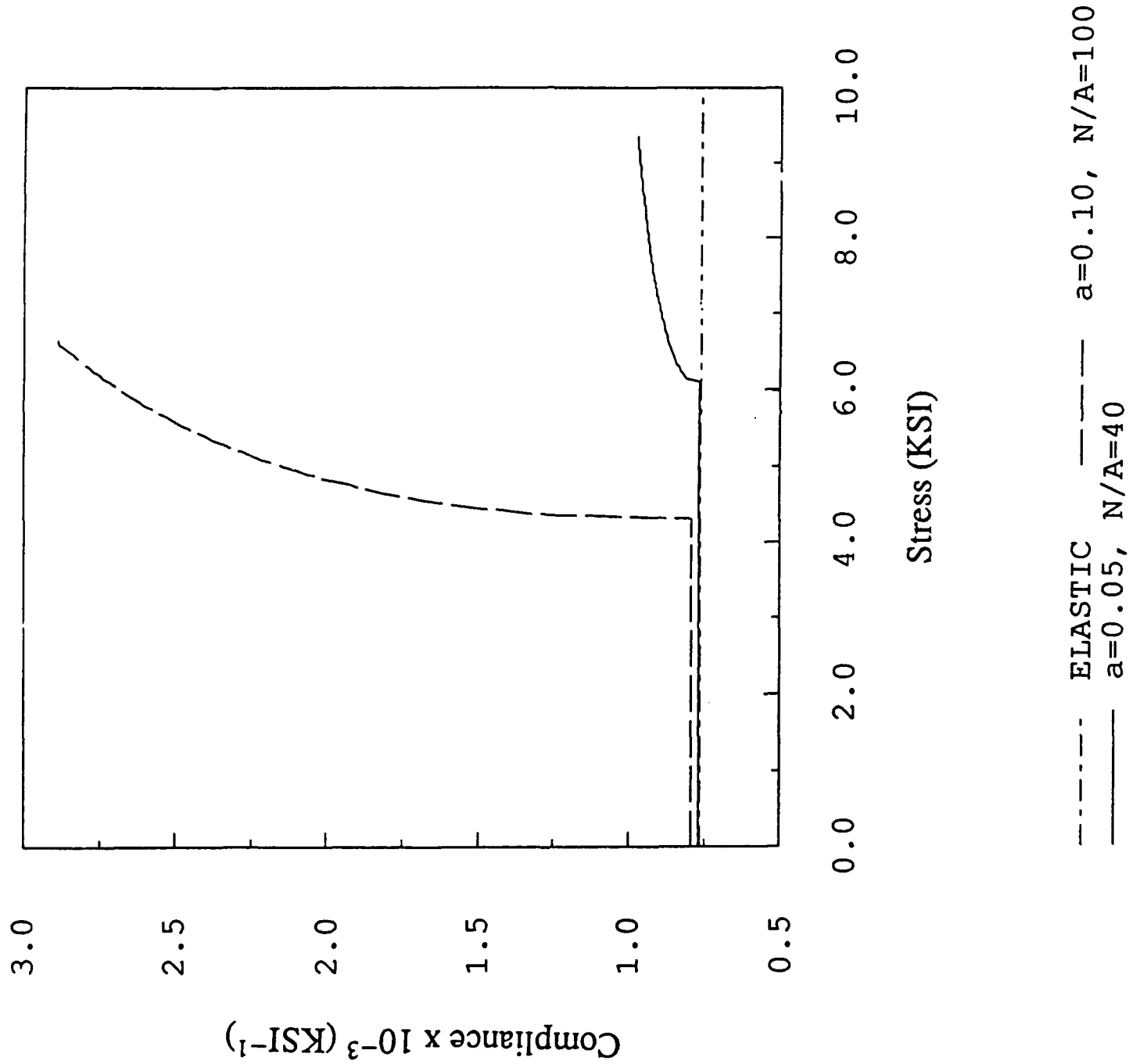

Stress (KSI)

Compliance x 10^{-3} (KSI^{-1})
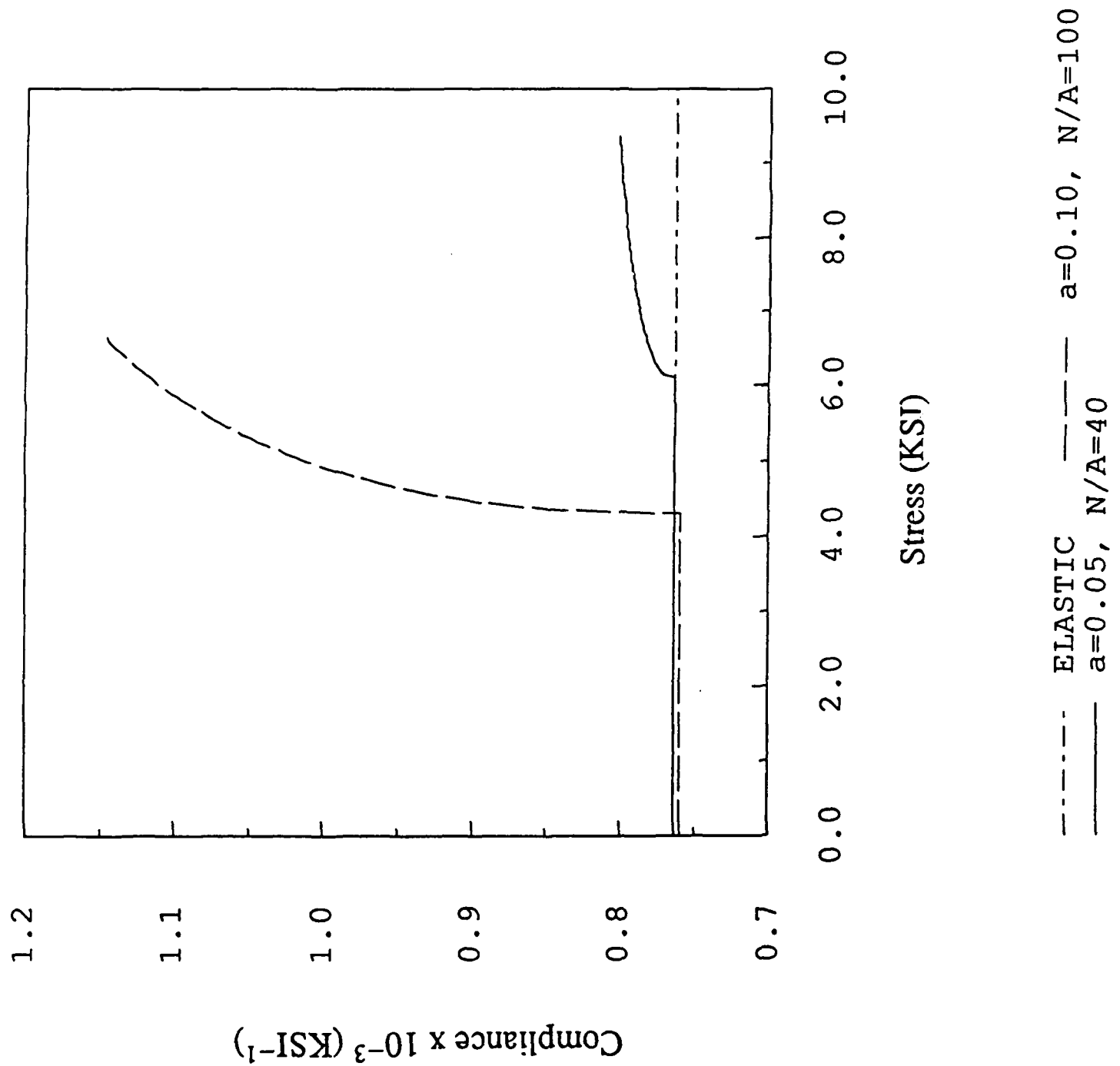
ELASTIC

a=0.10, N/A=100

a=0.05, N/A=40

Figure 12. The overall compliance S_{11} vs. the axial stress p for two different sets of a and N/A values. Note that $\alpha_i = 20°$.

Figure 13. The overall compliance S_{12} vs. the axial stress p for two different sets of a and N/A values. Note that $\alpha_i = 20°$.
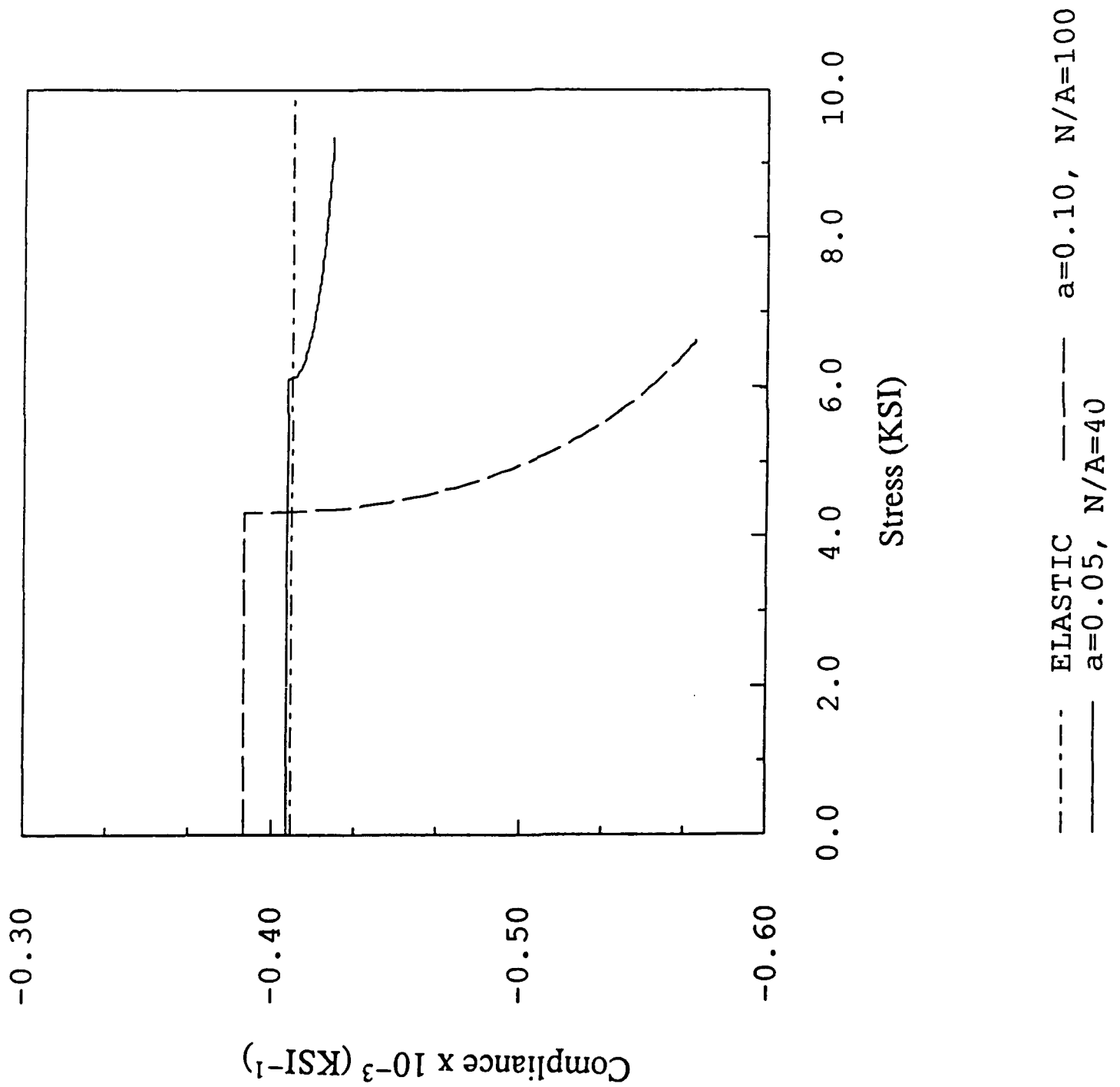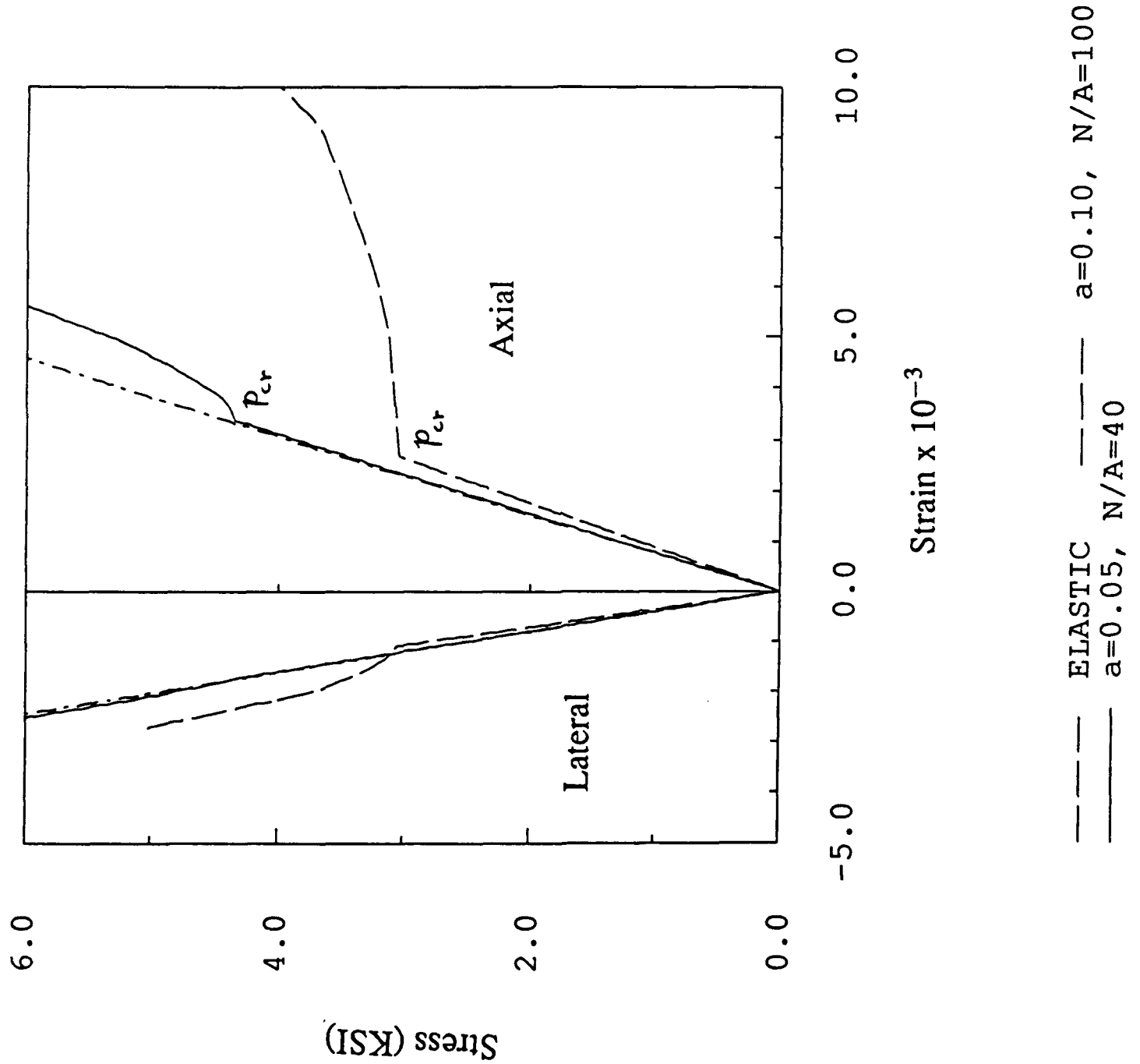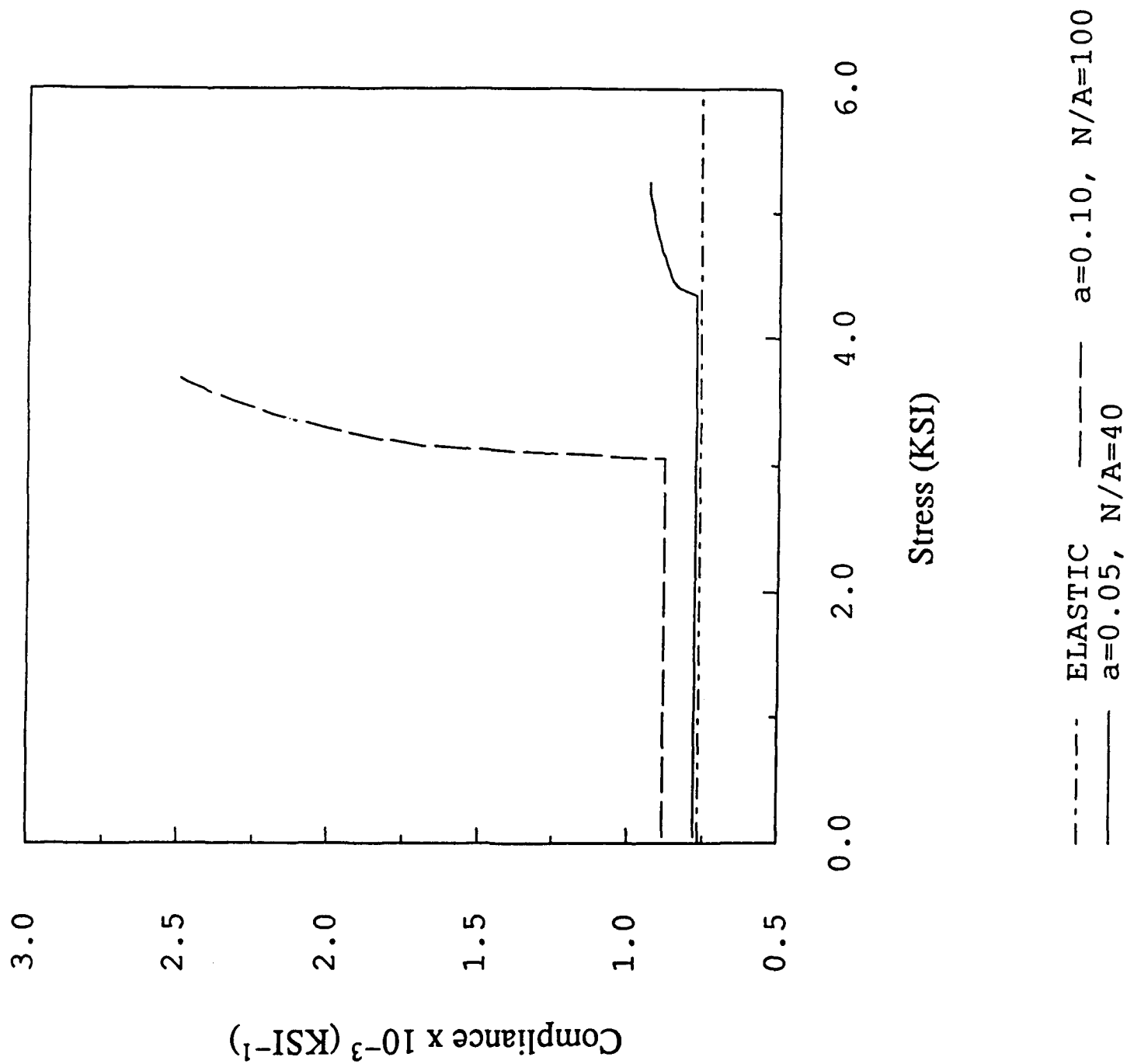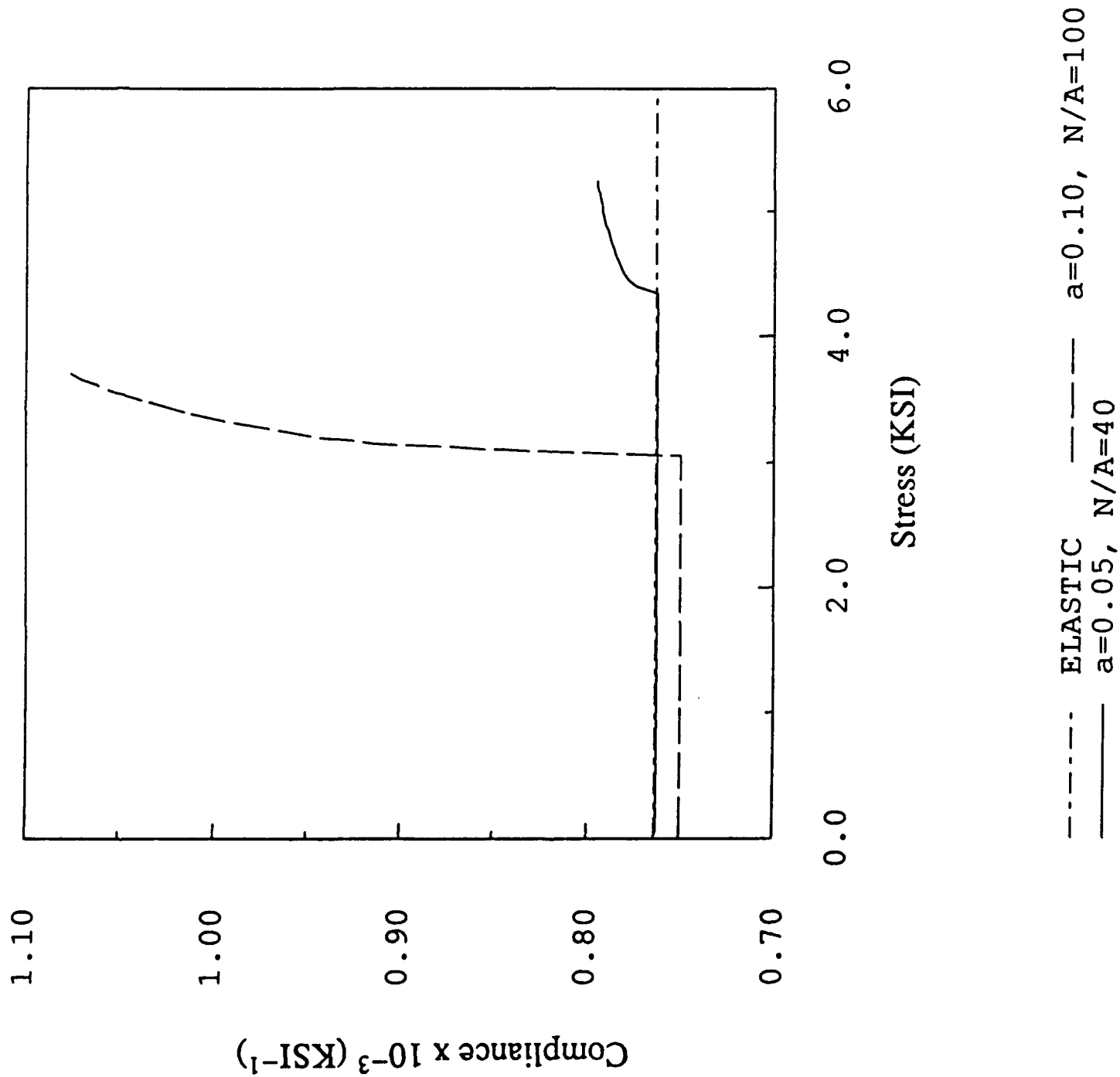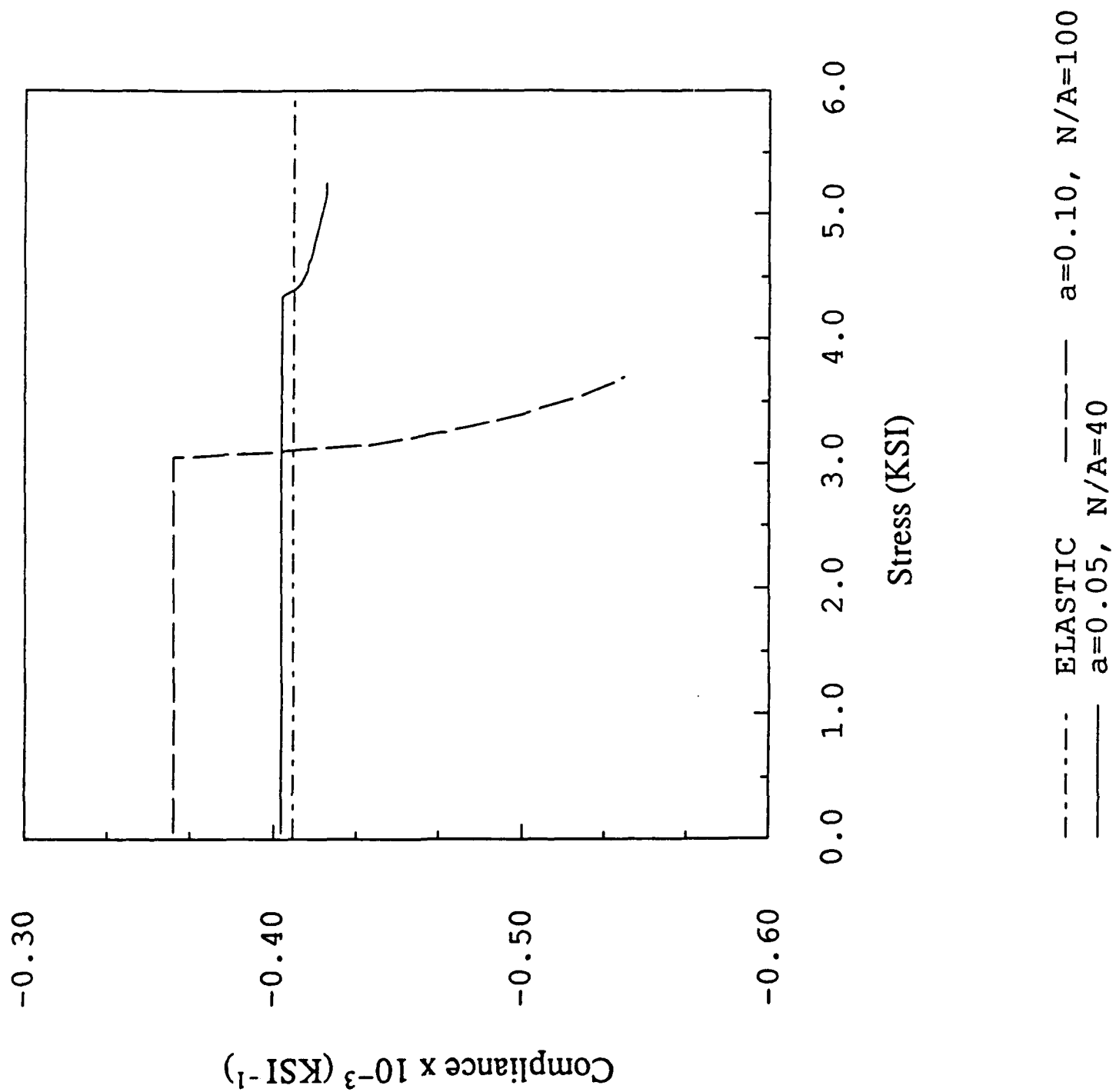
A Three-Dimensional Statistical Micromechanical
Theory for Brittle Solids with Interacting Microcracks

III.0. Abstract

A three-dimensional statistical micromechanical theory is presented to investigate the overall nonlinear mechanical responses of microcrack-weakened brittle solids. The macroscopic stress-strain relations of elastic solids with interacting microcracks are micromechanically derived by taking the *ensemble average* over all possible realizations which feature the same material mesostructural geometry. Approximate analytical solutions of a two-crack interaction model are introduced to account for microcrack interaction among many randomly oriented and distributed microcracks. The overall effective compliances of microcrack-weakened brittle solids are derived by further taking the *volume average* of the *ensemble-averaged* stress-strain relations over the entire material mesostructural domain of a representative volume element. Moreover, some special cases are investigated by using the proposed framework and other existing methods. It is emphasized that no Monte Carlo simulations are needed in the proposed framework.

III.1. Introduction

The nonlinear mechanical responses of damaged solids due to the existence, growth, and nucleation of microdefects (such as microcracks and microvoids) are of significant importance to engineers, and have been the subject of many investigations. See Krajcinovic (1989) for an excellent literature review on damage mechanics. For brittle materials (e.g. concrete, rocks and ceramics), in particular, microcracks often control overall deformation and failure mechanisms. To date, the only exact results derived for microcrack-weakened brittle solids are for dilute microcrack concentrations, where microcrack interactions are entirely neglected. These micromechanical damage models are called "Taylor's models"; see, e.g., Krajcinovic and Fanella (1986), Fanella and Krajcinovic (1988), and Ju (1990) for some recent works.

On the other hand, several approximate micromechanical analyses ("effective medium methods") were proposed in the literature to account for interaction effects of distributed microcracks. For example, the "self-consistent method" (Hill (1965)) was first applied to microcrack-weakened solids by Budiansky and O'Connell (1976) with special attention directed to perfectly randomly distributed (isotropic) and *weakly* interacting microcracks. The self-consistent method was further developed by Horii and Nemat-Nasser (1983) to take into account the effects of *closed* microcracks undergoing frictional sliding. See also Sumarac and Krajcinovic (1987, 1989), Krajcinovic and Sumarac (1989), Ju (1991), Ju and Lee (1991), and Lee and Ju (1991). Christensen and Lo (1979) proposed a three-phase "geneialized self-consistent model". The "differential scheme" was investigated by Roscoe (1952, 1973), McLaughlin (1977), and Hashin (1988). Further, the "Mori-Tanaka method" was developed by Mori and Tanaka (1973), Benveniste (1986), and Zhao, Tandon and Weng (1989). Based on variational principles, Hashin and Shtrikman (1962, 1963) also proposed upper and lower bounds for composites with inclusions.

Some comparisons and assessments for the self-consistent method, the generalized self-consistent method, the Mori-Tanaka method, and/or the differential scheme were also presented by Horii and Sahasakmontri (1990), Laws and Dvorak (1987), Nemat-Nasser and Hori (1990), and Christensen (1990, for pure shear load only). It is noted that effective medium methods are only valid for *weak* or at most *moderate* microcrack concentrations. Overall effective compliances as well as anisotropy due to microcracks can be estimated by effective medium approximations.

When microcrack concentrations are higher and microcrack spacings are closer, *strong* microcrack interactions occur and effective medium theories are no longer appropriate. Emanating from this viewpoint, excellent strong microcrack interaction models were proposed by Horii and Nemat-Nasser (1985), Hori and Nemat-Nasser (1987) for two-dimensional deterministic microcracks (not at the overall constitutive level), and by Kachanov and Montagut (1986), Kachanov (1987), Chudnovsky et al. (1987a,b), Montagut and Kachanov (1988), Kachanov and Laures (1989), and Laures and Kachanov (1990) for two- and three-dimensional *deterministic* (specified) arbitrary microcrack arrays (at the overall constitutive level). Other literatures are cited and discussed in the reference papers. Moreover, the important and valuable work due to Kachanov (1987), Kachanov and Laures (1989) rely on Monte Carlo simulations of a large amount of deterministic microcrack arrays, and depend heavily on large-scale computations to obtain local stresses of many randomly located microcracks. Therefore, it is desirable to develop innovative and *simple* statistical micromechanical damage theories to account for interactions among randomly located and oriented microcracks *without* using extensive random microcrack simulations and large-scale iterative stress computations.

The purpose of the present work is to establish a three-dimensional statistical micromechanical framework to predict overall effective moduli for brittle solids with many interacting, randomly distributed microcracks. The proposed statistical framework considers the probability and conditional probability density functions of microcrack locations and relative configurations. See Batchelor (1970), Hinch (1977), Willis (1977), Chen and Acrivos (1978a,b) for references. In addition, the *ensemble* and *volume* averages of stresses, strains and compliances are systematically constructed based on analytical micromechanics solutions and statistical mechanics concepts. Therefore, statistical aspects are naturally embedded into damage theories and macroscopic (averaged) constitutive equations. As a result, we do not rely on heavy numerical stress computations or extensive Monte Carlo random simulations involving hundreds of deterministic microcrack arrays.

It is emphasized that the proposed method is fundamentally different from that proposed by Hudson (1980, 1981, 1986). Hudson's method, though using the ensemble average approach, is based on a second order stiffness theory and thus leads to irrational behaviors for microcracked solids with moderate or high microcrack concentrations (see Sayers and

Kachanov, 1991). That is, Hudson's method is designed for small microcrack density. The proposed approach is suitable for low, moderate or high microcrack concentrations.

A brief outline of this work is as follows. In section 2, an *ensemble average* approach to derive damaged stress-strain relations is introduced. Approximate closed-form analytical solutions are subsequently presented for the interaction problem of two aligned but arbitrarily located penny-shaped microcracks. The overall moduli of a representative volume element (unit cell) are then derived by further taking the *volume average* of *ensemble averaged* local stress-strain relations over the entire (unit cell) domain at the *mesostructural* level in Section 3. In Section 4, applications are made to a number of special cases. In particular, for the dilute microcrack concentration case, the present approach recovers the well-known Taylor's model by neglecting interactions among microcracks. Further, for *aligned* penny-shaped microcracks, the present method reveals that average tractions and overall compliances are changed by the presence and interaction of 3-D microcracks. This result is relevant to fiber breaking in unidirectionally reinforced fiber composites. Comparisons with the Taylor's model, the self-consistent method and the differential scheme are also presented. Finally, higher-order microcrack interaction models within the proposed framework are discussed in Section 5.

III.2. An ensemble average approach to 3-D aligned microcrack interaction and effective moduli

We first review some basic background related to the concept of volume-averaged (mesostructural) stress and strain tensors within the context of a representative volume element (RVE) or unit cell. The ensemble average of microcrack-induced strains and approximate analytical solutions of two arbitrarily located and oriented microcracks are subsequently given. Overall effective compliances of brittle solids with interacting microcracks are then derived within the framework of statistical micromechanics. Following current literatures, it is assumed that the volume-average stress $\bar{\sigma}$ approximately equal to the far-field stress σ^∞. This typical assumption may be removed and significant further improvements are very promising. These issues will be addressed in a forthcoming paper.

III.2.1. Ensemble average of microcrack-perturbed stresses and s- trains

Due to the existence and interaction of microcracks, local stresses and strains in the matrix material are perturbed. The ensemble average approach hinges on the concept that local stresses, strains and compliances (or stiffnesses) at a typical point within a RVE of a microcrack-weakened solid can be obtained by averaging over the ensemble of all *statistical realizations* of randomly distributed microcracks. Batchelor (1970), Batchelor and Green (1972), and Hinch (1977) applied this approach to the study of fluid suspensions within the framework of pairwise (second order) interaction. The ensemble average approach with pairwise interaction was later applied to composite materials with interacting inclusions (inhomogeneities) by Willis and Acton (1976), as well as Chen and Acrivos (1978a,b). Recently, Ju and Chen (1990a,b) proposed two-dimensional (second order and higher) micromechanical damage theories for brittle solids with interacting *slit* microcracks by employing the ensemble average method and micromechanical fracture mechanics. It is noted that local displacements, strains and stresses vary with *positions* within a RVE.

For simplicity, we consider a two-phase composite composed of a linear elastic matrix and many *penny-shaped* microcracks. The local strain tensor at a point x within the RVE takes the form:

$$\epsilon(\mathbf{x}) = \mathbf{S}^o : \sigma(\mathbf{x}) + \epsilon^*(\mathbf{x}, \mathcal{C}) \tag{1}$$

where ϵ and σ denote the local strain and stress, respectively; ϵ^* is the *perturbed* strain due to the existence and interaction of microcracks; and C denotes the set of all possible configurations of the microcracks. It is emphasized that ϵ^* is zero if $\mathbf{x}$ is a point in the matrix and non-zero if $\mathbf{x}$ is a point on the microcrack surfaces. Taking the ensemble average over Eq. (1), we arrive at

$$\langle\epsilon\rangle(\mathbf{x}) = \mathbf{S}^\circ : \langle\sigma\rangle(\mathbf{x}) + \langle\epsilon^*\rangle(\mathbf{x}) \tag{2}$$

where the angle brackets $\langle\cdot\rangle$ signify the ensemble average.

Throughout the development of this paper, for simplicity, we shall assume that the solid is *locally homogeneous* (Hinch (1977)) and penny-shaped microcracks do not intersect one another. *Locally homogeneity* implies that all probability density functions (PDF) do not vary under small translation on a macroscopic length scale. It can be shown (Ju and Chen (1990a)) that, in the case of microcracks, the perturbed strain can be expressed as

$$\langle\epsilon^*\rangle(\mathbf{x}) = f(\mathbf{x}) \int_{\mathcal{G}} \int_{S_i} \frac{1}{2}\langle[\![\mathbf{u}]\!] \otimes \mathbf{n} + \mathbf{n} \otimes [\![\mathbf{u}]\!]\rangle(\mathbf{x}'|\mathbf{x},\mathcal{G})f(\mathcal{G}) \, d\mathcal{G}dS \tag{3}$$

Here, $\mathcal{G} \equiv (a, \mathbf{n})$ indicates the microcrack length (radius) a and orientation $\mathbf{n}$. Furthermore, $\mathbf{x}'$ denotes a point on the surfaces (S_i) of a microcrack centered at $\mathbf{x}$; $f(\mathbf{x})$ is the PDF for a microcrack being centered at $\mathbf{x}$; $[\![\mathbf{u}]\!]$ is the vector of microcrack opening displacements; and $f(\mathcal{G})$ is the PDF for a microcrack with a geometry $\mathcal{G}$. If all penny-shaped microcracks are aligned (parallel) and of equal size, then there is no variation in $\mathcal{G}$. This could correspond to, for example, microcracks generated by fiber breaks in unidirectional fiber composites (see, e.g., Laws and Dvorak (1987)). In this event, Eq. (3) can be simplified as follows

$$\langle\epsilon^*\rangle(\mathbf{x}) = f(\mathbf{x}) \int_{S_i} \frac{1}{2}\langle[\![\mathbf{u}]\!] \otimes \mathbf{n} + \mathbf{n} \otimes [\![\mathbf{u}]\!]\rangle(\mathbf{x}'|\mathbf{x}) \, dS \tag{4}$$

It is well known that, for an open penny-shaped microcrack with radius a embedded in an infinite linear elastic isotropic matrix, the microcrack opening displacements at $\mathbf{x}'$ (at a distance ρ from the center of the microcrack) are:

$$\left\{ \begin{array}{c} [\![u_x']\!] \\ [\![u_y']\!] \\ [\![u_z']\!] \end{array} \right\} = \frac{8(1-\nu^2)}{\pi E(2-\nu)}\sqrt{a^2-\rho^2}\left\{ \begin{array}{c} 2s \\ 2t \\ (2-\nu)p \end{array} \right\} \tag{5}$$

where E and ν = the Young's modulus and Poisson's ratio of the virgin matrix material, respectively. Moreover, p, s and t = the z-direction normal, the x-direction shear and the

y-direction shear stresses projected on the microcrack surface in its local coordinates; see Fig. 1 for a schematic plot.

If all (open) microcracks are aligned (parallel), then we can define $n = (0, 0, 1)^T$. By substituting Eq. (5) into (4) and carring out the integration, we obtain (assuming equal microcrack size)

$$\langle e^* \rangle(\mathbf{x}) = f(\mathbf{x}) \frac{16(1 - \nu^2)}{3E(2 - \nu)} a^3 \, \mathbf{g} \cdot \langle \mathbf{T} \rangle \tag{6}$$

where (the Voigt's notation)

$$\langle \mathbf{e}^* \rangle \equiv \left\{ \begin{array}{c} \langle e_1^* \rangle \\ \langle e_2^* \rangle \\ \langle e_3^* \rangle \\ \langle e_4^* \rangle \\ \langle e_5^* \rangle \\ \langle e_6^* \rangle \end{array} \right\} \equiv \left\{ \begin{array}{c} \langle \epsilon_{xx}^* \rangle \\ \langle \epsilon_{yy}^* \rangle \\ \langle \epsilon_{zz}^* \rangle \\ 2\langle \epsilon_{xy}^* \rangle \\ 2\langle \epsilon_{yz}^* \rangle \\ 2\langle \epsilon_{zx}^* \rangle \end{array} \right\} \tag{7}$$

In addition, $\mathbf{g}$ is the transformation matrix and $\mathbf{T}$ is the *local* stress vector:

$$\mathbf{g} = \begin{bmatrix} 0 & 0 & 0 \\ 0 & 0 & 0 \\ 2 - \nu & 0 & 0 \\ 0 & 0 & 0 \\ 0 & 0 & 2 \\ 0 & 2 & 0 \end{bmatrix} \quad ; \quad \mathbf{T} = \left\{ \begin{array}{c} p \\ s \\ t \end{array} \right\} \tag{8}$$

In the event of distributed (nonuniform) microcrack lengths and orientations, similar expressions can be constructed accordingly.

On the other hand, the local stress vector $\langle \mathbf{T} \rangle$ can be shown to be (see Eq. (14) in Sec. 2.2):

$$\mathbf{T} = \mathbf{T}^\infty + \tilde{\mathbf{T}} \equiv \left\{ \begin{array}{c} p^\infty \\ s^\infty \\ t^\infty \end{array} \right\} + \left\{ \begin{array}{c} \tilde{p} \\ \tilde{s} \\ \tilde{t} \end{array} \right\} \tag{9}$$

Here, $\mathbf{T}^\infty$ denotes the unperturbed local stress vector due to remote loading, and $\tilde{\mathbf{T}}$ denotes the local stress perturbation due to three-dimensional microcrack interactions. In what follows, attention is focused on *pairwise* (second order) microcrack interactions. Higher order microcrack interactions will be discussed in Sec. 5. By assuming that all microcracks are aligned with a chosen global coordinate system, the stress $\mathbf{T}^\infty$ due to far field loads can be expressed as

$$\mathbf{T}^\infty = \mathbf{K}_0 \cdot \boldsymbol{\tau}^\infty \tag{10}$$

where

$$\mathbf{K}_0 = \begin{bmatrix} 0 & 0 & 1 & 0 & 0 & 0 \\ 0 & 0 & 0 & 0 & 0 & 1 \\ 0 & 0 & 0 & 0 & 1 & 0 \end{bmatrix} \quad ; \quad \boldsymbol{\tau}^\infty \equiv \begin{Bmatrix} \sigma_{xx}^\infty \\ \sigma_{yy}^\infty \\ \sigma_{zz}^\infty \\ \sigma_{xy}^\infty \\ \sigma_{yz}^\infty \\ \sigma_{zx}^\infty \end{Bmatrix} \tag{11}$$

The ensemble average of local stress perturbation, on the other hand, takes the form (assuming uniform size and aligned orientation):

$$\langle \tilde{\mathbf{T}} \rangle(\mathbf{x}) = \int_{\Xi} \langle \tilde{\mathbf{T}} \rangle(\mathbf{x}|\mathbf{x}_1) f(\mathbf{x}_1|\mathbf{x}) \, d\mathbf{x}_1 \tag{12}$$

where $\langle \tilde{\mathbf{T}} \rangle(\mathbf{x}|\mathbf{x}_1)$ = the ensemble-average stress perturbation for a microcrack centered at $\mathbf{x}$ over the subclass of realizations having a microcrack centered at $\mathbf{x}_1$; and $f(\mathbf{x}_1|\mathbf{x})$ = the conditional PDF for finding a microcrack centered at $\mathbf{x}_1$ given a microcrack centered at $\mathbf{x}$. Further, Ξ designates the active (open) integration domain which depends on the loading conditions.

The conditional PDF $f(\mathbf{x}_1|\mathbf{x})$ can be simplified to $f(\mathbf{x}_1)$ if microcracks do *not* intersect and *reasonable randomness* holds (Hinch (1977)). The *local homogeneity* assumption enables us to further approximate $f(\mathbf{x}_1)$ by $f(\mathbf{x})$. Therefore, Eq. (12) can be recast as:

$$\langle \tilde{\mathbf{T}} \rangle(\mathbf{x}) = f(\mathbf{x}) \int_{\Xi} \langle \tilde{\mathbf{T}} \rangle(\mathbf{x}|\mathbf{x}_1) \, d\mathbf{x}_1 \tag{13}$$

The quantity $\tilde{\mathbf{T}}(\mathbf{x}|\mathbf{x}_1)$ corresponding to pairwise microcrack interaction will be the main subject of Sec. 2.2.

III.2.2. Approximate explicit solutions for pairwise interaction of aligned microcracks

The objective of this section is to construct approximate closed-form *explicit* expressions for perturbed stresses $\tilde{\mathbf{T}}$ due to two-microcrack interaction so that the ensemble-average formalism proposed in Sec. 2.1 can be realized. It is possible, in principle, to derive expressions for $\tilde{\mathbf{T}}$ in the interaction problem involving two 3-D, arbitrarily oriented and located penny-shaped microcracks. However, the general solutions of two-microcrack interaction are rather complicated and no reasonably compact closed-form explicit solutions are possible (although numerical solutions are certainly feasible). Therefore, for demonstration purpose,

attention will be foucused on explicit solutions of two randomly located, aligned (parallel), equally sized, penny-shaped microcracks embedded in infinite linear elastic isotropic matrix.

The "pseudo-traction" method is adopted here to derive approximate expressions for $\tilde{\mathbf{T}}$ since *exact* solutions are not yet available. For mathematical simplicity, only the *first term* of Taylor's expansion of the local stress field is used to represent the average stress across the microcrack surface. Higher order terms in polynomial expansions may be included if desired, however, at the high cost of a much larger system of equations and much more complicated analytical expressions. Stemming from a different viewpoint, the more accurate "transmission factor"-type formulation proposed by Kachanov (1987) is well suited for deterministic, numerical computations. Within the framework of statistical ensemble average, nevertheless, closed-form explicit solutions for stress-interaction are warranted.

Figure 1 shows the local coordinate systems for microcracks 1 and 2 of radius a. The z-axis is chosen as the direction normal to a microcrack surface. In accord with the pseudo-traction concept, the problem of two interacting microcracks subjected to far field stresses can be decomposed into a homogeneous problem and two sub-problems (see also Ju and Chen (1990a)). 'n the homogeneous problem, a microcrack-free solid is subjected to applied stresses at far field. In the sub-problem j $(j = 1, 2)$, an infinitely extended solid contains only *one* penny-shaped microcrack and is subjected to zero remote stress at infinity. Since stresses vanish on microcrack surfaces (C_j), the following boundary conditions must be satisfied $(j = 1, 2)$:

$$-p_j + p_j^\infty + \tilde{p}_j = 0 \quad \cdot \quad -s_j + s_j^\infty + \tilde{s}_j = 0 \quad ; \quad -t_j + t_j^\infty + \tilde{t}_1 = 0 \qquad (14)$$

In the first sub-problem (containing only 'microcrack 1'), let us define a cylindrical coordinate system with the center of the 'microcrack 1' as its origin. Accordingly, the center location of the 'microcrack 2' can be characterized by (ρ, ϕ, z); see Fig. 1. For convenience, we shall introduce the following definitions:

$$\sigma_1 \equiv \sigma_{xx} + \sigma_{yy} \quad ; \quad \sigma_2 \equiv \sigma_{xx} - \sigma_{yy} - 2i\sigma_{xy} \qquad (15)$$

$$\sigma_z \equiv \sigma_{zz} \quad ; \quad \tau_z \equiv \sigma_{xz} + i\sigma_{yz} \qquad (16)$$

If the surfaces of the 'microcrack 1' are subjected to applied *normal* stress $p^{(1)}$, then perturbed

stresses at the 'microcrack 2' location are given by (Fabrikant (1989, p. 252–257)):

$$\sigma_1'^{(1)} = \frac{2p^{(1)}}{\pi} \left\{ (1+2\nu) \left[\frac{a(l_2^2 - a^2)^{1/2}}{l_2^2 - l_1^2} - \sin^{-1}\left(\frac{a}{l_2}\right) \right] + \frac{az^2[l_1^4 + a^2(2a^2 + 2z^2 - 3\rho^2)]}{(l_2^2 - l_1^2)^3(l_2^2 - a^2)^{1/2}} \right\}$$

$$\sigma_2'^{(1)} = \frac{2p^{(1)}}{\pi} \frac{al_1^2 e^{2i\phi}(l_2^2 - a^2)^{1/2}}{l_2^2(l_2^2 - l_1^2)} \left\{ (1-2\nu) + \frac{z^2[a^2(6l_2^2 - 2l_1^2 + \rho^2) - 5l_2^4]}{(l_2^2 - l_1^2)^2(l_2^2 - a^2)} \right\}$$

$$\sigma_z'^{(1)} = \frac{2p^{(1)}}{\pi} \left\{ \frac{a(l_2^2 - a^2)^{1/2}}{l_2^2 - l_1^2} - \sin^{-1}\left(\frac{a}{l_2}\right) - \frac{az^2[l_1^4 + a^2(2a^2 + 2z^2 - 3\rho^2)]}{(l_2^2 - l_1^2)^3(l^2 - a^2)^{1/2}} \right\} \tag{17}$$

$$\tau_z'^{(1)} = -\frac{2p^{(1)}}{\pi} \frac{zl_1 e^{i\phi}(l_2^2 - a^2)^{1/2}[a^2(4l_2^2 - 5\rho^2) + l_1^4]}{l_2(l_2^2 - l_1^2)^3}$$

where

$$l_1 \equiv \frac{1}{2} \left\{ [(a+\rho)^2 + z^2]^{1/2} - [(a-\rho)^2 + z^2]^{1/2} \right\}$$

$$l_2 \equiv \frac{1}{2} \left\{ [(a+\rho)^2 + z^2]^{1/2} + [(a-\rho)^2 + z^2]^{1/2} \right\} \tag{18}$$

Furthermore, when the surfaces of the 'microcrack 1' are loaded by the combined shear stresses $\tau^{(1)} = s^{(1)} + it^{(1)}$, then perturbed stresses at the 'microcrack 2' location are (Fabrikant (1989, p. 257–261)):

$$\sigma_1''^{(1)} = \frac{2(\bar{\tau}^{(1)} e^{i\phi} + \tau^{(1)} e^{-i\phi})}{\pi(2-\nu)} \left\{ -2(1+\nu)\frac{al_1(a^2 - l_1^2)^{1/2}}{l_2(l_2^2 - l_1^2)} + \frac{zl_1(l_2^2 - a^2)^{1/2}[a^2(4l_2^2 - 5\rho^2) + l_1^4]}{l_2(l_2^2 - l_1^2)^3} \right\}$$

$$\sigma_2''^{(1)} = \frac{-2e^{i\phi}}{\pi(2-\nu)} \left\{ 4(1-\nu)\frac{al_1(a^2 - l_1^2)^{1/2}}{l_2(l_2^2 - l_1^2)}\bar{\tau}^{(1)} + \frac{zl_1(l_2^2 - a^2)^{1/2}}{l_2(l_2^2 - l_1^2)} \left[\frac{4a^2}{l_2^2}\bar{\tau}^{(1)}e^{2i\phi} - \frac{a^2(4l_2^2 - 5\rho^2) + l_1^4}{(l_2^2 - l_1^2)^2}(\tau^{(1)} + \bar{\tau}^{(1)}e^{2i\phi}) \right] \right\}$$

$$\sigma_z''^{(1)} = -\frac{2(\bar{\tau}^{(1)} e^{i\phi} + \tau^{(1)} e^{-i\phi})}{\pi(2-\nu)} \frac{zl_1(l_2^2 - a^2)^{1/2}[a^2(4l_2^2 - 5\rho^2) + l_1^4]}{l_2(l_2^2 - l_1^2)^3}$$

$$\tau_z''^{(1)} = \frac{2}{\pi(2-\nu)} \left\{ \left[(2-\nu)\left(\frac{a(l_2^2 - a^2)^{1/2}}{l_2^2 - l_1^2} - \sin^{-1}\left(\frac{a}{l_2}\right) \right) + \frac{z(a^2 - l_1^2)^{1/2}[l_1^4 + a^2(2a^2 + 2z^2 - 3\rho^2)]}{(l_2^2 - l_1^2)^3} \right] \tau^{(1)} \right.$$
$$\left. + \left[\nu a(l_2^2 - a^2)^{1/2} + \frac{z(a^2 - l_1^2)^{1/2}[a^2(6l_2^2 - 2l_1^2 + \rho^2) - 5l_2^4]}{(l_2^2 - l_1^2)^2} \right] \frac{l_1^2 e^{2i\phi}}{l_2^2(l_2^2 - l_1^2)}\bar{\tau}^{(1)} \right\} \tag{19}$$

where $\bar{\tau}^{(1)}$ is the complex conjugate of $\tau^{(1)}$. The total perturbed stresses due to combined normal loading $p^{(1)}$ and shear loading $\tau^{(1)}$ are therefore obtained:

$$\sigma_1^{(1)} = \sigma_1'^{(1)} + \sigma_1''^{(1)} \quad ; \quad \sigma_2^{(1)} = \sigma_2'^{(1)} + \sigma_2''^{(1)}$$

$$\sigma_z^{(1)} = \sigma_z'^{(1)} + \sigma_z''^{(1)} \quad ; \quad \tau_z^{(1)} = \tau_z'^{(1)} + \tau_z''^{(1)} \tag{20}$$

It can be shown that the Cartesian stress components are

$$\sigma_{xx}^{(1)} = \frac{1}{2}\left[\sigma_1^{(1)} + \text{Re}(\sigma_2^{(1)}) \right] \quad ; \quad \sigma_{yy}^{(1)} = \frac{1}{2}\left[\sigma_1^{(1)} - \text{Re}(\sigma_2^{(1)}) \right]$$

$$\sigma_{zz}^{(1)} = \sigma_z^{(1)} \quad ; \quad \sigma_{xy}^{(1)} = \frac{1}{2}\text{Im}(\sigma_2^{(1)}) \tag{21}$$

$$\sigma_{yz}^{(1)} = \text{Im}(\tau_z^{(1)}) \quad ; \quad \sigma_{zx}^{(1)} = \text{Im}(\tau_z^{(1)})$$

where "Re" and "Im" are the real and imaginary parts, respectively, of a complex variable.

Eq. (21) can be recapitulated into the following matrix form:

$$
\boldsymbol{\tau}^{(1)} \equiv \left\{ \begin{array}{c} \sigma_{xx} \\ \sigma_{yy} \\ \sigma_{zz} \\ \sigma_{xy} \\ \sigma_{yz} \\ \sigma_{zx} \end{array} \right\}^{(1)} = \left[\begin{array}{ccc} \frac{b_1+b_2}{2} & \frac{c_1+c_2}{2} & \frac{d_1+d_2}{2} \\ \frac{b_1-b_2}{2} & \frac{c_1-c_2}{2} & \frac{d_1-d_2}{2} \\ b_3 & c_3 & d_3 \\ \frac{b_4}{2} & \frac{c_4}{2} & \frac{d_4}{2} \\ b_5 & c_5 & d_5 \\ b_6 & c_6 & d_6 \end{array} \right]^{(1)} \left\{ \begin{array}{c} p \\ s \\ t \end{array} \right\}^{(1)} \tag{22}
$$

where definitions of the parameters b_i, c_i, and d_i can be found in **Appendix I**. Symbolically, we can express $\boldsymbol{\tau}^{(1)}$ as a function of coordinates and normal and shear stresses as follows:

$$
\boldsymbol{\tau}^{(1)} \equiv \boldsymbol{\tau}(\rho, \phi, z; p_1, s_1, t_1) \tag{23}
$$

Since microcracks 1 and 2 are aligned, the perturbed normal and shear stresses along the surfaces at the 'microcrack 2' location are

$$
\begin{aligned}
\tilde{p}_2 &= \mathbf{e}_z \cdot \boldsymbol{\tau}^{(1)} \cdot \mathbf{e}_z = \sigma_{zz}^{(1)} \\
\tilde{s}_2 &= \mathbf{e}_z \cdot \boldsymbol{\tau}^{(1)} \cdot \mathbf{e}_x = \sigma_{zx}^{(1)} \\
\tilde{t}_2 &= \mathbf{e}_z \cdot \boldsymbol{\tau}^{(1)} \cdot \mathbf{e}_y = \sigma_{yz}^{(1)}
\end{aligned} \tag{24}
$$

where $\mathbf{e}_x$, $\mathbf{e}_y$, and $\mathbf{e}_z$ are the unit base vectors in the Cartesian (x, y, and z) coordinates.

Similarly, in the sub-problem 2 (containing only 'microcrack 2'), it can be shown that the perturbed normal and shear stresses along the surfaces at the 'microcrack 1' location are

$$
\tilde{p}_1 = \sigma_{zz}^{(2)} \quad ; \quad \tilde{s}_1 = -\sigma_{zx}^{(2)} \quad ; \quad \tilde{t}_1 = \sigma_{yz}^{(2)} \tag{25}
$$

where symbolic representations similar to Eq. (23) and (24) have been employed:

$$
\boldsymbol{\tau}^{(2)} \equiv \boldsymbol{\tau}(\rho, \pi - \phi, z; p_2, -s_2, t_2) \tag{26}
$$

Eq. (24) together with (25) then leads to

$$
\left\{ \begin{array}{c} \tilde{p}_1 \\ \tilde{s}_1 \\ \tilde{t}_1 \\ \tilde{p}_2 \\ \tilde{s}_2 \\ \tilde{t}_2 \end{array} \right\} = \left[\begin{array}{cccccc} 0 & 0 & 0 & b_4^{(2)} & -c_4^{(2)} & d_4^{(2)} \\ 0 & 0 & 0 & -b_5^{(2)} & c_5^{(2)} & -d_5^{(2)} \\ 0 & 0 & 0 & b_6^{(2)} & -c_6^{(2)} & d_6^{(2)} \\ b_4^{(1)} & c_4^{(1)} & d_4^{(1)} & 0 & 0 & 0 \\ b_5^{(1)} & c_5^{(1)} & d_5^{(1)} & 0 & 0 & 0 \\ b_6^{(1)} & c_6^{(1)} & d_6^{(1)} & 0 & 0 & 0 \end{array} \right] \left\{ \begin{array}{c} p_1 \\ s_1 \\ t_1 \\ p_2 \\ s_2 \\ t_2 \end{array} \right\} \tag{27}
$$

For convenience in the following derivations, let us define

$$\mathbf{T}_{1-2} \equiv \begin{Bmatrix} p_1 \\ s_1 \\ t_1 \\ p_2 \\ s_2 \\ t_2 \end{Bmatrix} \quad ; \quad \mathbf{T}_{1-2}^{\infty} \equiv \begin{Bmatrix} p_1^{\infty} \\ s_1^{\infty} \\ t_1^{\infty} \\ p_2^{\infty} \\ s_2^{\infty} \\ t_2^{\infty} \end{Bmatrix} \quad ; \quad \tilde{\mathbf{T}}_{1-2} \equiv \begin{Bmatrix} \tilde{p}_1 \\ \tilde{s}_1 \\ \tilde{t}_1 \\ \tilde{p}_2 \\ \tilde{s}_2 \\ \tilde{t}_2 \end{Bmatrix} \tag{28}$$

and $\alpha \equiv$ the 6×6 matrix in Eq. (27). With these notations at hand, Eq. (27) can be rewritten as

$$\tilde{\mathbf{T}}_{1-2} = \alpha \cdot \mathbf{T}_{1-2} \tag{29}$$

Since $\mathbf{T}_{1-2} = \mathbf{T}_{1-2}^{\infty} + \tilde{\mathbf{T}}_{1-2}$, $\tilde{\mathbf{T}}_{1-2}$ can be solved from Eq. (29)

$$\tilde{\mathbf{T}}_{1-2} = \tilde{\mathbf{K}} \cdot \mathbf{T}_{1-2}^{\infty} \quad ; \quad \text{where} \quad \tilde{\mathbf{K}} \equiv \alpha \cdot (\mathbf{I} - \alpha)^{-1} \tag{30}$$

Further, we define $\tilde{\mathbf{T}} \equiv (\tilde{p}_1, \tilde{s}_1, \tilde{t}_1)^T$ and $\mathbf{K}_1 \equiv$ the first three *rows* of $\tilde{\mathbf{K}}$. Hence, from Eq. (30), the perturbed stresses on surfaces of a microcrack due to the existence of a second microcrack are:

$$\tilde{\mathbf{T}} = \mathbf{K}_1 \cdot \mathbf{T}_{1-2}^{\infty} \tag{31}$$

Finally, since the two microcracks under consideration are aligned, it can be easily shown that

$$\mathbf{T}_{1-2}^{\infty} \equiv \begin{Bmatrix} p_1^{\infty} \\ s_1^{\infty} \\ t_1^{\infty} \\ p_2^{\infty} \\ s_2^{\infty} \\ t_2^{\infty} \end{Bmatrix} = \begin{bmatrix} 0 & 0 & 1 & 0 & 0 & 0 \\ 0 & 0 & 0 & 0 & 0 & 1 \\ 0 & 0 & 0 & 0 & 1 & 0 \\ 0 & 0 & 1 & 0 & 0 & 0 \\ 0 & 0 & 0 & 0 & 0 & 1 \\ 0 & 0 & 0 & 0 & 1 & 0 \end{bmatrix} \begin{Bmatrix} \sigma_{xx}^{\infty} \\ \sigma_{yy}^{\infty} \\ \sigma_{zz}^{\infty} \\ \sigma_{xy}^{\infty} \\ \sigma_{yz}^{\infty} \\ \sigma_{zx}^{\infty} \end{Bmatrix} \equiv \mathbf{K}_2 \cdot \boldsymbol{\tau}^{\infty} \tag{32}$$

From Eq. (32) and (31), we conclude that the *average* perturbed stress $\tilde{\mathbf{T}}$ over surfaces of a microcrack is simply:

$$\tilde{\mathbf{T}} = \mathbf{K} \cdot \boldsymbol{\tau}^{\infty} \quad ; \quad \text{where} \quad \mathbf{K} \equiv \mathbf{K}_1 \cdot \mathbf{K}_2 \tag{33}$$

Substitution of Eq. (33) into (13) then renders realizations for $\langle \tilde{\mathbf{T}} \rangle$ in the previous section. Therefore, the *ensemble average* approach is completely defined. For non-aligned penny-shaped microcracks, more complicated (though analogous) derivations will be involved.

III.2.3. Some test problems for two-microcrack interaction

A number of test problems are considered in this section to examine the performance of the approximate analytical solutions presented in Sec. 2.2. These include normal and

shear loadings for two aligned *coplanar* or *stacked* penny-shaped microcracks. It is not our intention, however, to propose highly accurate analytical solutions to compute *local* stresses and stress intensity factors (SIFs) at all points on microcrack surfaces for a two-microcrack interaction problem. Instead, reasonably accurate *analytical average* perturbed stresses (in terms of elementary functions) over microcrack surfaces are sought in order to exploit the ensemble average approach. In fact, if one is interested in deterministic 3-D microcrack interaction, excellent *numerical* method has been proposed by Kachanov and Laures (1989). It is noted that key steps in Kachanov and Laures (1989) method also focus on the computation of *average* pairwise "transmission factors" and *average* tractions. Once average tractions become known, one can certainly compute *projected* local stresses and SIFs at any point on microcrack surfaces. In general, the simple analytical solutions presented in Sec. 2.2 are not as accurate as those proposed in Kachanov and Laures (1989). Nonetheless, the latter relies on extensive numerical computations of transmission factors for all points on microcrack surfaces and is therefore not employed here.

It is emphasized that, given an existing microcrack, the location of the second microcrack is *random* within the ensemble average framework. Although stress interactions between two moderately spaced random microcracks are not very strong, their cumulative effects are important due to high spatial probability. On the other hand, stress interactions between two closely spaced random microcracks are strong yet their spatial probability is lower. Therefore, contributions from both closely and moderately spaced microcracks should be accounted for in the ensemble average approach. The ensemble-average spacing of microcrack arrays, clearly, depends on microcrack concentration.

Case I: *Two equal-size coplanar microcracks under normal loading.* Though numerical results for SIFs are available for two coplanar microcracks under normal and shear loadings (Fabrikant (1987, 1989)), exact results for average tractions projected over microcrack surfaces are not documented. Nevertheless, Kachanov and Laures (1989) show that their results for SIFs are very close to those of Fabrikant (1987, 1989) for two equal-size coplanar microcracks. Therefore, the average tractions computed by Kachanov and Laures (1989) should be quite accurate in the case of *coplanar* microcracks. The ratios of perturbed vs. far-field average normal stresses (p/p^∞) are listed in Table 1 for various $l/2a$ values (the Poisson ratio $\nu = 0.25$). Here, l signifies the center-to-center distance between two microcracks and

$2a$ is the microcrack size. For example, $l/2a = 1.00025$ means that the smallest distance between microcrack tips is only $0.00025a$. The results reported in Kachanov and Laures (1989) and relative differences between the two results are also given in **Table 1** for comparison. From **Table 1**, it is clear that interaction renders average stress amplification. The effect of microcrack interaction decays as the distance between two microcracks increases. Moreover, the differences between our simple calculations and those of Kachanov and Laures (1989) are very small in general.

Case II: *Two equal-size coplanar microcracks under shear loading.* The ratios of perturbed vs. far-field average shear stresses (τ/τ^∞) are listed in **Table 2** for various $l/2a$ values (the Poisson ratio $\nu = 0.5$). From **Table 2**, it is seen again that interaction renders average stress amplification. The differences between our simple calculations and those of Kachanov and Laures (1989) are again rather small; see **Table 2**.

Case III: *Two equal-size stacked microcracks under normal loading.* The ratios of perturbed vs. far-field average normal stresses (p/p^∞) are listed in **Table 3** for various $l/2a$ values (the Poisson ratio $\nu = 0.25$). Obviously, from **Table 3**, interaction renders strong average stress *shielding*. The degree of shielding in this case is much stronger than the degree of amplification in Cases I or II. Fabrikant (1989) did not provide numerical results for SIFs nor average stresses for two stacked microcracks under normal or shear loadings. Therefore, exact results are not available. For comparison, the differences between our simple calculations and those of Kachanov and Laures (1989) are listed in **Table 3**. It is observed that the difference is not very significant if $l/2a$ is greater than 0.5. The difference increases as the two microcracks move closer, due to sharp variations of stress fields in the close neighborhood of interacting microcracks.

Case IV: *Two equal-size stacked microcracks under shear loading.* The ratios of perturbed vs. far-field average normal stresses (p/p^∞) are given in **Table 4** for various $l/2a$ values (the Poisson ratio $\nu = 0.25$). From **Table 4**, interaction renders average stress *shielding* when the distance l is small and very weak stress *amplification* when $l/2a > 0.5$. The differences between our simple calculations and those of Kachanov and Laures (1989) are small for $l/2a$ greater than 0.25; see **Table 4**.

Since pairwise microcrack interactions are random (probabilistic) within the framework of the ensemble average approach, the errors associated with the present approximate analysis should be statistically averaged over all possible realizations. Therefore, the (pairwise)

ensemble-average error of the present method should be small as long as the microcrack concentration is not too high.

III.3. Effective moduli of brittle solids with interacting microcracks

With the ensemble average framework and analytical pairwise interaction solutions at hand, we are now ready to construct the *ensemble-average* constitutive equations of brittle solids with many randomly located, interacting microcracks. By substituting Eq. (10) and (33) into (9) and taking the ensemble average, we arrive at

$$\langle \mathbf{T} \rangle = (\mathbf{K}_0 + f(\mathbf{x})\langle \mathbf{K} \rangle) \cdot \boldsymbol{\tau}^{\infty} \qquad (34)$$

where

$$\langle \mathbf{K} \rangle \equiv \int_{\Xi} \mathbf{K} \, d\mathbf{x}_1 = \int_{\Xi} \mathbf{K} r^2 \sin \psi \, dr d\psi d\theta \qquad (35)$$

In the foregoing equations, it is implicitly assumed that all microcracks are of equal size and of same orientation. In addition, the spherical coordinate system (r, ψ, θ) is used to describe the random location $(\mathbf{x}_1)$ of the second microcrack relative to the first random microcrack centered at $\mathbf{x}$. Note that ψ varies from 0 to π and θ ranges from 0 to 2π. If we normalize r with respect to the microcrack radius a (i.e., $\xi \equiv r/a$), then Eq. (35) can be recast as

$$\langle \mathbf{K} \rangle \equiv a^3 \langle \hat{\mathbf{K}} \rangle = a^3 \int_{\Xi} \mathbf{K} \xi^2 \sin \psi \, d\xi d\psi d\theta \qquad (36)$$

Combining Eq. (6), (34) and (36), we obtain the *local* ensemble-average damage-induced strain (at a typical point $\mathbf{x}$):

$$\langle \mathbf{e}^* \rangle(\mathbf{x}) = \langle \mathbf{S}^* \rangle(\mathbf{x}) \cdot \boldsymbol{\tau}^{\infty} \qquad (37)$$

Here the ensemble averaged, damage-induced *local* compliance has two components:

$$\langle \mathbf{S}^* \rangle(\mathbf{x}) = \langle \mathbf{S}^{*1} \rangle(\mathbf{x}) + \langle \mathbf{S}^{*2} \rangle(\mathbf{x}) \qquad (38)$$

where

$$\langle \mathbf{S}^{*1} \rangle(\mathbf{x}) = \frac{16(1-\nu^2)}{3E(2-\nu)} f(\mathbf{x}) a^3 \mathbf{g} \cdot \mathbf{K}_0$$

$$\langle \mathbf{S}^{*2} \rangle(\mathbf{x}) = \frac{16(1-\nu^2)}{3E(2-\nu)} f^2(\mathbf{x}) a^6 \mathbf{g} \cdot \langle \hat{\mathbf{K}} \rangle \qquad (39)$$

It is noteworthy that Eq. (39) actually reveals physical *nonlocal effects* in constitutive equations through the *ensemble averaging* process. That is, the stress-strain laws at a material point $\mathbf{x}$ within a RVE depend on the constitutive laws of *all neighboring* points. This is a *physical* nonlocal approach, at variance with *postulated* nonlocal theories due to Eringen and Edelen (1972).

To obtain *volume averaged* moduli due to microcracks within a RVE, one simply applies the volume-average operator to Eq. (38)–(39). As a consequence, we have

$$\overline{\langle S^* \rangle} \equiv \frac{1}{V} \int_V \langle S^* \rangle(x) \, dx = \frac{1}{V} \left[\int_V \langle S^{*1} \rangle(x) \, dx + \int_V \langle S^{*2} \rangle(x) \, dx \right] \tag{40}$$

where

$$\overline{\langle S^{*1} \rangle} = \frac{16(1 - \nu^2)}{3E(2 - \nu)} g \cdot K_0 \, a^3 \frac{\int_V f(x) \, dx}{V}$$

$$\overline{\langle S^{*2} \rangle} = \frac{16(1 - \nu^2)}{3E(2 - \nu)} g \cdot \langle \hat{K} \rangle \, a^6 \frac{\int_V f^2(x) \, dx}{V} \tag{41}$$

Let us assume that there are N microcracks in the RVE; i.e,

$$\int_V f(x) \, dx = N \tag{42}$$

Further, consider the case in which the variance of the PDF $(f(x))$ for locations of microcracks is *small* (e.g., uniform probability). We may therefore write

$$\int_V f^2(x) \, dx \simeq \frac{\left[\int_V f(x) \, dx \right]}{V} = \frac{N^2}{V} \tag{43}$$

Substitution of Eq. (42) and (43) into (41) then leads to

$$\overline{\langle S^{*1} \rangle} = \frac{16(1 - \nu^2)}{3E(2 - \nu)} g \cdot K_0 \, \omega$$

$$\overline{\langle S^{*2} \rangle} = \frac{16(1 - \nu^2)}{3E(2 - \nu)} g \cdot \langle \hat{K} \rangle \, \omega^2 \tag{44}$$

where

$$\omega \equiv \frac{Na^3}{V} \tag{45}$$

is the (volume-average) microcrack concentration parameter. It is noted that $\overline{\langle S^{*1} \rangle}$ actually corresponds to the first order contribution due to non-interacting microcracks; i.e., the simple Taylor's model is recovered. Moreover, $\overline{\langle S^{*2} \rangle}$ represents the second order contribution due to pairwise microcrack interaction.

Finally, the overall (volume-ensemble averaged) effective moduli for a microcrack weakened solid is obtained by adding the elastic compliance S^o to $\overline{\langle S \rangle}$:

$$\overline{\langle S \rangle} \equiv S^o + \overline{\langle S^{*1} \rangle} + \overline{\langle S^{*2} \rangle} \tag{46}$$

In particular, in the case of 3-D linear isotropic elasticity, $\mathbf{S}^o$ reads

$$\mathbf{S}^o = \frac{1}{E}\begin{bmatrix} 1 & -\nu & -\nu & 0 & 0 & 0 \\ -\nu & 1 & -\nu & 0 & 0 & 0 \\ -\nu & -\nu & 1 & 0 & 0 & 0 \\ 0 & 0 & 0 & 2(1+\nu) & 0 & 0 \\ 0 & 0 & 0 & 0 & 2(1+\nu) & 0 \\ 0 & 0 & 0 & 0 & 0 & 2(1+\nu) \end{bmatrix} \quad (47)$$

It is emphasized that the *local* macroscopic constitutive laws for a RVE are recovered by the volume averaging process.

III.4. Some numerical examples

In this section, some numerical examples involving aligned microcracks are presented to illustrate the proposed ensemble-volume average approach in three-dimension. In the first example, effects of microcrack interactions are neglected and the well-known Taylor's model is recovered. Subsequently, the proposed second order (in microcrack concentration) microcrack interaction model is implemented. Finally, we compare the results of the present approach with some existing methods, including the Taylor's model, the self-consistent method and the differential scheme. Closed microcrack contributions to compliances are neglected in this work.

III.4.1. Dilute non-interacting aligned microcracks

Let us consider the case in which effects of microcrack interactions are totally neglected. This can be done by simply dropping the term $\overline{\langle S^{\cdot 2}\rangle}$ in Eq. (46):

$$\overline{\langle S\rangle} = S^0 + \overline{\langle S^{\cdot 1}\rangle} \tag{48}$$

From Eq. (8), (11), and (44), we obtain

$$\overline{\langle S^{\cdot 1}\rangle} = \frac{16(1-\nu^2)\omega}{3E(2-\nu)} \begin{bmatrix} 0 & 0 & 0 & 0 & 0 & 0 \\ 0 & 0 & 0 & 0 & 0 & 0 \\ 0 & 0 & 2-\nu & 0 & 0 & 0 \\ 0 & 0 & 0 & 0 & 0 & 0 \\ 0 & 0 & 0 & 0 & 2 & 0 \\ 0 & 0 & 0 & 0 & 0 & 2 \end{bmatrix} \tag{49}$$

Combination of Eq. (47) and (49) then yields

$$\overline{\langle S\rangle} = \begin{bmatrix} S^0_{11} & S^0_{12} & S^0_{13} & 0 & 0 & 0 \\ S^0_{21} & S^0_{22} & S^0_{23} & 0 & 0 & 0 \\ S^0_{31} & S^0_{32} & \overline{S}_{33} & 0 & 0 & 0 \\ 0 & 0 & 0 & S^0_{44} & 0 & 0 \\ 0 & 0 & 0 & 0 & \overline{S}_{55} & 0 \\ 0 & 0 & 0 & 0 & 0 & \overline{S}_{66} \end{bmatrix} \tag{50}$$

where $1 = xx$, $2 = yy$, $3 = zz$, $4 = xy$, $5 = yz$, $6 = zx$ (Voigt's notation); S^0_{ij} components are given in (47), and

$$\overline{S}_{33} = S^0_{33} + S^{\cdot 1}_{33}$$

$$\overline{S}_{55} = S^0_{55} + S^{\cdot 1}_{55} \tag{51}$$

$$\overline{S}_{66} = S^0_{66} + S^{\cdot 1}_{66}$$

in which

$$S_{33}^{*1} \equiv \frac{16(1 - \nu^2)}{3E} \, \omega$$

$$S_{56}^{*1} = S_{66}^{*1} \equiv \frac{32(1 - \nu^2)}{3E(2 - \nu)} \, \omega \tag{52}$$

It is observed that only the three compliance components in Eq. (51) are changed due to the presence of randomly located, aligned, penny-shaped microcracks. One notes that Eq. (50)–(52) indeed recover the well-known Taylor's model. Further, the effective constitutive equations belong to the category of transverse isotropy. This is typical of *fiber breaks* in unidirectional reinforced fiber composites.

III.4.2. Aligned interacting penny-shaped microcracks

We now focus on the proposed ensemble-volume averaged, pairwise interaction model. For a given microcrack concentration ω, the overall effective moduli in Eq. (46) can be evaluated by carrying out the integration in Eq. (36). That is, one needs to perform integration for the matrix **K** over the active microcrack domain (ζ, ψ, θ). It is emphasized that the values of K decay rapidly as the distance between a pair of random microcracks increase. Therefore, compliance contributions due to remote integration region can be neglected.

The integration in Eq. (DC) can be effectively computed by the Gauss quadrature scheme with three independent variables – ζ, ψ and θ; see **Table 5** for convergence behavior. Our numerical experiments show that use of $\zeta_{max} = 20$ (or $r_{max} = 20a$) is quite acceptable; i.e., contributions from the $\zeta > 20$ domain can indeed be neglected. In **Table 5**, the minimum radius of integration for r (or ζ) is assumed to be $r_{min} = 2a$ (or $\zeta_{min} = 2$). The only *nonzero* components in $\langle \hat{\mathbf{K}} \rangle$ are simply $\langle \hat{K}_{13} \rangle$, $\langle \hat{K}_{26} \rangle$ and $\langle \hat{K}_{35} \rangle$ (the latter two are equal). It is observed that the normal component ($\langle \hat{K}_{13} \rangle$) is much greater than the shear components ($\langle \hat{K}_{26} \rangle$ and $\langle \hat{K}_{35} \rangle$). Furthermore, use of $r_{min} = 2a$ implies that the minimum allowable distance between any two microcrack centers is $2a$. The fore, according to the "face-center cubic" calculation, the maximum allowable ω is $1/4\sqrt{2} \simeq 0.1768$ for $r_{min} = 2a$. Note that the maximum allowable microcrack density would be 0.741 if ω is defined as $4\pi Na^3/3V$ (Budiansky and O'Connell, 1976).

To achieve higher maximum permissible microcrack densities, various minimum radii of integration r_{min} are used to compute $\langle \hat{\mathbf{K}} \rangle$; see **Table 6** for details. The value of ζ_{max} is

chosen as 20.0 in **Table 6**. We observe significant increases in both $\langle \hat{K}_{13} \rangle$ and $\langle \hat{K}_{26} \rangle$ as ζ_{min} decreases. The maximum microcrack concentration ω corresponding to the $\zeta_{min} = 1.1a$ case is found to be 1.0627 (or 4.451 if the definition in Budiansky and O'Connell (1976) is employed). It is emphasized that **Table 6** is *not* a summary of convergence behavior, but a display of $\langle \hat{K} \rangle$ for different maximum allowable microcrack densities.

For convenience, let us define $\langle \hat{K}_{13} \rangle \equiv \hat{k}_1$ and $\langle \hat{K}_{26} \rangle = \langle \hat{K}_{35} \rangle \equiv \hat{k}_2$. Therefore, according to Eq. (8) and (44), we obtain

$$\overline{\langle \mathbf{S}^{\cdot 2} \rangle} = \frac{16(1 - \nu^2)}{3E(2 - \nu)} \, \omega^2 \begin{bmatrix} 0 & 0 & 0 & 0 & 0 & 0 \\ 0 & 0 & 0 & 0 & 0 & 0 \\ 0 & 0 & (2-\nu)\hat{k}_1 & 0 & 0 & \\ 0 & 0 & 0 & 0 & 0 & 0 \\ 0 & 0 & 0 & 0 & 2\hat{k}_2 & 0 \\ 0 & 0 & 0 & 0 & 0 & 2\hat{k}_2 \end{bmatrix} \tag{53}$$

Adding Eq. (53) to (50), we thus arrive at the expression for overall effective complaince with second order microcrack interaction. Apart form the three compliance components $\overline{\langle S_{33} \rangle}$, $\overline{\langle S_{55} \rangle}$ and $\overline{\langle S_{66} \rangle}$, it is seen that all other components are identical to the elastic components. In particular, the three compliance components which change under microcrack interaction take the following explicit forms:

$$\overline{\langle S_{33} \rangle} = S_{33}^0 + \frac{16(1 - \nu^2)}{3E} \left(\omega + \hat{k}_1 \omega^2 \right)$$

$$\overline{\langle S_{55} \rangle} = \overline{\langle S_{66} \rangle} = S_{55}^0 + \frac{32(1 - \nu^2)}{3E(2 - \nu)} \left(\omega + \hat{k}_2 \omega^2 \right) \tag{54}$$

III.4.3. Comparison with some existing methods

The effects of fiber breaks and aligned penny-shaped microcracks on the stiffness of unidirectional fiber composites have been studied extensively in the literature. We refer to Laws and Dvorak (1987) for excellent presentation by using the self-consistent method and the differential scheme. It is noted that, in Laws and Dvorak (1987), the microcrack density is defined as $\alpha \equiv 8Na^3/V$; i.e., their α is equal to 8ω in this paper. The maximum microcrack concentration considered in Laws and Dvorak (1987) is $\omega = \alpha/8 = 0.125$. The macroscopic (overall) material behavior is, not surprisingly, transversely isotropic. It should be realized that the Taylor's model, the self-consistent method and the differential scheme

all belong to the category of "effective medium" approaches. Namely, theses methods do *not* depend on the distributions of microcrack locations at all.

In the following numerical computations, the Young's modulus E_0 is taken as 0.5 MPa and the shear modulus G_0 as 0.2 MPa ($\nu = 0.25$) for the virgin matrix material. The overall (ensemble-volume averaged) longitudinal normal and shear compliances, $\overline{\langle S_{33} \rangle}$ and $\overline{\langle S_{55} \rangle}$, are plotted against the microcrack concentration parameter ω in Figures 2 and 3, respectively. The values of $\hat{k}_1$ and $\hat{k}_2$ in Eq. (54) are taken as 1.049792 and 0.355988, respectively, which correspond to $\zeta_{min} = 1.1$ (i.e., the maximum allowable density $\omega = 1.0627$). Note that, once more, $\omega = 1$ corresponds to $\alpha = 8$ in Laws and Dvorak (1987). For comparison, the results obtained by using the Taylor's model, the self-consistent method and the differential scheme are also displayed in Figures 2 and 3. We would like to comment that: (a) the Taylor's model is really suitable for dilute microcrack concentrations; (b) the self-consistent method and the differential scheme are suitable for low or moderate ω; and (c) the proposed statistical pairwise microcrack interaction model is suitable for moderately high (not extremely high) ω.

Figures 4 and 5 show the effect of microcrack density ω on the normalized longitudinal Young's modulus E_L/E_0 and shear modulus G_L/G_0 for four different models. We have employed the standard notation: $E_L \equiv \overline{\langle S_{33} \rangle}$ and $G_L \equiv \overline{\langle S_{55} \rangle}$. In addition, it is straightforward to express the normalized moduli in Figures 4 and 5 as follows for the Taylor's model

$$\frac{E_L}{E_0} = \frac{1}{1 + 5\omega} \quad ; \quad \frac{G_L}{G_0} = \frac{1}{1 + 2.28571\omega} \tag{55}$$

and for the present model

$$\frac{E_L}{E_0} = \frac{1}{1 + 5\omega(1 + 1.05\omega)} \quad ; \quad \frac{G_L}{G_0} = \frac{1}{1 + 2.28571\omega(1 + 0.356\omega)} \tag{56}$$

III.5. Higher order ensemble-average formulation of microcrack interaction

The statistical micromechanical model presented so far is based on the concept of *pairwise* microcrack interaction. This pairwise microcrack interaction mechanism essentially corresponds to a *second order* damage theory since it involves terms of ω^2. The classical Taylor's model, on the other hand, is a first order microcrack theory since it involves only terms of ω. Within the context of the ensemble-volume average approach, one can systematically incorporate many-microcrack interaction mechanisms into the proposed ensemble average framework (see Ju and Chen (1990. . In essence, one needs to re-derive the ensemble average of the **perturbation** in local stress field due to n-microcrack *interactions* $(n \geq 3)$; see Eq. (9)-(12). That is, by formulating and computing higher order corrections on local stress fields $\langle T \rangle$ due to neighboring microcrack interactions, one can construct higher oder microcrack interaction models.

To illustrate the foregoing statements, let us consider a three-microcrack (third order in ω) interaction mechanism within the proposed framework of the ensemble-volume average approach. For simplicity, we assume that all microcracks are aligned and of equal size. Following the definitions and assumptions described in Section 2.1, one can recapitulate the local ensemble stress perturbation in Eq. (9):

$$\langle \tilde{T} \rangle + \langle \tilde{\tilde{T}} \rangle \equiv \langle \left\{ \begin{array}{c} \tilde{p} \\ \tilde{s} \\ \tilde{t} \end{array} \right\} \rangle + \langle \left\{ \begin{array}{c} \tilde{\tilde{p}} \\ \tilde{\tilde{s}} \\ \tilde{\tilde{t}} \end{array} \right\} \rangle \tag{57}$$

where $\langle \tilde{T} \rangle$ is the first order local ensemble stress perturbation due to pairwise microcrack interactions (see Eq. (9), (12)), and $\langle \tilde{\tilde{T}} \rangle$ is the second order local ensemble stress perturbation due to the higher (third) order microcrack interactions. In particular, $\langle \tilde{\tilde{T}} \rangle$ can be expressed as (cf. Eq. (12))

$$\langle \tilde{\tilde{T}} \rangle = \int_{\Xi} \langle \tilde{\tilde{T}} \rangle (x; x_1 | x_2) f(x_2 | x; x_1) \, dx_2 \tag{58}$$

Here, $\langle \tilde{\tilde{T}} \rangle (x; x_1 | x_2)$ is the second order ensemble-average *stress perturbation* of a microcrack centered at x, given a microcrack centered at x_1, over a subclass of realizations which have a microcrack centered at x_2. Further, $f(x_2 | x; x_1)$ is the conditional probability density function (PDF) for finding a microcrack centered at x_2 given two microcracks fixed at x and at x_1. The conditional PDF $f(x_2 | x; x_1)$ can be further simplified to $f(x)$ by the assumptions of local

homogeneity and reasonable randomness (i.e. statistical independence). The active (open) integration domain Ξ depends on loading conditions and ranges of microcrack interactions.

The solutions of $\tilde{T}$ (or the total stress vector T) for a system of three (or many) arbitrarily located microcracks were previously investigated by Kachanov and Laures (1989). In particular, Kachanov and Laures (1989) pursued extensive numerical computations to obtain the "transmission factors" for local stresses. Alternatively, one can derive approximate analytical closed-form solutions for $\tilde{T}$ by following the procedures presented in Sec. 2.2 of this paper.

For clarity, let us express T and $\langle e^* \rangle(x)$ as follows (cf. Eq. (34), (37) and (38), assuming local homogeneity and reasonable randomness):

$$\langle T \rangle = \langle T^\infty + \tilde{T} + \tilde{\tilde{T}} \rangle = (K_0 + f(x)\langle K \rangle + f^2(x)\langle K' \rangle) \cdot \tau^\infty \qquad (59)$$

$$\langle e^* \rangle(x) = \left\{ \langle S^{*1} \rangle(x) + \langle S^{*2} \rangle(x) + \langle S^{*3} \rangle(x) \right\} \cdot \tau^\infty \equiv \langle S^* \rangle(x) \cdot \tau^\infty \qquad (60)$$

where $\tilde{\tilde{T}} \equiv K' \cdot \tau^\infty$ and (cf. Eq. (39))

$$\langle S^{*1} \rangle(x) \equiv \frac{16(1 - \nu^2)}{3E(2 - \nu)} f(x) a^3 g \cdot K_0 \qquad (61)$$

$$\langle S^{*2} \rangle(x) \equiv \frac{16(1 - \nu^2)}{3E(2 - \nu)} f^2(x) a^6 g \cdot \langle \hat{K} \rangle \qquad (62)$$

$$\langle S^{*3} \rangle(x) \equiv \frac{16(1 - \nu^2)}{3E(2 - \nu)} f^3(x) a^9 g \cdot \langle \hat{K}' \rangle \qquad (63)$$

In Eq. (63), we have defined $\langle \hat{K}' \rangle \equiv 1/a^6 \langle K' \rangle$. It is emphasized that both K_0 and $\hat{K}$ are expressed *explicitly* in *closed-form* formulas. Similarly, $\hat{K}'$ (or $\tilde{\tilde{T}}$) can also be constructed in closed-form as follows. One starts by expanding Eq. (14) into nine linear equations with $j = 1, 2, 3$. Then, one obtains expressions similar to Eq. (22), with the understanding that permutations 1-2, 2-3, 3-1 are involved. Eq. (24) in Sec. 2.2 is modified to include the third microcrack's contribution to stress perturbations. Subsequently, Eq. (27) is expanded to a 9 by 9 system with α denoting a 9 by 9 coefficient matrix. Therefore, we arrive at explicit formulas similar to Eq. (30)–(33); and $\hat{K}'$, $\tilde{\tilde{T}}$ can be expressed in closed-form as in the two-microcrack interaction problem. Finally, it is noted that the computation of $\langle \hat{K}' \rangle$ involves integration over the domain of all possible positions of two active neighboring microcracks (cf. Eq. (36)).

Following the standard procedures presented in Sec. 3, it can be shown that (S^{*3}) in Eq. (39) introduces the third order terms (in ω^3) to overall compliance due to third order microcrack interactions. Therefore, a third order statistical micromechanical model can be actually constructed. By repeating the foregoing procedures, we can formulate a complete (though very complicated) hierarchical family of statistical microcrack theories of arbitrary (desired) orders.

III.6. Conclusions

An innovative three-dimensional statistical micromechanical theory for microcrack-weakened brittle solids is presented based on the concepts of ensemble-volume average and pairwise microcrack interaction. A physically *"nonlocal"* description of the material behavior can be obtained during the *ensemble average* process. The overall compliances of microcrack-weakened brittle solids are derived by performing ensemble-volume averaged integration over the entire domain of a representative unit cell. To account for microcrack interaction effects, the ensemble average integration is performed over a finite "interaction radius". The proposed approach is fundamentally different from existing effective medium methods which do not depend on locations and configurations of microcracks, Further, the proposed microcrack interaction framework does not require the use of Monte Carlo simulation. Some numerical examples are given to illustrate the proposed model. The resulting predictions are compared with other existing methods. Higher order microcrack interaction formulation is also briefly presented.

III.7. References

1. BATCHELOR, G. K., (1970), "The stress system in a suspension of force-free particles", *J. Fluid Mech.*, vol. 41, pp. 545–570.

2. BATCHELOR, G. K. AND GREEN, J. T., (1972), "The determination of the bulk stress in a suspension of spherical particles to order c^{2}", *J. Fluid Mech.*, vol. 56, part 3, pp. 401–427.

3. BENVENISTE, Y., (1986), "On the Mori-Tanaka's method in cracked bodies", *Mech. Res. Comm.*, vol. 13, pp. 193–201.

4. BUDIANSKY, B. AND O'CONNELL, R. J., (1976), "Elastic moduli of a cracked solid", *Int. J. Solids & Struct.*, vol. 12, pp. 81–97.

5. CHEN, H. S. AND ACRIVOS, A., (1978a), "The solution of the equations of linear elasticity for an infinite region containing two spherical inclusions", *Int. J. Solids & Struct.*, vol. 14, pp. 331–348.

6. CHEN, H. S. AND ACRIVOS, A., (1978b), "The effective elastic moduli of composite materials containing spherical inclusions at non-dilute concentrations", *Int. J. Solids & Struct.*, vol. 14, pp. 349–364.

7. CHRISTENSEN, R. M., (1990), "A critical evaluation for a class of micromechanics models", *J. Mech. Phys. Solids*, vol. 38, no. 3 pp. 379–404.

8. CHRISTENSEN, R. M. AND LO, K. H., (1979), "Solutions for effective shear properties in three phase sphere and cylinder models", *J. Mech. Phys. Solids*, vol. 27, pp. 315–330.

9. CHUDNOVSKY, A., DOLGOPOLSKY, A. AND KACHANOV, M., (1987a), "Elastic interaction of a crack with a microcrack array–I. formulation of the problem and general form of the solution", *Int. J. Solids & Struct.*, vol. 23, no. 1, pp. 1–10.

10. CHUDNOVSKY, A., DOLGOPOLSKY, A. AND KACHANOV, M., (1987b), "Elastic interaction of a crack with a microcrack array–II. Elastic solution for two crack configurations", *Int. J. Solids & Struct.*, vol. 23, no. 1, pp. 11–21.

11. ERINGEN, A. C. AND EDELEN, D. G. B., (1972), "On nonlocal elasticity", *Int. J. Eng. Sci.*, vol. 10, pp. 233–248.

12. FABRIKANT, V. I., (1987), "Close interaction of coplanar circular cracks in an elastic medium", *Acta Mechanica*, vol. 67, pp. 39-59.

13. FABRIKANT, V. I., (1989) "Applications of potential theory in mechanics: a selection of new results", Kluwer Academic Publishers, Dordrecht, The Netherlands.

14. FANELLA, D. AND KRAJCINOVIC, D., (1988), "A micromechanical model for concrete in compression", *Eng. Fract. Mech.*, vol. 29, no. 1, pp. 49–66.

15. HASHIN, Z. AND SHTRIKMAN, S., (1962), "On some variational principles in anisotropic and nonhomogeneous elasticity", *J. Mech. Phys. Solids*, vol. 10, pp. 335–342.

16. HASHIN, Z. AND SHTRIKMAN, S., (1963), "A variational approach to the theory of the elastic behavior of multiphase materials", *J. Mech. Phys. Solids*, vol. 11, pp. 127–140.

17. HASHIN, Z., (1988), "The differential scheme and its application to cracked materials", *J. Mech. Phys. Solids*, vol. 36, pp. 719–734.

18. HILL, R., (1965), "A self-consistent mechanics of composite materials", *J. Mech. Phys. Solids*, vol. 13, pp 213–222.

19. HINCH. E. J., (1977), "An averaged-equation approach to particle interactions in a fluid suspension", *J. Fluid Mech.*, vol. 83, pp. 695–720.

20. HORI, M. AND NEMAT-NASSER, S., (1987), "Interacting micro-cracks near the tip in the process zone of a macro-crack", *J. Mech. Phys. Solids*, vol. 35, pp. 601–629.

21. HORII, H. AND NEMAT-NASSER, S., (1983), "Overall moduli of solids with microcracks: load-induced anisotropy", *J. Mech. Phys. Solids*, vol. 331, pp. 155–171.

22. HORII, H. AND NEMAT-NASSER, S., (1985), "Elastic fields of interacting inhomogeneities", *Int. J. Solids & Struct.*, vol. 21, pp. 731–745.

23. HORII, H. AND SAHASAKMONTRI, K., (1990), "Mechanical properties of cracked solids: validity of the self-consistent method", in *Micromechanics and Inhomogeneity*, ed. by G. J. Weng, M. Taya and H. Abe, pp. 137–159, Springer-Verlag, New York.

24. HUDSON, J. A., (1980), "Overall properties of a cracked solid", *Math. Proc. Camb. Phil. Soc.*, vol. 88, pp. 371–384.

25. HUDSON, J. A., (1981), "Wave speeds and attenuation of elastic waves in material containing cracks", *Geophys. J. R. astr. Soc.*, vol. 64, pp. 133–150.

26. HUDSON, J. A., (1986), "A higher order approximation to the wave propagation constants for a cracked solid", *Geophys. J. R. astr. Soc.*, vol. 87, pp. 265–274.

27. JU, J. W., (1990), "A micromechanical damage model for uniaxially reinforced composites weakened by interfacial arc microcracks", *J. Appl. Mech.*, ASME, accepted for publication.

28. JU, J. W., (1991), "On two-dimensional self-consistent micromechanical damage models for brittle solids", *Int. J. Solids & Struct.*, vol. 27, no. 2, pp. 227–258.

29. JU, J. W. AND CHEN, T. M., (1990a), "On two-dimensional statistical micromechanical damage models for brittle solids with interacting microcracks. Part I : General formulations", *J. Appl. Mech.*, submitted for publication, Oct. 1990.

30. JU, J. W. AND CHEN, T. M., (1990b), "On two-dimensional statistical micromechanical damage models for brittle solids with interacting microcracks. Part II : Evolutionary models", *J. Appl. Mech.*, submitted for publication, Oct. 1990.

31. JU, J. W. AND LEE, X., (1991), "On three-dimensional self-consistent micromechanical damage models for brittle solids. Part I: Tensile loadings", *J. Eng. Mech.*, vol. 117, no. 7, to appear July 1991.

32. KACHANOV, M., (1987), "Elastic solids with many cracks: a simple method of analysis", *Int J. Solids & Struct.*, vol. 23, pp. 23–43.

33. KACHANOV, M. AND MONTAGUT, E., (1986), "Interaction of a crack with certain microcrack arrays", *Eng. Fracture Mech.*, vol. 25, pp. 625–636.

34. KACHANOV, M. AND LAURES, J.-P., (1989), "Three-dimensional problems of strongly interacting arbitrarily located penny-shaped cracks", *Int. J. of Fract.*, vol. 41, pp. 289–313.

35. KRAJCINOVIC, D., (1989), "Damage mechanics", *Mech. Mater.*, vol. 8, no. 2-3 (Dec. 1989), pp. 117–197.

36. KRAJCINOVIC, D. AND FANELLA, D., (1986), "A micromechanical damage model for concrete", *Eng. Fract. Mech.*, vol. 25, pp. 585–596.

37. KRAJCINOVIC, D. AND SUMARAC, D., (1989), "A mesomechanical model for brittle deformation processes: part I", *J. Appl. Mech.*, vol. 56, pp. 51–62.

38. LAURES, J.-P. AND KACHANOV, M., (1990), "Three-dimensional interactions of a crack front with arrays of penny shaped microcracks", *Int. J. Fract.*, to appear.

39. LAWS, N. AND DVORAK, G. J., (1987), "The effect of fiber breaks and aligned penny-shaped cracks on the stiffness and energy release rates in unidirectional composites", *Int. J. Solids & Struct.*, vol. 23, no. 9, pp. 1269–1283.

40. LEE, X. AND JU, J. W., (1991), "On three-dimensional self-consistent micromechanical damage models for brittle solids. Part II: Compressive loadings", *J. Eng. Mech.*, vol. 117, no. 7, to appear July, 1991.

41. McLAUGHLIN, R., (1977), "A study of the differential scheme for composite materials", *Int. J. Engng. Sci.*, vol. 15, pp. 237–244.

42. MONTAGUT, E. AND KACHANOV, M., (1988), "On modeling a microcracked zone by weakened elastic material and on statistical aspects of crack-microcrack interactions", *Int. J. Fract.*, vol. 37. R 55–R 62.

43. MORI, T. AND TANAKA, K., (1973), "Average stress in matrix and average elastic energy of materials with misfitting inclusions", *Acta Metallurgica*, vol. 21, pp. 571–574.

44. NEMAT-NASSER, S. AND HORI, M., (1990), "Elastic solids with microdefects", in *Micromechanics and Inhomogeneity*, pp. 297–320, ed. by G. J. Weng, M. Taya and H. Abe, Springer-Verlag, New York.

45. ROSCOE, R. A., (1952), "The viscosity of suspensions of rigid spheres", *Brit. J. Appl. Phys.*, vol. 3, pp. 267–269.

46. ROSCOE, R. A., (1973), "Isotropic composites with elastic or viscoelastic phases: general bounds for the moduli and solutions for special geometries", *Rheol. Acta*, vol. 12, pp. 404–411.

47. SAYERS, C. M. AND KACHANOV, M., (1991), "A simple technique for finding effective elastic constants of cracked solids for arbitrary crack orientation statistics", *Int. J. Solids & Struct.*, vol. 27, no. 6, pp. 671–680.

48. SUMARAC, D. AND KRAJCINOVIC, D., (1987), "A self-consistent model for microcrack-weakened solids", *Mech. Mater.*, vol. 6, pp. 39–52.

49. SUMARAC, D. AND KRAJCINOVIC, D., (1989), "A mesomechanical model for brittle deformation processes: part II", *J. Appl. Mech.*, vol. 56, pp. 57–62.

50. WILLIS, J. R. AND ACTON, J. R., (1976), "The overall elastic moduli of a dilute suspension of spheres", *Quart. J. Mech. Appl. Math.*, vol. 29, part 2, pp. 163–177.

51. ZHAO, Y. H., TANDON, G. P. AND WENG, G. J., (1989), "Elastic moduli for a class of porous materials", *Acta Mechanica*, vol. 76, pp. 105–130.

Table 1. Two equal-size coplanar microcracks under normal loading ($\nu = 0.25$)

$l/2a$	Present	Kachanov	Difference(%)
1.00025	1.0354	1.0837	4.46
1.005	1.0348	1.0779	4.00
1.05	1.0296	1.0529	2.21
1.1	1.0251	1.0398	1.41
1.15	1.0215	1.0315	0.97
1.25	1.0161	1.0214	0.52
1.5	1.0088	1.0104	0.16
2.0	1.0035	1.0038	0.03
2.5	1.0018	1.0019	0.01

Table 2. Two equal-size coplanar microcracks under shear loading ($\nu = 0.5$)

$l/2a$	Present	Kachanov	Difference(%)
1.005	1.0681	1.1017	3.05
1.05	1.0580	1.0703	1.15
1.25	1.0317	1.0292	0.24
1.5	1.0174	1.0144	0.30
1.75	1.0106	1.0084	0.22
2.0	1.0070	1.0054	0.16
2.5	1.0035	1.0026	0.09
3.5	1.0013	1.0006	0.07

Table 3. Two equal-size stacked microcracks under normal loading ($\nu = 0.25$)

$l/2a$	Present	Kachanov	Difference(%)
0.05	0.5004	0.5583	10.37
0.25	0.5383	0.6689	19.52
0.35	0.5836	0.7158	18.47
0.5	0.6667	0.7777	14.27
0.75	0.7928	0.8562	7.40
1.0	0.8754	0.9073	3.52
1.5	0.9505	0.9588	0.87

Table 4. Two equal-size stacked microcracks under shear loading ($\nu = 0.25$)

$l/2a$	Present	Kachanov	Difference(%)
0.05	0.5549	0.6613	16.09
0.25	0.8214	0.8886	7.56
0.5	1.0002	0.9837	1.68
0.75	1.0233	1.0053	1.79
1.0	1.0180	1.0084	0.95
1.25	1.0120	1.0072	0.48
1.5	1.0080	1.0055	0.25
2.0	1.0039	1.0031	0.08
2.5	1.0021	1.0026	0.05

Table 5. Convergence behavior of $\langle \hat{K} \rangle$ vs. ξ_{max} (given $\xi_{min} = 2$)

$\xi_{max} = r_{max}/a$	$\langle \hat{K}_{13} \rangle$	$\langle \hat{K}_{26} \rangle = \langle \hat{K}_{35} \rangle$
4.0	0.150807	0.059503
6.0	0.168554	0.066656
8.0	0.173029	0.068467
10.0	0.174644	0.069121
20.0	0.176139	0.069728
40.0	0.176327	0.069804
80.0	0.176351	0.069828
160.0	0.176354	0.069829
320.0	0.176354	0.069829
640.0	0.176354	0.069829

Table 6. Numerical integration of $\langle \hat{\mathbf{K}} \rangle$ for different ξ_{min} (given $\xi_{max} = 20$)

$\xi_{min} = r_{min}/a$	$\langle \hat{K}_{13} \rangle$	$\langle \hat{K}_{26} \rangle = \langle \hat{K}_{35} \rangle$
2.0	0.176139	0.069728
1.75	0.305726	0.105974
1.5	0.601154	0.195689
1.25	0.850189	0.281202
1.125	0.975302	0.327491
1.1	1.049792	0.355988

III.8. Appendix I: Parameters for Eq. (22)

The parameters b_i, c_i and d_i in Eq. (22) can be shown to be:

$$b_1 = \frac{2}{\pi}\left[(1+2\nu)k_1 + \frac{az^2}{g_2}k_2\right]$$

$$b_2 = \frac{2}{\pi}ag_3^2\left[(1-2\nu)k_1 + \frac{z^2}{g_2}k_3\right]\cos 2\phi$$

$$b_3 = \frac{2}{\pi}\left[k_1 - \frac{az^2}{g_2}k_2\right]$$

$$b_4 = \frac{2}{\pi}ag_3^2\left[(1-2\nu)k_1 + \frac{z^2}{g_2}k_3\right]\sin 2\phi \qquad (64)$$

$$b_5 = -\frac{2}{\pi}zg_2g_3k_4\sin\phi$$

$$b_6 = -\frac{2}{\pi}zg_2g_3k_4\cos\phi$$

$$c_1 = f_3\cos\phi$$

$$c_2 = f_4\cos\phi + f_5\cos 3\phi + f_6(\cos\phi + \cos 3\phi)$$

$$c_3 = f_4\sin\phi + f_5\sin 3\phi + f_6(\sin 3\phi + \sin\phi)$$

$$c_4 = -2f_6\cos\phi \qquad (65)$$

$$c_5 = f_7 + f_8\cos 2\phi$$

$$c_6 = f_8\sin 2\phi$$

$$d_1 = f_3\sin\phi$$

$$d_2 = -f_4\sin\phi + f_5\sin 3\phi + f_6(\sin 3\phi - \sin\phi)$$

$$d_3 = f_4\cos\phi - f_5\cos 3\phi + f_6(\cos\phi - \cos 3\phi)$$

$$d_4 = -2f_6\sin\phi \qquad (66)$$

$$d_5 = f_8\sin 2\phi$$

$$d_6 = f_7 - f_8\cos 2\phi$$

where

$$f_1 = \frac{g_1}{g_5}$$

$$f_2 = \frac{g_2}{g_5}$$

$$f_3 = \frac{8}{\pi(2-\nu)} \left[-2(1+\nu)a g_3 f_1 + z g_2 g_3 k_4 \right]$$

$$f_4 = -\frac{8(1-\nu)}{\pi(2-\nu)} a g_3 f_1$$

$$f_5 = -\frac{8}{\pi(2-\nu)} z g_3 f_2 g_4^2 \tag{67}$$

$$f_6 = \frac{2}{\pi(2-\nu)} z g_2 g_3 k_4$$

$$f_7 = \frac{2}{\pi} \left(k_1 + \frac{1}{2-\nu} z g_1 k_2 \right)$$

$$f_8 = \frac{2}{\pi(2-\nu)} g_3^2 (\nu a f_2 + z g_1 k_3)$$

$$g_1 = (a^2 - l_1^2)^{1/2}$$

$$g_2 = (l_2^2 - a^2)^{1/2}$$

$$g_3 = \frac{l_1}{l_2} \tag{68}$$

$$g_4 = \frac{a}{l_2}$$

$$g_5 = l_2^2 - l_1^2$$

$$k_1 = a f_2 - \sin^{-1}(g_4)$$

$$k_2 = \frac{l_1^4 + a^2(2a^2 + 2z^2 - 3\rho^2)}{g_5^3}$$

$$k_3 = \frac{a^2(6l_2^2 - 2l_1^2 + \rho^2) - 5l_2^4}{g_5^3} \tag{69}$$

$$k_4 = \frac{a^2(4l_2^2 - 5\rho^2) + l_1^4}{g_5^3}$$

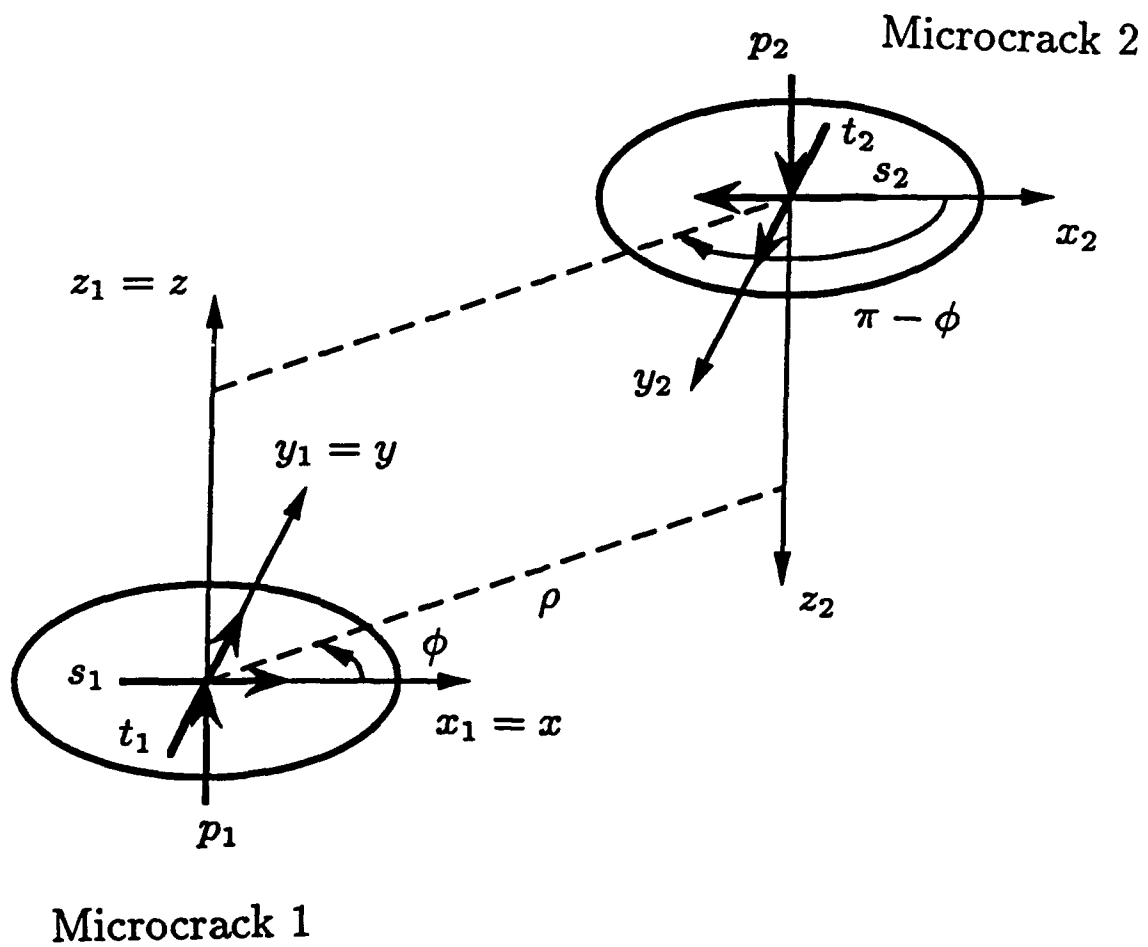## III.9. Figure captions

Figure 1.   Coordinate systems for two microcracks.
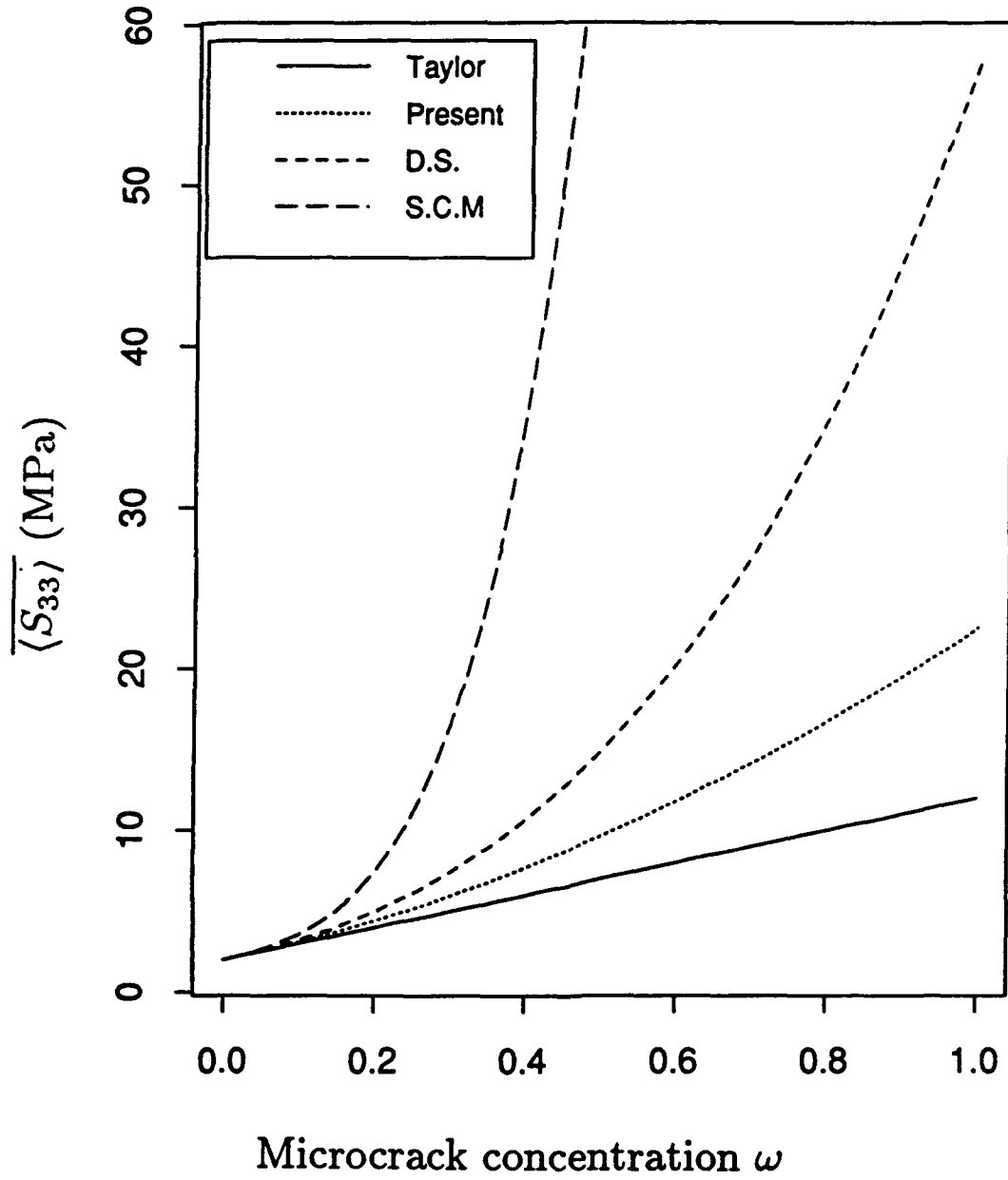
Figure 2.   Comparison of overall longitudinal normal compliance $\overline{\langle S_{33}\rangle}$.
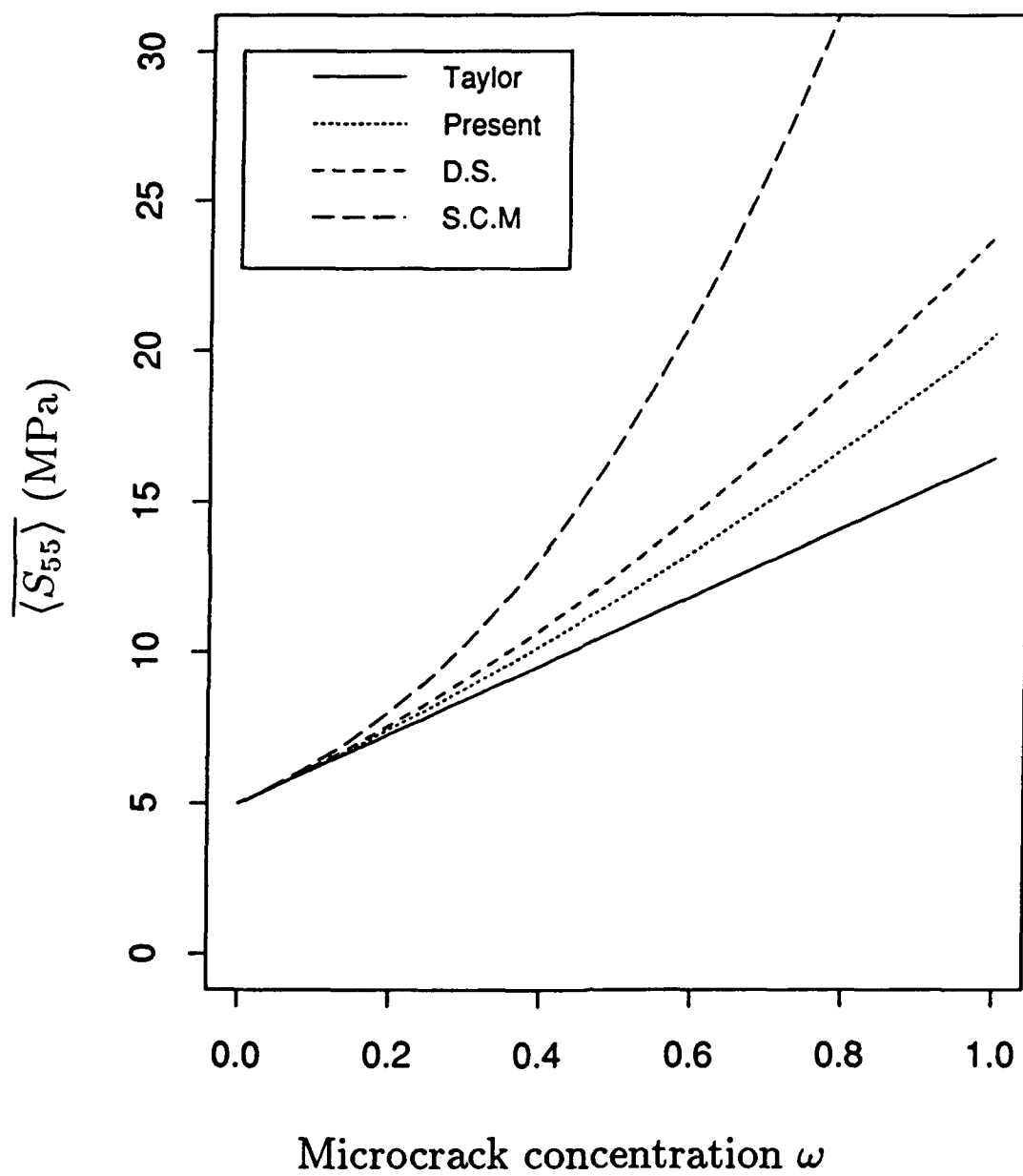
Figure 3.   Comparison of overall longitudinal shear compliance $\overline{\langle S_{55}\rangle}$.

Figure 4.   Comparison of normalized longitudinal Young's modulus.

Figure 5.   Comparison of normalized longitudinal shear modulus.

Figure 1. Coordinate systems for two microcracks.

Figure 2. Comparison of overall longitudinal normal compliance $\overline{\langle S_{33} \rangle}$.

Figure 3. Comparison of overall longitudinal shear compliance $\overline{\langle S_{55} \rangle}$.
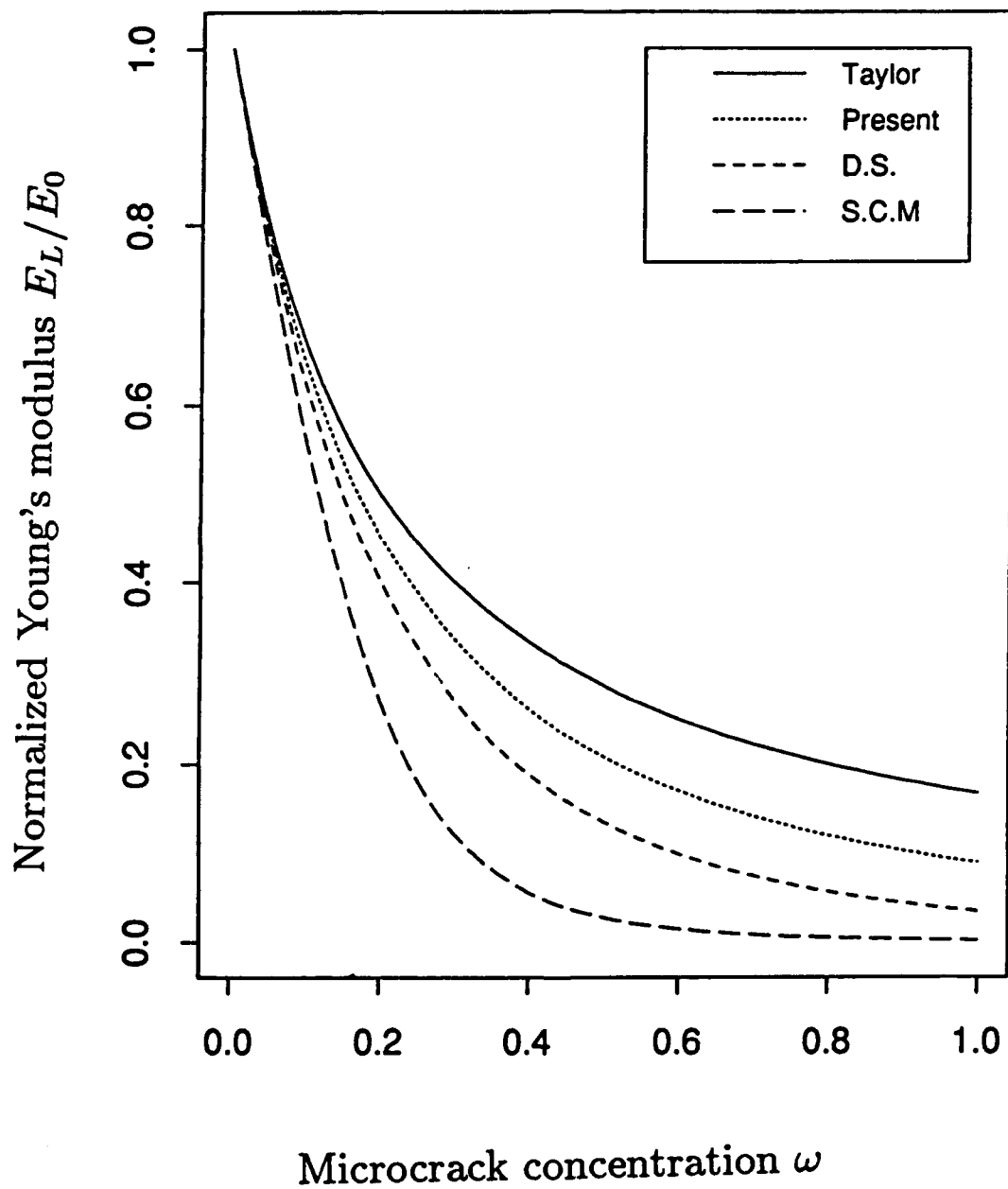
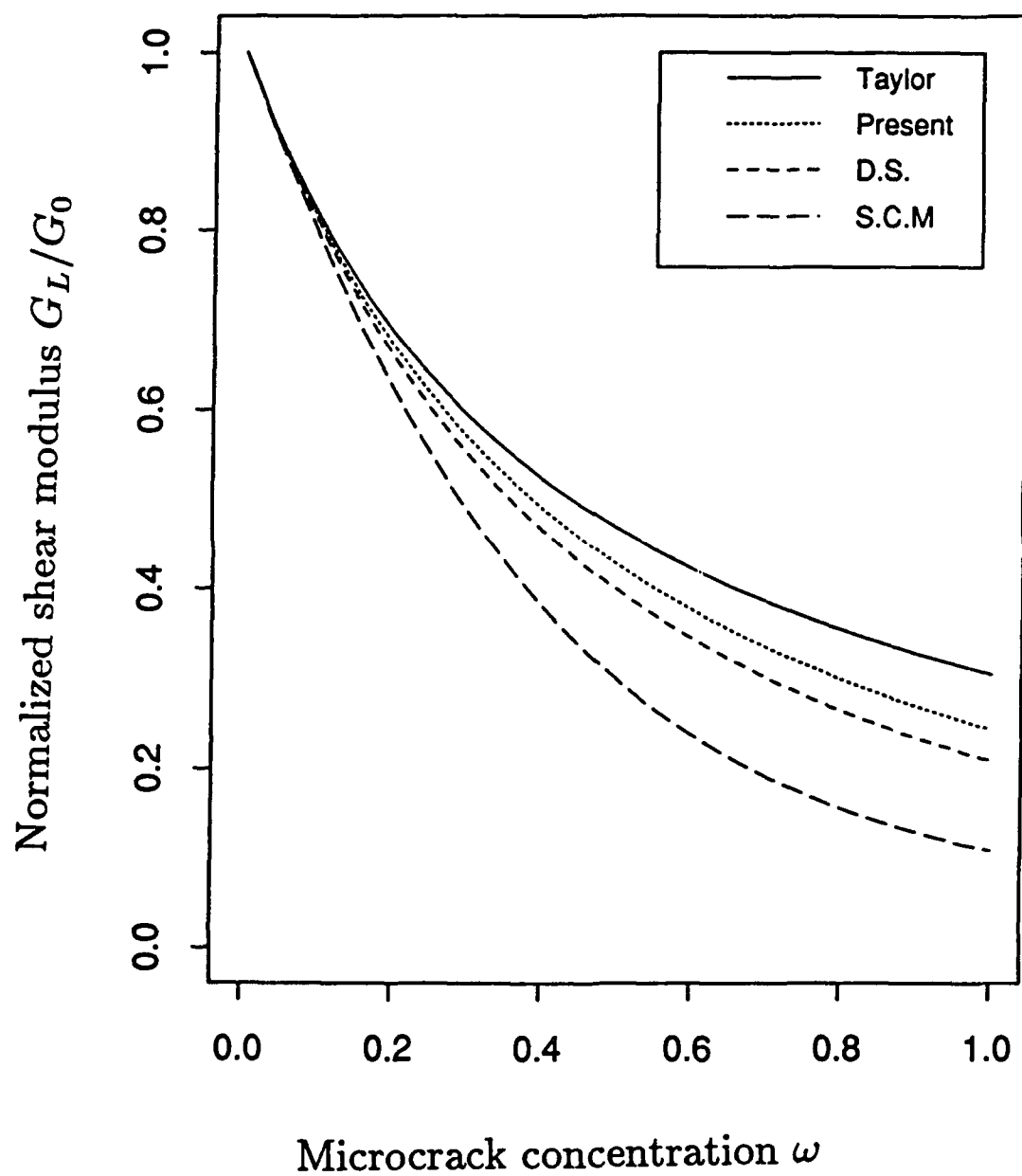**Figure 4.** Comparison of normalized longitudinal Young's modulus.

Figure 5. Comparison of normalized longitudinal shear modulus.